

Review

# Municipal Solid Waste Fly Ash-Derived Zeolites as Adsorbents for the Recovery of Nutrients and Heavy Metals—A Review

Christian Vogelsang<sup>1,\*</sup> and Muhammad Umar<sup>2</sup><sup>1</sup> Norwegian Institute for Water Research, Økernveien 94, N-0579 Oslo, Norway<sup>2</sup> Walkerton Clean Water Centre, 20 Ontario Rd, Walkerton, ON N0G 2V0, Canada; mumar@wcwc.ca

\* Correspondence: christian.vogelsang@niva.no

**Abstract:** Though fly ash from the incineration of municipal solid waste (MSW-FA) is considered hazardous waste, its huge and increasing volumes and potential value due to high concentrations of salts and heavy metals such as copper and zinc have attracted commercial interest in mining it for resources. The associated treatments used for extracting these resources may make it economically feasible to extract other constituents from the residuals, adding another potential pathway towards a zero-waste society. This review assesses the feasibility of using zeolites, synthesized from precursors extracted from MSW-FA, as sorbents for the recovery of nutrients (ammonium, nitrate, and phosphate) and heavy metals. It is possible to tailor the properties of the zeolites; however, the large variability in reported adsorption capacities and specificities, as well as the inherent heterogenic nature and variable composition and concentrations of most nutrient- or heavy metal-rich waste streams, make such tailoring challenging. A remaining important issue is the transfer of unwanted micropollutants from the MSW-FA or waste stream to the final products and the loss of surfactants from surfactant-modified zeolites during adsorption and/or desorption of nitrate and/or phosphate. Nonetheless, the recovery process is benefited by high concentrations of the target compounds and low concentrations of competing ions.

**Keywords:** waste-as-resource; zeolite precursor; sorption; surface-modified zeolites; ammonium; phosphate; reuse; regeneration



**Citation:** Vogelsang, C.; Umar, M. Municipal Solid Waste Fly Ash-Derived Zeolites as Adsorbents for the Recovery of Nutrients and Heavy Metals—A Review. *Water* **2023**, *15*, 3817. <https://doi.org/10.3390/w15213817>

Academic Editors:  
Monika Wawrzekiewicz and  
Anna Wołowicz

Received: 4 September 2023  
Revised: 24 October 2023  
Accepted: 26 October 2023  
Published: 31 October 2023



**Copyright:** © 2023 by the authors. Licensee MDPI, Basel, Switzerland. This article is an open access article distributed under the terms and conditions of the Creative Commons Attribution (CC BY) license (<https://creativecommons.org/licenses/by/4.0/>).

## 1. Introduction

There is an increasing interest in using incineration to dispose of municipal solid waste (MSW) due to the large reduction in weight (up to 70%) and volume (up to 90%), the concomitant recovery of energy and heat, and the destruction of most of the hazardous organic contaminants and pathogens. The globally generated amount of MSW increased significantly from 1.3 billion tons per annum in 2012 to 2.1 billion tons in 2018 [1], which is expected to increase further to 3.4 billion tons per year by 2050 [2]. Upon incineration, three main residues are produced: bottom ash, fly ash (FA), and air pollution control (APC) residues. Approximately 250–300 kg of bottom ash, 25–30 kg of fly ash, and APC residues are generated for each ton of MSW incinerated [3]. The bottom ash residue is utilized in many applications, particularly in building and construction work. The FA residue, however, is generally regarded as toxic waste due to its high content of heavy metals, salts, and organic micropollutants such as dioxins and furans [4] owing to the volatilization and condensation of different elements during the incineration. Therefore, nearly all MSW incineration FA (MSW-FA) is stabilized/solidified and deposited as toxic waste in landfills, and due to their enormous volumes, taking up valuable space. However, a shift in focus from environmental impacts to resource recovery has identified the potential value of embedded salts and metals in the MSW-FA, and some progress has been made in recovering these resources [5–7].

The principal components of FA are CaO, SiO<sub>2</sub>, Al<sub>2</sub>O<sub>3</sub>, and Fe<sub>2</sub>O<sub>3</sub>, resembling the main components of volcanic material, a precursor of natural zeolites. Zeolites are crystalline

micro- and mesoporous materials widely used as catalysts and sorbents [8]. However, most of the zeolites that are used today are synthesized since natural zeolites vary too much in mineralogical and chemical composition, crystal structure, and pore sizes, both between and within the mineral deposits they are extracted from, to be used for applications that require zeolites with specific and predictable properties [9]. Zeolites are primarily synthesized from pure silica ( $\text{SiO}_2$ ) and alumina ( $\text{Al}_2\text{O}_3$ ), though the search for and use of alternative economical and abundant sources has increased in the last decades [10]. Due to its low cost, availability, abundance, and resemblance to volcanic material, it is relatively common to synthesize zeolite from coal-derived FA [11]. MSW-FA usually contains much less silica and alumina than coal-derived FA [10,11]. Moreover, the often-high levels of leachable toxic compounds in this type of FA need to be reduced [12].

Zeolites are commonly used in separation processes in, e.g., the petrochemical and pharmaceutical industries as they can be made fairly specific to the target molecules, and since the main mechanisms behind the separation process (molecular sieving, electrostatic interaction, and polarization) are always reversible, zeolites are believed (under ideal situations) to be able to undergo a virtually unlimited number of adsorption–desorption cycles [8]. This is important from a cost-efficiency perspective too, as the high initial costs can be compensated by the longer life, assured by excellent stability and ease of regeneration.

Zeolites, depending on their chemical composition and pore structures as well as the operating conditions, can be used as sorbents for the removal of mono-, di-, and trivalent cations such as ammonium ( $\text{NH}_4^+$ ) and heavy metals ( $\text{Pb}^{2+}$ ,  $\text{Cu}^{2+}$ ,  $\text{Cd}^{2+}$ ,  $\text{Zn}^{2+}$ ,  $\text{Cr}^{3+}$ , and  $\text{Ni}^{2+}$ ) from industrial and municipal wastewaters [13]. And, by subsequent desorption and refinement, if needed, these adsorbates can be recovered for further downstream applications [11,14]. Furthermore, certain surface modifications of the zeolites can also be used as sorbents to remove anions such as phosphate ( $\text{PO}_4^{3-}$ ), nitrate ( $\text{NO}_3^-$ ), and arsenate ( $\text{H}_2\text{AsO}_4^-$ ,  $\text{HAsO}_4^{2-}$ ,  $\text{AsO}_4^{3-}$ ). However, the recovery of the adsorbates and the regeneration of the SMZ may be low.

The need to drastically improve the recovery of phosphorous from available sources due to the reduced availability of non-renewable phosphate rock is well known. Crop residues, food waste, manure, and human excreta are such sources, and multiple methods and strategies are currently under development to facilitate cost-effective means to harvest phosphorous from these, including from domestic wastewater [15], primarily for use in agriculture [16]. Nitrogen, on the other hand, is not a scarce resource, but the industrial production of mineral fertilizers consumes extensive amounts of energy and natural gas as feedstock for the hydrogen gas in the production of ammonia. Jensen and Kongshaug (2003) [17] estimated that fertilizer production accounted for approximately 1.2% of global energy consumption, of which about 93% was consumed by nitrogen-based fertilizers. Moreover, extensive nitrogen removal up to 85% at wastewater treatment plants (WWTP), as proposed by the European Commission in the revised version of the urban waste water treatment directive [18], implies a huge increase in investments, operating costs, and energy consumption to comply with the more stringent discharge requirements for nitrogen while losing approximately 60% of the nitrogen as nitrogen gas.

This review focuses on the feasibility of extracting Al and Si from MSW-FA and using these as precursors in the synthesis of zeolites to be used as sorbents for the recovery of nutrients and heavy metals from sources rich in these adsorbates. Potential sources could, for instance, be liquid manure fractions, rejection water after anaerobic digestion of food or sewage sludge, urine, concentrated black water after fermentation, industrial waste streams, or leachates from landfills or mines/mining areas [19–22]. Many of these sources are rich in constituents that may be transferred to the zeolite precursors if appropriate measures are not in place, which may then also end up as problematic contaminants in the recovered nutrients or heavy metals.

The second chapter of the review gives a brief overview of what zeolites are and how they are synthesized, particularly considering the shortcomings of using MSW-FA as source material and reviewing various extraction and purification methods to generate zeolite

precursors. The third chapter analyzes how zeolite properties and application conditions influence cation (e.g., ammonium) and heavy metal adsorption, while the fourth chapter examines the possibility of using surface-modified zeolites to adsorb anions such as nitrate and phosphate. The fifth chapter considers different approaches to recover and reuse substances and to regenerate the zeolite's adsorption capacity, and in the final chapter, the review discusses the possibilities and limitations from a somewhat broader perspective and pinpoints which topics need to be addressed in the future to assess the feasibility of using MSW-FA this way.

## 2. Zeolites

### 2.1. The Crystalline Structure of Zeolites

A zeolite is a crystalline substance with a structure characterized by a framework of linked tetrahedra, each consisting of four oxygen atoms surrounding a cation (typically  $\text{AlO}_4^{5-}$  and/or  $\text{SiO}_4^{4-}$ ). The tetrahedra are linked in rings, normally between 4 and 12 atoms, that are units in a more complex three-dimensional framework containing open cavities in the form of channels and cages, as illustrated in Figure 1. The difference in valence between silicon (+4) and aluminium (+3) leads to an excess of negative charge in the crystalline structure, which is neutralized by the presence of compensation cations ( $\text{Na}^+$ ,  $\text{K}^+$ ,  $\text{Li}^+$ ,  $\text{Ca}^{2+}$ ,  $\text{Mg}^{2+}$ , etc.) that do not occupy fixed positions but are free to move in the channels of the lattice framework [23]. Thus, the negative charge of zeolites is not localized but is more or less uniformly distributed in the framework, also called "framework charge" [24]. The compensation cations can be replaced by other cations (i.e., they are exchangeable). The channels or pores are typically smaller than 20 Å; hence, zeolites are classified as microporous materials [8], yet the pores are large enough to allow the passage of small compounds [25]. Therefore, they are also called "molecular sieves". Note that only the trivalent aluminium brings any negative charge into the frame; hence, the lower the Si:Al ratio, the more negatively charged and hydrophilic the zeolite framework, and conversely, the higher the Si:Al ratio, the more hydrophobic the zeolite framework.

There is a clear link between the crystalline structure of a zeolite and its properties, as well as the types of applications it would be suitable for. Hence, it is crucial to be able to characterize in detail both its chemical composition and its three-dimensional physical structure. The most relevant and commonly applied methods to characterize the crystalline structure of zeolites are:

- X-ray diffraction (XRD) is used to study the crystal structure and size of zeolite, the approximate extent of heteroatom substitution, and the presence of defects in zeolites [26].
- Transmission electron microscopy (TEM) is used for the characterization of zeolite structures, for instance, structure determination of new zeolites, study of growth mechanisms of nano-sized zeolites and pore structures of hierarchical micro- and meso-porous zeolites, and analysis of metal sites in zeolites [27].
- Fourier transform infrared spectroscopy (FTIR) is used to specify the functional units of zeolites and to predict the reaction mechanisms in the zeolite framework. The FTIR spectrum is also used to indicate the secondary building units that were found in the zeolite structure [26].
- A scanning electron microscope (SEM) is used to study the surface of solids and give information about their morphology and textural properties [26].
- Raman spectroscopy can be used to determine the framework type and symmetry of zeolites, identify the chemical composition and acidity of zeolites, and study the host-guest interactions and catalytic reactions of zeolites [28,29].

A wide range of improvements to these methods and new methodologies have emerged in the last decades, and in combination, these methods now constitute a strong set of tools to characterize and understand many fundamental aspects relevant for the development and application of zeolites [30].

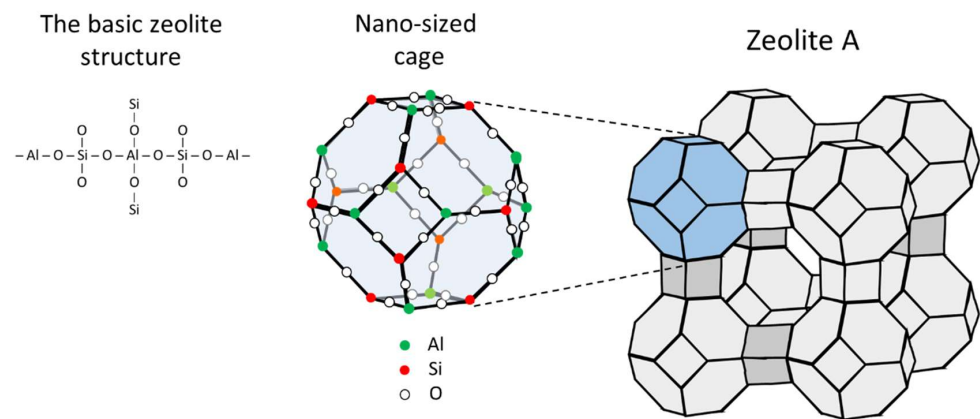


**Figure 1.** Illustration of zeolite A from the basic structure via the nano-sized cage with a Si/Al ratio of 1 to the full characteristic zeolite A crystalline structure (LTA).

## 2.2. Naturally and Synthesized Zeolites

About 60 varieties of natural zeolites have been identified, distinguished by their framework structure and crystalline system [8,31,32]. Large deposits of sedimentary zeolite have been found, generally in volcanoclastic rocks, though only rocks with zeolite content >50% may be of economic interest [8]. As can be seen from the ternary diagram in Figure 2, the volcanic ashes that these natural zeolites are developed from are usually very rich in silica ( $\text{SiO}_2$ ) and/or alumina ( $\text{Al}_2\text{O}_3$ ). However, as already mentioned, the mineralogical and chemical composition and the crystal structure and pore sizes are typically varying much in naturally occurring zeolites, both between and within the mineral deposit from which they are extracted [9]. Due to the possibility of synthesizing zeolites with a higher degree of ordering in the crystalline structure and with standardized pore sizes, resulting in more uniform and predictable properties, a lot of research has been put into developing zeolites that facilitate targeted applications in the process industry as heterogeneous catalysts, sorbents, and ion exchange resins [8].

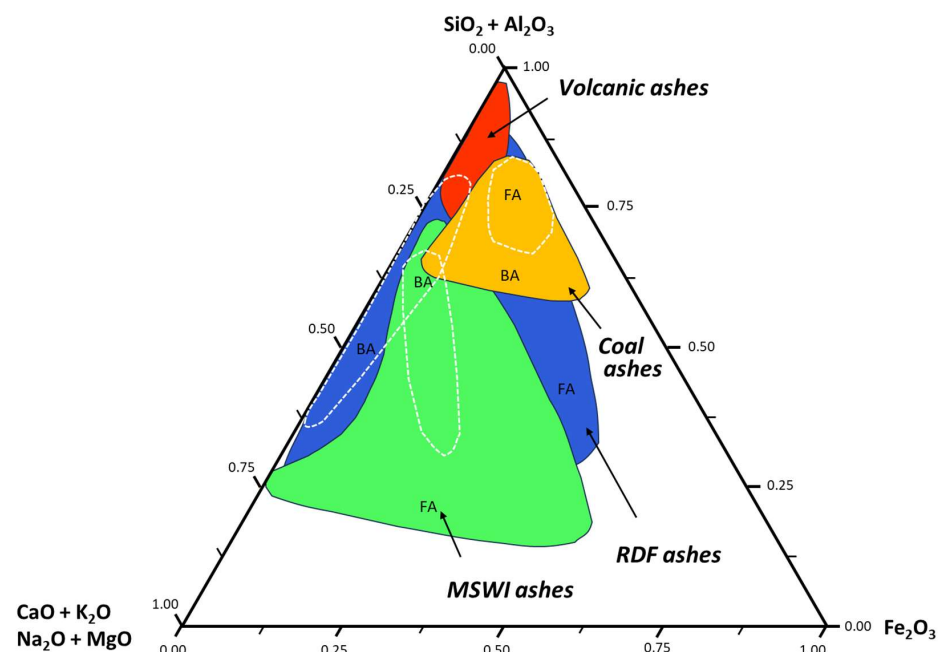


**Figure 2.** Ternary diagram showing relative proportions of  $\text{SiO}_2$ ,  $\text{Al}_2\text{O}_3$ ,  $\text{CaO}$ ,  $\text{K}_2\text{O}$ ,  $\text{Na}_2\text{O}$ ,  $\text{MgO}$ , and  $\text{Fe}_2\text{O}_3$  in various fly ashes (FA) and bottom ashes (BA). Refuse-derived fuels (RDF) are produced from various types of waste, such as MSW, industrial waste, or commercial waste. Reproduced from Brännvall and Kumpiene (2016) [33] with permission from the Royal Society of Chemistry.

### 2.3. Zeolite Synthesis

Historically, zeolites have mostly been prepared by hydrothermal synthesis at moderate temperatures (353–523 K) under autogenous pressure [8,34]. Until the end of the 1950s, only purely inorganic systems had been used. This imposed a major constraint on the Si/Al ratio of the framework, which was always very low, thereby generating very hydrophilic zeolites with great cation exchange properties. However, by introducing different organic additives to the reaction mixtures, the Si/Al ratio could be drastically raised, with the first high-silica zeolite (beta) having a Si/Al ratio of 5 to 100 and then the first zeolite having a pure silica endmember (ZSM-5; Silicalite-1). This was possible since the organic molecules could act as void fillers (probably the role of small neutral organic molecules such as, e.g., 1-propanol, 1-propanamine, and 1,6-hexanediol in the synthesis of ZSM-5) or as structure-directing agents (SDA) promoting the crystallization of different zeolite phases [8]. The relatively large organic molecules compensate for a lower number of negative framework charges than the small inorganic cations (e.g.,  $\text{Na}^+$ ,  $\text{K}^+$ ) used in the pure inorganic system; hence, a lower number of trivalent metal ions ( $\text{Al}^{3+}$ ) are incorporated in the framework. By varying the size of the organic molecule, the maximum trivalent ion concentration can be modulated [8]. Hence, it has been possible to synthesize zeolites with larger pore volumes than those present in natural zeolites [35]. However, other parameters also influence the final structure of the synthesized zeolites: the composition of the reaction mixture, crystallization time, temperature, and the  $\text{SiO}_2/\text{Al}_2\text{O}_3$  molar ratio in the reaction mixture. Today, several different methods (e.g., hydrothermal, solvothermal, ionothermal, and solven-free methods) and strategies are applied to synthesize zeolites to improve specific qualities of the end product, increase reaction rates, and save energy [11,36]. Due to the obvious benefits of increased access to the internal structure while still having a high specific surface area, significant attention has been given to the possibility of producing zeolites with mesoporous characteristics (20 to 500 Å). According to [8], the most versatile and promising route to the preparation of micromesoporous hierarchical systems is probably the recrystallization of preformed zeolites in the presence of a surfactant [37,38]; the zeolite crystals are partially destroyed with an alkali solution, and the zeolite fragments extracted from the crystals generate mesoporosity and are reassembled in a mesostructured phase with the help of the surfactant. The treatment conditions ( $\text{OH}^-$ /zeolite ratio, temperature, and time) determine the degree of dissolution of the zeolite crystals and, ultimately, influence the characteristics of the final products. Low dissolution degrees favor the formation of mesoporous crystals coated with a thin film of mesostructured phases, while composites of cocrystallized phases are obtained upon increasing the dissolution degree. Finally, when the dissolution of the zeolite crystals is complete, mesostructured materials with mesoporous walls formed by the assembly of zeolite fragments are produced [8,39]. An alternative method to generate mesoporous structures is to synthesize nanosheets or nanosponges using a dual-pyrogenic surfactant as described by [39] for a ZSM-5-type zeolite, an MFI-type zeolite as described by Schick et al. (2011) [40], or a \*BEA-type zeolite as described by Hanache et al. (2019) [41]. The dual-pyrogenic surfactant plays several roles: as a structuring agent of the zeolitic framework, as a crystal growth inhibitor along the b-axis (formation of the nanosheets), and as a mesopore generator [41].

### 2.4. MSW-FA as Source to Silicate and Alumina in Zeolite Synthesis

Using silicate and aluminate from pure chemicals makes the production of zeolites expensive; hence, a lot of research has been carried out to find alternative sources to silicate and aluminate from cheaper and more abundant sources during the last decades [10]. The prerequisites for such sources are that they must be cheap, readily available, generated in large quantities, and rich in silica and/or alumina with a low content of contaminating elements [11]. Fly ash from coal-burning is one such source that has been researched considerably. As can be seen from the ternary diagram in Figure 2, these fly ashes are very rich in silica and alumina, more so than the bottom ashes (BA) from coal burning.

The fly ash fraction of the MSW incineration (MSWI) residues consists of grayish, fine, irregular-shaped dust-like particles [42]. The size of the particles is in the range of ca. 1–2000  $\mu\text{m}$ , but the main weight fraction appears to be within a relatively narrow size range of 50–200  $\mu\text{m}$  [43–47]. The average specific surface area of FA is typically in the range of 250–850  $\text{m}^2/\text{kg}$  [48,49], while the specific densities of the particles are typically 1.7–2.4  $\text{kg}/\text{m}^3$  [12].

In terms of the silica and alumina content in ashes from the incineration of MSW, the situation is the opposite of that of coal-burning ashes; the BA are much richer in silica and alumina than MSW-FA and similar to BA from coal-burning. However, the composition of MSW-FA is greatly dependent on the MSW sources [50,51] and the type of incinerators [52]. The reported concentrations of Al and Si in MSW-FA indicate that the relative contents of  $\text{SiO}_2$  and  $\text{Al}_2\text{O}_3$  are in the range of 12–41 weight% and 5–24 weight%, respectively, with typical values of ca. 20 weight%  $\text{SiO}_2$  and ca. 10 weight%  $\text{Al}_2\text{O}_3$ . A summary of the reported elemental composition of MSW-FA is shown in Table 1. FA contains both amorphous (i.e., glassy, soft, malleable, and opaque) and crystalline phases (i.e., hard, brittle, and transparent or translucent). Typically dominating crystalline structures in MSW-FA are quartz ( $\text{SiO}_2$ ), gismondine ( $\text{CaAl}_2\text{Si}_2\text{O}_8 \cdot 4\text{H}_2\text{O}$ ; a zeolite mineral), gehlenite ( $\text{Ca}_2\text{Al}[\text{AlSiO}_7]$ ), feldspars ( $\text{K-Na}[\text{AlSi}_3\text{O}_8]$ - $\text{Ca}[\text{Al}_2\text{Si}_2\text{O}_8]$ ), hematite ( $\text{Fe}_2\text{O}_3$ ), anhydrite ( $\text{CaSO}_4$ ), gypsum ( $\text{CaSO}_4 \cdot 2\text{H}_2\text{O}$ ), calcite ( $\text{CaCO}_3$ ), sylvite (KCl), and lime (CaO) [53–57].

MSW-FA also contains significant amounts of Cl, Ca, Na, and K, where most of the alkali metals (Na and K) are present as water-soluble chlorides. Most of the Ca is present as calcium oxide (CaO), probably due to the decomposition of calcite ( $\text{CaCO}_3$ ) [58] and to the excessive use of lime in the scrubbing process [59]. The high levels of chloride probably originate from the significant volumes of polyvinyl chloride (PVC) present in MSW [59]. Fly ash from grate furnaces is particularly rich in Cl, Na, and K, mainly in the forms of NaCl and KCl [60,61]. The high content of certain heavy metals (Pb, Cd, Zn, Cd, etc.) in the MSW-FA (see Table 1) is also problematic. Moreover, the FA may contain significant concentrations of organic micropollutants such as polycyclic hydrocarbons (PAH; 18–5600  $\mu\text{g}/\text{kg}$ ), chlorobenzenes (CB; 0.03–890  $\mu\text{g}/\text{kg}$ ), polychlorinated biphenyls (PCB; <40  $\mu\text{g}/\text{kg}$ ), polychlorinated dibenzo-p-dioxins (PCDD; 0.7–1000  $\mu\text{g}/\text{kg}$ ), and furans (PCDF; 1.4–370  $\mu\text{g}/\text{kg}$ ) [4]. Therefore, proper management of MSW-FA involves some sort of stabilization or solidification of the FA prior to landfilling or other confined placement to minimize potential leakage of salts, heavy metals, and organic micropollutants [62]. Examples of stabilization or solidification processes are the use of hydraulic binders, including cement, lime, and/or pozzolanic materials; the use of chemical precipitation; the use of aging and weathering through hydration, carbonation, or oxidation/reduction; and the use of thermal treatment by sintering, vitrification, and melting [62].

Another important issue regarding MSW-FA is that their composition will vary much more than FA from the incineration of fuel that is more homogeneous (e.g., coal-burning). The relative abundance of each component is influenced by (1) the composition of the incinerated waste and (2) the conditions during incineration. The former is usually affected by human habits, socioeconomic factors, and the recycling system before incineration [63], while the latter is affected by the types of fuel, operating parameters, types of furnaces, and the APC system design used [64].

Hence, both the inherent low and potentially highly variable concentrations of silica and alumina in MSW-FA and the potentially high contamination level of inorganic and organic micropollutants disqualify it from being an interesting raw source for zeolite synthesis directly [65,66].

**Table 1.** Chemical composition range of FA/APC residues from MSW incineration based on reported literature values [12,62,66–76].

Element	Unit	Fly Ash/APC Residues		
		Min	Max	Median
<i>Main elements</i>				
Si	g/kg	36	190	-
Al	g/kg	6.4	93	-
Fe	g/kg	0.76	71	-
Ca	g/kg	46	361	-
Mg	g/kg	1.1	19	-
K	g/kg	17	109	-
Na	g/kg	6.2	84	-
Ti	g/kg	0.7	12	-
S	g/kg	1.4	32	-
Cl	g/kg	45	380	-
P	g/kg	1.7	9.6	-
Mn	g/kg	0.2	1.7	-
TOC	g/kg	4.9	17	-
LOI	g/kg	11	120	-
SiO <sub>2</sub>	%	11.5	41.4	19.1
Al <sub>2</sub> O <sub>3</sub>	%	4.7	24.3	10.9
CaO	%	17	31.5	22.0
SO <sub>3</sub>	%	3	10.2	6.4
Na <sub>2</sub> O	%	3.8	9.6	5.9
K <sub>2</sub> O	%	2	8.1	4.5
Fe <sub>2</sub> O <sub>3</sub>	%	1.3	5.9	2.5
MgO	%	1.7	6.9	2.7
<i>Minor elements</i>				
As	mg/kg	18	960	-
Cd	mg/kg	16	1660	-
Cr	mg/kg	72	570	-
Cu	mg/kg	16	2220	-
Hg	mg/kg	0.1	51	-
Ni	mg/kg	19	710	-
Pb	mg/kg	254	27,000	-
Zn	mg/kg	4308	41,000	-

### 2.5. Producing Zeolite-Like Material from MSW Fly Ash

As described above, there are three main limitations to using MSW-FA as a source for producing zeolites: (i) the Al and Si content is too low; (ii) the elemental composition is variable and partially unpredictable; and (iii) there is a high level of salts and toxic contaminants that may leach out and have negative health and/or environmental implications depending on the applications of the zeolites or how any residues from the production process are managed.

The general stepwise approach to synthesising zeolites from MSW-FA is to remove as much of the compounds that are not needed or hamper the process (especially salts) in a pre-treatment step (see Section 2.5.1), and then get all alumina and silica over to a dissolved or amorphous (i.e., non-crystalline) state (see Section 2.5.2) in a Si/Al ratio and concentration that is appropriate for (re)crystallization to the preferred type(s) of zeolites. As some heavy metals in the MSW-FA may have commercial interest, both separate extraction and solidification may be adequate management strategies for these (see Section 2.5.4), while organic micropollutants such as dioxins (PCDDs) and furans (PCDFs) need additional strategies (see Section 2.5.5).

There are relatively few studies that have published results from the synthesis of zeolites from MSW-FA, and as far as the authors have found, all have used some sort of hydrothermal treatment (see Section 2.5.3). The examples in Table 2 show the main types and details related to both applied pre-treatments, hydrothermal treatments, and post-treatments that were applied in each case, as well as details regarding the final zeolite products. In the following sections, some of these will be discussed in more detail.

**Table 2.** Examples of zeolite synthesis from MSW-FA using hydrothermal treatment. BET = Brunauer–Emmett–Teller specific surface area; WGP = waste glass powder; WMS = wet magnet-separated; Cal = calcination; Gr = grinding; AF = alkali fusion; DI = deionized water; DW = deionized water washing; Acid = acid treatment; CTAB = cetyltrimethylammonium bromide; HYD = hydrolysis; w/ST = with stirring or shaking; MWA = microwave-assisted; CRY = crystallization; N.S.: Not specified.

Ref.	Al, Si Sources					Pre-Treatment		Hydrothermal Treatment				Products			
	Type	In MSW-FA		BET	CEC	Initial Si/Al Ratio	Type	Type	Additives	L/S	Temp	Time	Zeolite	BET	CEC
		Si	Al	m <sup>2</sup> /g	meq/g					-	mL/g	°C		h	m <sup>2</sup> /g
[77]	MSW-FA	9.5% SiO <sub>2</sub>	5.5% Al <sub>2</sub> O <sub>3</sub>	N.S.	N.S.	1.5	DW, Cal <sup>1</sup> , Acid <sup>1</sup> , DI	Autoclave w/ST	1–2 M NaOH	25	60	20–30	Zeolite A	N.S.	N.S.
									0.5–2 M NaOH	25	100–120	20–48	Zeolite P	N.S.	N.S.
[78]	MSW-FA (<75 μm, WMS)	22.0% SiO <sub>2</sub>	10.2% Al <sub>2</sub> O <sub>3</sub>	2.54	0.078	1.9	No	N.S.	3.5 M NaOH	5–15	130–190	24	Gismondine	45	0.8
									6 M NaOH				Gmelinite	N.S.	0.65
[79]	MSW-FA (water-cooled)	47.1% SiO <sub>2</sub>	12.4% Al <sub>2</sub> O <sub>3</sub>	0.5	N.S.	4	Gr	Autoclave	2 M NaOH	30	200	>24	Zeolite-like	54	N.S.
[65]	MSW-FA, WGP, Al <sub>2</sub> O <sub>3</sub> powder	0.3% Si	2.2% Al	N.S.	0.20	1	No	Heater w/ST	2.5 M NaOH	10	60	24	Zeolites Y, A and L (perlielite)	N.S.	1.00
							AF (1.2 g NaOH/g FA, 550 °C, 1 h)	Aging w/ST	WGP, Al <sub>2</sub> O <sub>3</sub> powder	10	Room	24	-	-	-
								CRY	No	-	90	24	Zeolite-like	N.S.	1.00
								HYD	DI	100	105	24	-	-	-
[80]	MSW-FA	12.2% Si	0.8% Al	8.59	N.S.	40	AF (1.5 g NaOH/g FA, 400 °C, 40 min)	Sealed reactor	1.2% CTAB <sup>2</sup>	Filtrate	105	24	-	-	-
								Cal	-	-	550 °C	3	ZSM-23	651	N.S.
								Aging w/ST	DI	9	Room	24	-	-	-
[54]	MSW-FA and coal-FA	45.5% SiO <sub>2</sub>	22.6% Al <sub>2</sub> O <sub>3</sub>	N.S.	0.64	1.8	Gr, AF (1.2 g NaOH/g FA, 550 °C, 1 h)	CRY	No	-	90	6–10	Zeolite X	200	2.5
											≥130	14–18	Zeolite HS	N.S.	N.S.
[81]	MSW-FA	N.S.	N.S.	N.S.	N.S.	N.S.	No	MWA	DI, 1.5 mol NaH <sub>2</sub> PO <sub>4</sub> /kg FA	2	200	1/6	Zeolite-like	N.S.	N.S.
[82]	MSW-FA	N.S.	N.S.	N.S.	N.S.	N.S.	No	MWA	1 M Na <sub>2</sub> HPO <sub>4</sub>	3	150	1/3	Zeolite-like	N.S.	N.S.
[83]	MSW-FA	4.3% Si	2.4% Al		0.023		AF (2 g NaOH/g FA, 550 °C, 1 h)	MWA	DI	3.3	100	0.5	Zeolite-like	N.S.	1.17
							No	MWA	DI	3.3	100	0.5	Zeolite-like	N.S.	0.43

Note: <sup>1</sup> Calcination at 800 °C for 2 h and acid treatment with 3 M HCl (1 mL/g FA) for 30 min; <sup>2</sup> pH adjusted to 10 using 1 M H<sub>2</sub>SO<sub>4</sub>.

### 2.5.1. Specific Leaching of Salt as Pre-Treatment

As indicated above, washing the FA with clean water to leach out salts, primarily chlorides (e.g., NaCl, KCl, CaCl<sub>2</sub>, and CaCl<sub>2</sub>·Ca(OH)<sub>2</sub>·H<sub>2</sub>O), could be an effective pre-treatment step [59]. When removing the salts, as little as possible of the heavy metals should be included to secure their potential reuse value. Moreover, removing the salts will also increase the concentration of Al and Si in the residual solids. [84] found that a single wash cycle with water (L/S ratio of 2) for 60 min extracted more than 65% of Cl, greater than 50% of K and Na, and about 20% of Ca. When the L/S ratio was increased to 20, ca. 95% of Cl and ca. 50% of Ca were washed out, but with no additional effect on K and Na. However, by increasing the L/S ratio, the leaching of certain heavy metals (Pb, Cu, Zn), and particularly Cr (8%), was increased. A limited loss of Al and Si was observed, but the total loss of mass was not provided. Though [71] did a similar washing test with MSW-FA (L/S ratio of 2) but for a shorter time (15 min) and measured a total mass loss of ca. 12% due to the removal of chloride- and sulphate-based salts as well as elevated levels of Pb in the leachate (34 mg/L). Additionally, Weibel et al. (2017) [58] observed fairly similar levels of loss of Cl (73%), K (ca. 67%), and Na (58%) from MSW-FA as Wang et al. (2001) [84] when using treated process water (pH 7.9–9.5) from the incineration plant in the washing step with a L/S ratio of 10 for 1 h with a final pH of 10.8. In contrast to [84], they observed no depletion of Cr, Pb, Cu, or Zn. Pb-bearing sulphates were dissolved but were cemented as PbCu<sup>0</sup> on the surface of Al<sup>0</sup> particles. Aluminium was dissolved and recovered as precipitated aluminium hydroxide (Al(OH)<sub>3</sub>). However, significant amounts of Si (21%) were lost during the washing process. It must be noted that this MSW-FA had very low CaO content (<1%) compared to “normal” MSW-FA (17–31.5%; Table 1) as it contained no lime from the scrubbing treatment. Chuai et al. (2022) [85] found that the injected CaO in the scrubber promoted the formation of Ca<sub>3</sub>(AsO<sub>4</sub>)<sub>2</sub>, CaCrO<sub>4</sub>, and PbCl<sub>2</sub>, which significantly reduced the leaching rate of Pb and As from the FA. The cementation of soluble metal salts into less soluble silicates, hydroxides, and carbonates was also observed by Todorovic et al. (2003) [86] for Hg, Mn, Pb, and Zn, and notably also for Al and Si (leaching less than 3%). In addition to the presence and nature of the cementitious material, the process is dependent on the amount of water that is added, the temperature, and the time it is allowed to work; it may take weeks or months to complete [86,87]. In addition, Kiyaki et al. (2002) [88] eliminated NaCl and KCl from the MSW-FA by washing with deionized water (L/S ratio not stated), increasing the relative contents of SiO<sub>2</sub> and Al<sub>2</sub>O<sub>3</sub> from 9.5% and 5.5% in the initial MSW-FA to 28.0% and 17.0%, respectively.

### 2.5.2. Generating Al- and Si-Containing Zeolite Precursors

Different options to extract and purify Si and Al to generate the Al- and Si-containing zeolite precursors from Si- and/or Al-rich materials are briefly illustrated in Figure 3.

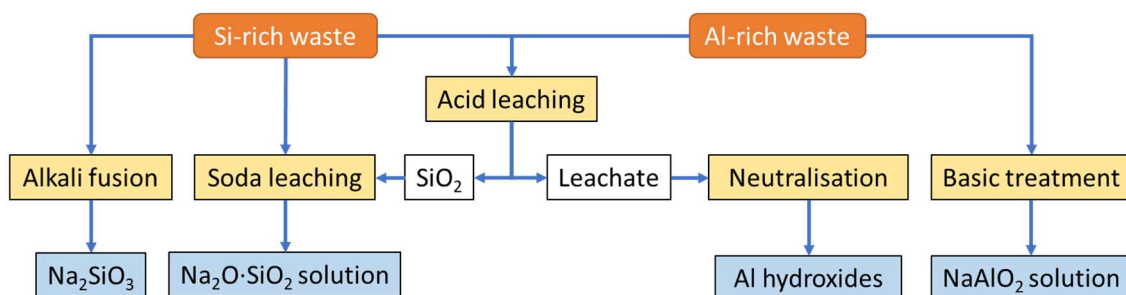


**Figure 3.** Simplified experimental flowsheet for the extraction of Si and Al and subsequently the preparation of microporous materials from Si and Al wastes.

Since silicas are completely dissolved at basic conditions (pH > 10), alkali leaching (usually with soda) at pH 11–12 can be used to produce sodium silicate (Na<sub>2</sub>O·SiO<sub>2</sub>) solutions, so-called desilication [89]. This process is also used to leach silicon from the

zeolite framework to tailor hierarchical or mesoporous zeolites [90]. At this pH, aluminium is also highly soluble, while most transition metals and alkali earth metals remain largely insoluble [91]. Hence, aluminium metal can be leached with soda to generate a sodium aluminate ( $\text{NaAlO}_2$ ) solution [92]. Iron should be oxidized to  $\text{Fe}^{3+}$  by air or oxidants prior to the alkali leaching to precipitate it as stable  $\text{Fe}(\text{OH})_3$  at pH 11 [93]. Bac et al. (2010) [79] produced a pure silica residue as a by-product when synthesizing zeolites from Si-rich (47%  $\text{SiO}_2$ ) MSW-FA. The  $\text{SiO}_2$  was extracted from the sodium silicate filtrate (residue from the separated zeolites; see details in Table 2) by mixing 1:1 with 2 M  $\text{NH}_4\text{NO}_3$  and vigorous stirring at room temperature for six hours, followed by filtering the flocculated  $\text{SiO}_2$  and freeze-drying. The residual  $\text{SiO}_2$  yield could be regulated by the amount of NaOH used in the hydrothermal process (inverse relationship), as this also regulates zeolite production. Lin and Chen (2021) [80] used both air-cooled and water-cooled MSW-FA in their tests and found that the rapid cooling of the FA provided by the water immediately after the incineration process increased the amorphous fraction in FA and thereby also increased the  $\text{SiO}_2$  yield.

Alkaline fusion, in which the FA is mixed with NaOH at high temperatures (typically 400–600 °C for about 1 h) followed by the addition of water and vigorous stirring, is often used as a pre-treatment to hydrothermal treatment (see examples in Table 2) to accelerate and make the dissolution of silicates and aluminates more efficient than normal alkali leaching as the quartz is transformed into an amorphous state.

Since the Si/Al ratio in zeolites has a significant effect on its sorption properties, as will be discussed in more detail in the next chapter, it will be beneficial to be able to extract the Al and Si content of the MSW-FA into separate amorphous zeolite precursors (i.e., pure compounds such as  $\text{Na}_2\text{SiO}_3$  and  $\text{Al}(\text{OH})_3$  or solutions such as  $\text{Na}_2\text{O}\cdot\text{SiO}_2$  and  $\text{NaAlO}_2$ ) so that the Si/Al ratio can be more easily tailored. Hence, the  $\text{SiO}_2$  residue extracted from the by-product [79] may be reused in zeolite synthesis to modify the precursor mix. However, the main target compounds for adsorption by zeolites in this review are cations; hence, zeolites with low Si/Al ratios that will be hydrophilic and strongly negatively charged will usually be better adsorbents for cations (see Section 3.3).

Most metal hydroxides, including aluminium hydroxides, are readily soluble in acidic conditions, while both crystalline and amorphous silicas are stable [94]. When clay minerals and materials based on silicates and aluminosilicates are treated with acids (typically hydrochloric or sulphuric acid), all the components of the clay minerals except  $\text{SiO}_2$  are substantially leached out by the acid, leaving internal cavities as pores in the final product, making acid leaching a simple and cost-effective method to prepare quite pure silica [95]. Temuujin et al. (2003) [96] found that when leaching vermiculite, 2 M HCl at 80 °C for 2 h gave the silicate product the highest specific surface area. In a similar study, [95] leached phlogopite and found that 5 M  $\text{HNO}_3$  at 90 °C for 15 min gave the most porous silica product. Though, when leaching chlorite,  $\text{H}_2\text{SO}_4$  (5 N at 90 °C for 1.5 h) gave a silica product with a higher specific surface area than when using HCl or  $\text{HNO}_3$  [64]. However, the resulting leachate may also contain significant amounts of heavy metals if these have not been removed during pre-treatment (see Section 2.5.4). However, Al can be precipitated as aluminium hydroxides by neutralization [97]. Several studies on coal FA have suggested protocols for generating pure silica and alumina [89,98–101]. Zhao et al. (2023) [99] suggested a cascade extraction method in which the raw coal FA was desilicated by alkali leaching to release silicon species, harvested as  $\text{CaSiO}_3$  after adding  $\text{Ca}(\text{OH})_2$  to the supernatant of the desilication unit. The solid residue from the desilication unit was mixed with  $\text{Na}_2\text{CO}_3$  and sintered to facilitate the dissolution of Al and Fe species that would subsequently be acid-leached and stepwise precipitated as  $\text{Fe}(\text{OH})_3$  and  $\text{Al}(\text{OH})_3$  based on pH. The sintered residue was recovered as silica gel. However, in coal-based FA, a large fraction of the Al is often found as acid-stable mullite ( $3\text{Al}_2\text{O}_3\cdot 2\text{SiO}_2$  or  $2\text{Al}_2\text{O}_3\cdot\text{SiO}_2$ ) [102,103] that needs to be activated by, e.g., sintering for acidic leaching to be efficient [99]. In MSW-FA, mullite is usually miniscule or absent [54,55,104].

Supplementary (waste) sources of Al and/or Si may also be used to increase the concentrations of Si and Al and/or to provide a tailored Si/Al ratio. In addition, Deng et al. (2106) [65] used waste glass powder and Al<sub>2</sub>O<sub>3</sub> powder to increase the very Si- and Al-poor MSW-FA (0.3% Si and 2.2% Al) in their study (see Table 2). Table 3 lists Al-rich (>10% Al<sub>2</sub>O<sub>3</sub>) waste sources that may be used as secondary sources to generate zeolite precursors [36,91].

**Table 3.** Al and Si sources from different waste products that contain a minimum of up to 10% Al. Sources: [91,105]; MSW-FA see Table 1.

Waste Material	Al <sub>2</sub> O <sub>3</sub>	SiO <sub>2</sub>	CaO
Aluminium scrap	Al <sub>met</sub> > 90–99%		
Aluminium dust	Al <sub>total</sub> 25–40 Al <sub>met</sub> 15–25	6–11	1–4
Black aluminium dross	42–88	1.3–14	0.6–1
White aluminium dross	40–50		
Spent Fluid Catalytic Cracking catalysts	40–50	40–50	0–1
Coal combustion ashes	15–40	40–60	3–15
Aluminium salt slag	20–30 Al <sub>met</sub> 5–10	2–10	
Coal gasification ashes	5–30	25–60	2–30
Liquid Crystal Displays glass panel	15–25	50–75	0–7
MSW-FA	5–24	12–41	15–50
Electric furnace steel reduction slag	15–20	15–20	50–60
Lithium slag	15–20	50–55	10–12
Red mud from the Bayer process (dried)	10–20	3–50	2–40
Drilling and cutting muds (dried)	5–20	30–70	2–30
MSW-BA	1–20	5–50	10–50
Waste porcelain	19	70	3
Blast furnace iron slag	10–15	30–40	40–50
Wood ash	0.5–15	10–70	10–70
Waste foundry sand	0–15	75–90	0–5
Palm oil fuel ash (POFA)	0.5–12	45–75	3–15
Zinc slag	7–10	15–20	15–20
Electric furnace steel oxidation slag	5–10	10–15	20–25

### 2.5.3. Hydrothermal Zeolite Synthesis from MSW-FA

A typical hydrothermal zeolite synthesis can be briefly described as follows [34]: The amorphous reactants containing silica and alumina (aqueous aluminosilicate gel) are mixed with a cation source, usually in a basic (high pH) medium, and heated, often (for reaction temperatures above 100 °C), in a sealed autoclave. After an “induction period”, crystalline zeolite products can be detected, and gradually, essentially all amorphous material is replaced by an approximately equal mass of zeolite crystals, which are recovered by filtration, washing, and drying. As indicated by the hydrothermal treatment examples in Table 2, NaOH is typically used both to increase the pH and to bring the cation (Na<sup>+</sup>) to the process.

The main factors that determine the zeolite yield are the amounts of amorphous Si and Al that are brought into the hydrothermal process (see Section 2.5.2), the amount of alkali (NaOH) that is mixed with the FA, the liquid-to-solid (L/S) ratio, the temperature, and the duration of the hydrothermal process.

NaOH reacts with  $\text{SiO}_2$  and  $\text{Al}_2\text{O}_3$  to generate soluble silicate and aluminate, and the amount of NaOH partially determines which zeolites are formed. Miyake et al. (2002) [77] found that zeolite A was converted to zeolite P when the NaOH concentration increased, while Yang et al. (1998) [78] found that gismondine was generated in 3.5 M NaOH while gmelinite was formed in 6 M NaOH (see Table 2). Some of the studies used alkali fusion as a pre-treatment to improve the dissolution of the more resilient Si and Al states (see Section 2.5.2), and the fused components were brought into the subsequent hydrothermal process.

The L/S ratio affects the concentrations of Si and Al and, therefore, the formation and growth of zeolites [80]. The L/S ratio should be low enough to give an aluminosilicate gel concentration that promotes the formation of the zeolite crystal structure, though the L/S ratio should still be high enough to give sufficient space for crystal structure formation and growth of the synthetic zeolite [80]. The L/S ratios applied in the traditional hydrothermal processes reported in Table 2 were typically in the range of 10–30.

Both the nucleation rate and the crystal growth rate increase with an increase in temperature [80]. However, as the formation of zeolite is thermodynamically metastable, it is important to control the reaction temperature. bac et al. (2010) [79] reported that the temperature was a critical factor determining the zeolitic material that was produced (hydroxy-sodalite and/or Na-P1 zeolite at 100 °C and hydroxycancrinite at 200 °C) as well as the quantity of produced zeolites (ca. doubled with an increase from 100 °C to 200 °C). Furthermore, Miyake et al. (2002) [77] also reported a shift in the type of zeolite that was produced when the temperature was increased from 60 °C to 100–120 °C (see Table 2).

The hydrothermal treatment needs to be given sufficient time for the crystallization process. Several hours to tens of hours are recommended for optimal zeolite yield [54,65,77]. In practice, most studies have used about 24 h (see Table 2). Lin et al. (2018) [106] reported that the zeolites A and X that initially developed dissociated and transformed to sodalite and type P zeolite when the crystallization time was prolonged and sufficient alkaline aluminosilicate gels were present.

The introduction of microwave-assisted hydrothermal treatment has significantly reduced both the energy consumption and time required for the zeolite synthesis, as the microwaves can accelerate the heating rate, facilitate the dissolution of  $\text{SiO}_2$  and  $\text{Al}_2\text{O}_3$ , and increase the nucleation rate. In addition, Qiu et al. (2016,2017) [81,82] demonstrated that the microwave-assisted hydrothermal treatment only took 10–20 min to generate zeolites from MSW-FA (see Table 2). However, the current microwave hydrothermal reactors only meet laboratory requirements; hence, industrial-scale devices need to be developed [51].

Of the examples of zeolite synthesis from MSW-FA shown in Table 2, the work done by Lin et al. (2021) [80] is the only one that included the use of a structural agent or soft template (the surfactant CTAB) in the hydrothermal process. CTAB needs to be removed afterwards, and this was done by calcination at 550 °C for 3 h.

#### 2.5.4. Controlled Acid Leaching and Solidification of Heavy Metals

As indicated in Table 1, MSW-FA usually contains significant amounts of heavy metals. Jin et al. (2013) [107] tested the leachability of selected heavy metals (Cr, Cu, Zn, and Pb) from MSW-FA without any pre-treatment using the modified BCR sequential extraction procedure [108]. They found that as much as 30% of Pb was found in the first fraction with exchangeable metals soluble in water or slightly acidic conditions. A total of 48% of the Cr, 65% of the Cu, 36% of the Zn, and another 25% of the Pb were found in the second and third fractions together, indicating that these may leach out of the MSW-FA if the environmental conditions promote leaching (i.e., oxidizing or reducing conditions). Similar observations have been made by others (e.g., Bayuseno et al. (2009) [109]). Hence, MSW-FA should be regarded as hazardous waste due to leachable heavy metals.

There are two main strategies that may prevent negative impacts from the heavy metals typically found in MSW-FA: (1) controlled removal by acid leaching before the residual FA (or extracted Al and Si) is used in the synthesis of zeolites; and (2) solidification within the crystalline structure of the zeolite. When selecting the first strategy, it will be

important to not lose significant amounts of Al at the same time, as Al may leach out at low pHs (see Section 2.5.2). When selecting the second strategy, it is important that the heavy metals do not leach out over time when the zeolites are applied as adsorbents in those environments and that the heavy metals significantly hamper or limit the adsorption capacity or rates of the zeolites.

### Controlled Acid Leaching of Heavy Metals

Most heavy metals show increased leaching rates at low pH, making acid leaching a commonly used method to facilitate their recovery from the MSW-FA [6,12,71]. Though some of the most abundant heavy metals in MSW-FA (Pb, Zn, Cu, and Cd) are amphoteric, meaning that they are characterized by a high leaching potential under both high- and low-pH conditions but not in between [66]. However, the same is the case for Al, as discussed in Section 2.5.2 [110].

Leaching of heavy metals has been done in full scale in Switzerland since 1997 using the FLUWA process, currently treating >60% of all FA in Switzerland [111]. The process uses scrub water from wet flue gas cleaning to leach heavy metals from MSW-FA. Weibel et al. (2017) [58] showed that the main parameters controlling the mobilization of the heavy metals were pH and redox conditions, the L/S ratio, the extraction time, and temperature. The exothermic reaction between CaO in the FA and the scrub water brought the temperature in the process up to ca. 60 °C. The ideal leaching pH was determined to be  $\leq 3.8$ , but the variable buffer capacity of the FA (due to carbonates) made it challenging to control the pH with the addition of HCl (32%), particularly in a continuous process [6]. They argued that the process must be individually adjusted to the composition of the FA being processed and the scrub water used in each specific FLUWA process. The acidic FA leaching resulted in depletion factors of 40% for Zn, 53% for Cd, 8% for Pb, and 6% for Cu, with the extraction of Pb and Cu primarily limited by the cementation process and the formation of a  $\text{PbCu}^0$ -alloy-phase [58]. The addition of hydrogen peroxide ( $\text{H}_2\text{O}_2$ ; 40 L, 35% per ton FA) during the acid FA leaching (termed optimized acidic leaching) and a high L/S ratio (3.5) prevented this reduction through oxidation of the redox-sensitive metals (mainly Pb, Cu, and Cd), and thus significantly higher depletion factors for Pb (57%), Cu (30%), and Cd (92%) were achieved with an extraction time of 75 min [58].  $\text{Fe}^{2+}$  was converted into  $\text{Fe}^{3+}$ , which was precipitated as Fe-hydroxide and accumulated in the remaining filter cake. And moreover,  $\text{Al}_0$  was oxidized by  $\text{H}_2\text{O}_2$  and quickly precipitated as aluminium-hydroxide, so no  $\text{Al}_0$  was available for contact reduction of more noble dissolved metals [58]. By twerking the different parameters, as much as 60–80% Zn, 80–95% Cd, and 50–85% Pb and Cu are stated to be extracted by optimized acidic leaching [6,58,111].

The treated FA was dewatered on a vacuum belt filter, with the heavy metals being accumulated in the leachate, which can later be used for heavy metal recovery. In 2012, the FLUREC process was implemented in full scale at the MSW incineration plant in Zuchwil, Switzerland, to recover ca. 300 tons of high-purity Zn (>99.995%) from the heavy-metal-enriched filtrate from the FLUWA process [7].

The total mass loss during the optimized acid leaching was 32%, but the concomitant losses of Al and Si were 14% and 15%, respectively; hence, the overall enrichments of Al and Si were relatively marginal, from 31.8 g Al/kg to 35.9 g Al/kg (13% increase) and 69.5 g Si/L to 77.9 g/kg (12% increase). If calculated as  $\text{Al}_2\text{O}_3$  and  $\text{SiO}_2$ , these concentrations make up 6.4% and 15.6%, respectively. FA from coal-burning, which has been used extensively as an Al- and Si-source for zeolite synthesis, contains  $\text{Al}_2\text{O}_3$  and  $\text{SiO}_2$  in the ranges of 12.5–35.6% and 28.5–59.7% with mean values of 24.3% and 46.6%, respectively [112]. However, as shown in Table 1, alumina and silica contents vary considerably in MSW-FA, and with median concentrations of ca. 10.9% and 19.1% for  $\text{Al}_2\text{O}_3$ - and  $\text{SiO}_2$ , respectively, the potential concentrations after optimized acid leaching would be 12.3%  $\text{Al}_2\text{O}_3$  and 21.4%  $\text{SiO}_2$ . These values are still below the range of their contents in FA from coal burning.

### Solidification of Heavy Metals

Several studies have shown that heavy metals in MSW-FA can be stabilized by hydrothermal treatment, with significantly reduced leaching from the generated product [51,78,106,107,113–115]. Bayuseno et al. (2009) [109] compared the leaching behavior of Pb, Zn, Cu, Cr, Cd, Ni, and As in raw MSW-FA, washed MSW-FA, and their hydrothermal products by the toxicity characteristic leaching procedure (TCLP). The hydrothermal treatment (10 mL 0.5 M NaOH/g, 180 °C for 48 h) significantly reduced the concentrations of all heavy metals in the leachate from both raw and washed MSW-FA to below or close to the TCLP limits set by the US EPA. Despite significant differences in the compositions (as determined by XRD analysis) of the initial raw and washed MSW-FA, there was no significant difference between the leaching characteristics of the hydrothermal products. It was supposed that the observed reduction in mobilization of heavy metals was caused by the incorporation of metals in phases with low solubility, such as tobermorite-11 Å, katoite, and zeolitic compounds [109].

Xie et al. (2010) [114] studied the stabilization of As, Ba, Cd, Cr, Cu, Ni, Pb, and Zn by hydrothermal treatment (L/S ratio = 2, 260 °C for 1 h) using 0.1–0.5% carbohydrazide (CHZ) as a strong reducing agent (to accelerate the degradation of PCDD/Fs; see Section 2.5.5) and ferrous sulphate (5 g Fe/kg FA) as an auxiliary agent. The addition of CHZ alone seemed to interfere with the stabilization of As, Cd, Ni, and Ba, but with the combination of 0.1% CHZ and ferrous sulphate, all heavy metals were well stabilized.

With microwave-assisted hydrothermal treatment, the solidification of heavy metals is accelerated from hours to minutes [116], and with additives such as phosphates [81,82,117] and Na<sub>2</sub>S [118], the solidification has also been shown to be improved. Qiu et al. (2016) [81] found that the heavy metals (Cd, Cr, Cu, Ni, Pb, and Zn) were sufficiently solidified by the microwave-assisted hydrothermal process (200 °C for 10 min) when applying 1.5 mol NaH<sub>2</sub>PO<sub>4</sub>/kg MSW-FA (L/S ratio of 2 mL/g FA) to reach the local regulatory limits, and the pH safety range was widened from 7.5–11 to 5–13. Similarly, Xu et al. (2023) [118] found that the addition of 3 M Na<sub>2</sub>S (L/S ratio of 2 mL/g FA) to the microwave-assisted hydrothermal process (125 °C for 10 min) was enough for the leaching concentration of heavy metals to meet the same regulatory limits. The heavy metals were apparently solidified in the zeolites by adsorption and precipitation. They also noted that the cost of Na<sub>2</sub>S is lower than that of most traditional additives, such as NaOH and Na<sub>2</sub>HPO<sub>4</sub>. Moreover, large-scale use of a limited resource such as phosphate in applications that apparently render the phosphorous unavailable for further reuse or recovery is not sustainable.

It is important to notice that, since the heavy metals are solidified into the hydrothermal product and that a significant fraction of the total MSW-FA (pre-treated or not) may be lost during the hydrothermal treatment process, the specific concentrations of the heavy metals in the products may be similar or even higher than in the original MSW-FA [107]. However, as the concentrations of heavy metals in the hydrothermal liquid are likely to exceed the discharge standard, a relevant wastewater treatment system may be required [51].

### 2.5.5. Destruction of Dioxins and Furans

Dioxins and furans are highly toxic, persistent, and bioaccumulating pollutants often present in MSW-FA and must be carefully managed to limit their risk to the environment and humans [119]. Though thermal treatment at high temperatures decomposes dioxins [120], the issues of high energy consumption and flue gas treatment cannot be ignored [51]. Subcritical hydrothermal treatment (i.e., occurring below the vapor–liquid critical point of water at 374.3 °C and 22.1 MPa) can also degrade dioxins efficiently [121,122], and since the process occurs in a closed autoclave system, dioxin vapor can be prevented from diffusing into the air, posing fewer health threats to operators [51]. Jin et al. (2013), Yamaguchi et al. (1996) and Hu et al. (2012) [123–125] have shown that dioxins can be effectively degraded at 250–300 °C by hydrothermal treatment.

As discussed for the solidification of heavy metals (see Section 2.5.4), adding compounds such as methanol [124], Fentons reagent [125], Fe<sub>2</sub>(SO<sub>4</sub>)<sub>3</sub>/FeSO<sub>4</sub> [125,126], CHZ [114],

or aerating with oxygen [123] may improve the degradation of dioxins. However, the overall toxicity may increase due to the transformation into more toxic degradation by-products [114,126]. In a recent review by Chen et al. (2019) [51], they suggest, when adopting the traditional hydrothermal method to degrade dioxins, to first treat the MSW-FA directly without any additive. If the residual dioxins still exceed the standard upper limit for recycling (50 ng-TEQ/kg) after being treated at 300 °C, then the dioxin degradation efficiency may be improved by aerating with oxygen and adding alkaline substances, organic solvents, or iron salts. Microwave-assisted hydrothermal treatment with Na<sub>2</sub>HPO<sub>4</sub> has also been shown to be efficient in degrading dioxins, reaching 91.8% degradation of dioxins at 220 °C for 2 h after adding 10 wt% Na<sub>2</sub>HPO<sub>4</sub>, though the degradation of furans was less [127].

By removing the chlorine-based salts (e.g., NaCl, KCl, and CaCl<sub>2</sub>), the chance of producing dioxins and furans (PCDD/Fs) during the subsequent heat treatments will also be reduced [125,127].

#### 2.5.6. Production Efficiency and Waste Management Related to Production of Zeolites from MSW-FA

The synthesis of zeolites described herein makes use of waste that would otherwise be landfilled as hazardous waste. And, as described in Section 2.5.1, a significant fraction of the MSW-FA may also be recovered as salts for reuse. Moreover, some heavy metals may also be recovered from the FA for potential reuse. Important aspects related to reuse are discussed in more detail in Sections 5 and 6.

However, traditional synthesis strategies are often characterized by high energy consumption, low efficiency, potential water pollution, and the substantial use of expensive and environmentally unfriendly organic templates (e.g., CTAB) [128]. The organic mesoporous templates need to be removed after the hydrothermal synthesis by dissolution or calcination at high temperatures, and when using calcination, greenhouse gases and/or toxic gases are inevitably released [128]. The low concentrations of Si and Al (high L/S ratio) that are often required to compose an aqueous clear solution suitable for the successful crystallization of zeolite result in a low yield of zeolite products and require multiple recycling treatments for the excessive residual solution [128]. Moreover, the long-time need for crystallization combined with the low product yield in a batch production system results in low production efficiency [128].

So-called “green synthesis protocols” have been developed to limit these environmental impacts, and some of these have already been used to synthesize zeolites from MSW-FA as described above:

- The use of organic templates for zeolite synthesis is avoided by using Na<sub>2</sub>O [118].
- Alkali fusion is a quasi-solid-state synthesis method that uses much less water [54,65,80,83].
- The microwave-assisted methods use mild reaction conditions, have a high energy efficiency, and the crystallization rate is significantly accelerated [81–83].
- Recovery of residual SiO<sub>2</sub> from the hydrothermal synthesis process reduces waste production and can be used to modify the precursor mix and reduce the need for “external” supplements of Si [79].

More examples of “green synthesis protocols” can be found in Pan et al. (2019) [128]. Here we will mention two in particular:

- Continuous-flow synthesis: The use of a tubular reactor in a continuous-flow synthesis of zeolites makes it possible to complete the crystallization in a matter of seconds or minutes due to the large heat transfer coefficient [128]. Liu et al. (2016) [129] synthesized ZSM-5 from a well-mixed and pre-heated precursor solution containing NaOH, pure colloidal silica, aluminium hydroxide (with gibbsite structure), and tetrapropylammonium hydroxide (TPAOH) as structural agents (50 NaOH:Al<sub>2</sub>O<sub>3</sub>:300 SiO<sub>2</sub>:20 TPAOH:2300 H<sub>2</sub>O). The precursor solution was continuously fed (1 mL/min) into a millimetre-sized (Di 2.18 mm) continuous flow reactor together with pre-heated (370 °C) pressurized water (1.6 mL/min), resulting in complete crystallization within

tens of seconds. Because the actual reactor volume was quite small (15.6 mL), the continuous flow process generated a very high space–time yield (ca. 7000 kg/m<sup>3</sup>h) [129].

- Collecting generated off-gases: Gases such as ammonia and hydrogen are often generated in generous amounts during hydrothermal synthesis. López-Delgado et al. (2020) [130] developed a conceptual design that included the recovery of 76 Nm<sup>3</sup> NH<sub>3</sub> (from aluminium nitride) and 106 Nm<sup>3</sup> H<sub>2</sub> per ton of aluminium waste (77% Al<sub>2</sub>O<sub>3</sub> and 4 wt% SiO<sub>2</sub>) used in the one-step hydrothermal process (10 kg Al waste, 5.3 kg NaOH pellets, 22.9 kg waterglass, and 132 L tap water at 1 bar and 80 °C for 12 h). To avoid gas generation inside the reactor, the aluminium waste was partially hydrolyzed with water and NaOH in a separate compartment.

As a final remark, it should be noted that MSW-FA is, as has been pointed out several times, a waste product with potentially hazardous concentrations of heavy metals and organic micropollutants such as dioxins and furans and should be managed accordingly, taking all necessary measures to minimize the risk to the environment and humans handling MSW-FA.

### 3. Targeted Sorption of Cations

#### 3.1. Zeolites as Cation Exchange Resins

A wide range of zeolites, both natural and synthetic, have been used to capture different compounds in different types of matrices. Zeolites with a low Si:Al ratio will be negatively charged (and hydrophilic), and the dominant mechanism for capturing compounds will most probably be the exchange of the compensation cations (e.g., Na<sup>+</sup>, K<sup>+</sup>, Ca<sup>2+</sup>, etc.) with the target cations [13]. Hence, cations that fit well into the three-dimensional crystalline structure and show stronger affinity to the negatively charged framework are more likely to be adsorbed. A theoretical cation exchange capacity (CEC) of a zeolite can be calculated as the amount of exchangeable cations that can be accommodated by a weight unit of zeolite material using the idealized chemical formula of the zeolite and assuming all exchangeable cations are sodium. Table 4 shows the CEC range of natural and synthetic zeolites typically used in wastewater treatment, together with key structural and chemical features. According to Perego et al. (2013) [13], the CEC of natural zeolites depends on several factors, including the structure and electrostatic field strength of the framework, its cation charge density, the composition and pH of the contacting solution, the raw mineral composition and workup, as well as the process apparatus and operating conditions (e.g., continuous stirred tank vs. fixed bed column, contact time, and solid:liquid ratio) used for the measurements. Hence, comparison of reported CEC in the literature is extremely difficult and often contradictory, and the operating CEC is generally far below (till a half) the theoretical one [13].

**Table 4.** Selected natural and synthetic hydrophilic zeolites applied in wastewater effluent treatment. Framework type code (FTC); window size refers to the largest channel; Si/Al ratio range; exchangeable cations more frequently found; theoretical cation exchange capacity (CEC) range as calculated from the idealized chemical formula assuming sodium as only an exchangeable cation. Sources: [31,131–134].

Zeolite	Structure		Chemistry		
	FTC	Window Å	Si/Al mol/mol	Cation -	CEC meq/g
<i>Natural zeolites</i>					
Clinoptilolite	HEU	3.1 × 7.5	4.0–5.7	Na, K, Ca	2.0–2.6
Chabazite	CHA	3.8	1.4–4.0	Na, K, Ca	2.5–4.7
Phillipsite	PHI	3.8	1.1–3.3	Na, K, Ca	2.9–5.6
Analcime	ANA	1.6 × 4.2	1.5–2.8	Na	3.6–5.3

Table 4. Cont.

Zeolite	Structure		Chemistry		
	FTC	Window Å	Si/Al mol/mol	Cation -	CEC meq/g
Erionite	ERI	3.6 × 5.1	2.6–3.8	Na, K, Ca	2.7–3.4
Faujasite	FAU	7.4	2.1–2.8	Na, K, Mg	3.0–3.4
Ferrierite	FER	4.2 × 5.4	4.9–5.7	Ca	2.1–2.3
Heulandite	HEU	3.1 × 7.5	4.0–6.2	Na, K, Ca, Sr	2.2–2.5
Laumontite	LAU	6.5 × 7.0	1.9–2.4	Na, K, Mg	3.8–4.3
<i>Synthetic zeolites</i>					
X	FAU	7.4	1.0–1.5	-	2.7–6.0
Y	FAU	7.4	<3	-	3.9
Mordenite <sup>1</sup>	MOR	6.5 × 7.0	4.0–5.7	Na, K, Ca	2.0–2.4
A	LTA	4.1 × 4.5	1.0–3.2	-	3.9–5.3
NaP1	GIS	2.9	1.7–3.9	-	2.0

Note: <sup>1</sup> Mordenite is a natural zeolite, but the synthetic version of the zeolite is more commonly use.

A summary of the factors that determine the cation selectivity of the zeolites and their adsorption rates and capacities is provided below.

### 3.2. Sorption Mechanisms

Adsorption is a surface phenomenon in which the adsorbate (i.e., cation) transfers onto the adsorbent (i.e., zeolite). The main adsorption mechanisms are chemisorption (involving strong covalent bonding), physisorption (involving weak van der Waals forces), and electrostatic interaction (involving attraction between ions or molecules with full permanent charges of opposite signs) [135]. For the latter to occur, an ion exchange with the already-present compensation ions (or counterions) needs to occur. Both physisorption and electrostatic interactions may govern the adsorption of cationic materials to zeolites, but the latter is generally believed to be the most important [136].

For a cation to be adsorbed to a particular site on a zeolite, it first needs to travel by diffusion from the bulk liquid phase through the stagnant liquid film layer outside the zeolite surface. The concentration gradient over the stagnant film governs the driving force; higher bulk concentrations give faster diffusion. As most of the surface of the zeolite is within its porous structure, the cation needs to fit into these pores and diffuse through the interior voids of the crystalline structure of the zeolite. For the electrostatic interaction to be active, the cation needs to exchange places with the existing compensation ion; hence, the electrostatic force between the cation and the anionic charge of the zeolite surface needs to be stronger than that between the surface and the compensation ion. In many cases, particularly for heavy metals, the cations are divalent (e.g., Pb<sup>2+</sup>, Cu<sup>2+</sup>, Zn<sup>2+</sup>, Cd<sup>2+</sup>, Ni<sup>2+</sup>), while the compensation ions are monovalent (e.g., K<sup>+</sup>, Na<sup>+</sup>), and therefore two compensation ions need to be exchanged for the cation to take its place [132,135]. Though the opposite can also be the case, Lin et al. (2015) [137] measured the adsorption rate of ammonium (NH<sub>4</sub><sup>+</sup>) in swine manure by a calcium-rich chabazite and argued that the diffusion rate of Ca<sup>2+</sup> for the exchange with NH<sub>4</sub><sup>+</sup> was the rate-limiting step in the adsorption as compared to the exchange between Na<sup>+</sup> and NH<sub>4</sub><sup>+</sup>.

#### 3.2.1. Adsorption of Heavy Metals

As summarized by de Magalhães et al. (2022) [132], the reported sorption kinetics of heavy metals such as Pb<sup>2+</sup>, Cd<sup>2+</sup>, Cr<sup>3+</sup>, Ni<sup>2+</sup>, Zn<sup>2+</sup>, Cu<sup>2+</sup>, As<sup>5+</sup>, and Cr<sup>6+</sup> by zeolites with

low Si/Al ratios (i.e., strongly negatively charged) all seem to be satisfactorily fitted by a pseudo-second-order kinetic model given by the general model equation [138]:

$$t/q_t = 1/k_2 q_e^2 + t/q_e, \quad (1)$$

where  $k_2$  is the pseudo-second-order rate constant of adsorption (g/mg·min);  $q_e$  and  $q_t$  are the amount of metal ions adsorbed (mg/g) at equilibrium and at time  $t$ , respectively;  $t$  is adsorption time (min). The initial sorption rate is given by  $h = k_2 q_e^2$ .

However, de Magalhães (et al. (2022) [132] argued that the intraparticle diffusion model, which assumes that the diffusion of the adsorbate into the pores of the adsorbate is the rate-limiting step in the adsorption process, would make a more appropriate model:

$$q_t = k_i t^{1/2}, \quad (2)$$

where  $k_i$  is the intraparticle diffusion constant (mg/g·h<sup>0.5</sup>) and  $t$  is the time in hours.

Empirical models such as the pseudo-second-order kinetic model cannot explain the adsorption mechanism [132]. The adsorption isotherm models, however, can do that based on the amount of adsorbate at the adsorbent surface and the concentration of the adsorbate in the liquid phase at a constant temperature. They can also be used to estimate the maximum adsorption capacity (mg/g). Two of the most commonly adopted models to represent adsorption isotherms are the Langmuir and Freundlich models [132]. The Langmuir model [139], which assumes a uniform distribution in a monolayer on the adsorbent surface that is also structurally and energetically homogeneous, takes the following form [138]:

$$C_e/q_e = 1/K_L q_{\max} + C_e/q_{\max}, \quad (3)$$

where  $C_e$  is the equilibrium concentration of heavy metals in solution (mg/L),  $q_e$  is the amount adsorbed at equilibrium (mg/g),  $K_L$  is the Langmuir constant (L/g), and  $q_{\max}$  is the maximum adsorption capacity (mg/g). The Freundlich model [140], which assumes multilayer adsorption on a heterogeneous surface of the adsorbent, can be expressed by [141]:

$$q_e = K_f C_e^{1/n}, \quad (4)$$

where  $K_f$  is the empirical constant of the Freundlich isotherm and  $n$  is the empirical parameter related to the intensity of the adsorption that depends on the heterogeneity of the material. If  $1/n$  is between 0.1 and 1, the adsorption process is favorable.

According to the summary made by de Magalhães et al. (2022) [132], for most of the reported zeolites (except scolecite), the adsorption of the above-mentioned heavy metals (Pb<sup>2+</sup>, Cd<sup>2+</sup>, Cr<sup>3+</sup>, Ni<sup>2+</sup>, Zn<sup>2+</sup>, Cu<sup>2+</sup>, As<sup>5+</sup>, and Cr<sup>6+</sup>) all seem to be well described by the Langmuir isotherm, hence indicating that a monolayer of heavy metal ions is adsorbed to the surface of the zeolites. However, Sprynskyy et al. (2006) [142] reported a better fit with the Freundlich isotherm at high metal concentrations when adsorbing Pb<sup>2+</sup>, Cu<sup>2+</sup>, Ni<sup>2+</sup>, and Cd<sup>2+</sup> on clinoptilolite, hence indicating more heterogenic adsorption coverage.

### 3.2.2. Adsorption of Ammonium

Most studies appear to report good agreement between adsorption rates of ammonium by most zeolites and pseudo-second-order kinetics [132,143–146] under appropriate pH conditions (see Section 3.3.7). Though some studies report good agreement with the Langmuir isotherm for the adsorption of ammonium by natural zeolites [137,144,147,148], most studies have found that the Freundlich isotherm gave the best fit, indicating that the adsorption process occurred on a heterogeneous surface [132,141,143,145,146,149]. Zhang et al. (2011) [146] found that the Langmuir isotherm gave the best fit for zeolites synthesized from low-calcium FA, while the Freundlich isotherm gave the best fit for zeolites synthesized from high-calcium FA.

Table 5 summarizes the apparent adsorption capacities reported for some different types of synthetic and natural zeolites. There are very large differences in the reported

adsorption capacities, but there is no clear correlation between the observed adsorption capacities and the type of zeolite, probably due to the many factors influencing the measured adsorption capacity, as will be outlined in more detail in the following.

**Table 5.** Reported apparent sorption capacity of ammonium ( $\text{NH}_4^+$ ) to different types of zeolites, natural or synthetic. The list is arranged according to decreasing adsorption capacities. Si/Al in the final zeolite product; BET = Brunauer–Emmett–Teller specific surface area; CEC = cation exchange capacity; N.S.: not specified.

Zeolite	Source	Si/Al mol/mol	BET $\text{m}^2/\text{g}$	$\text{NH}_4^+$ Adsorption mg $\text{NH}_4/\text{g}$	CEC meq/g	References
Magnetic clinoptilolite	Natural	N.S.	43.1	172	N.S.	[150]
Na-A	Natural	N.S.	430	116	N.S.	[151]
Mechanically activated clinoptilolite	Natural	N.S.	258	109	N.S.	[151]
NaP1	Coal FA	2.7	56.9	34.5	2.56	[126]
X, some A, P, and hydroxysodalite	Low-Ca coal FA	6.0	27.0	23.8	2.79	[146]
P1	Coal FA	3.5	18.5	22.9	N.S.	[148]
NaOH-treated zeolite Australia	Natural	N.S.	N.S.	19.5–20.0	N.S.	[141]
Clinoptilolite-Ca/-Na, Stilbite-Ca	Natural	2.9	25.8	17.0	N.S.	[149]
Sodalite	Coal FA	N.S.	15.5	16.0	2.92	[145]
NaP1, some analcime, chabazite	Coal FA	N.S.	N.S.	13.7	N.S.	[152]
Zeolite Australia as received	Natural	9.8	N.S.	8.6	N.S.	[141]
Na-X	Coal FA	1.12	165	5.0	18	[153]
NaP1/ $\text{Fe}_2\text{O}_3$	Coal FA	2.8	162	4.5	1.54	[154]
Gismondine	High Ca coal FA	4.7	45.5	3.2	0.69	[146]

### 3.3. Factors Affecting the Sorption of Cations

As indicated above, there are many factors that influence both the sorption rate of a cation and the sorption capacity of the zeolite. The most important ones are discussed briefly in the following.

#### 3.3.1. Framework Type vs. Size of the Cation

The framework type of each zeolite determines the dimensions of its internal pores and channels, as illustrated in Figure 1. Table 4 gives the size of the largest channel in some framework types occurring in zeolites used in effluent treatment. These vary from up to 7.5 Å, 7.0 Å, and 7.0 Å in HEU, MOR, and LAU, respectively, to 2.9 Å, 3.8 Å, and 3.8 Å in GIS, CHA, and PHI, respectively. The actual size of the cation is dependent on to what degree it is hydrated. Table 6 shows the radii of selected ions when they are unhydrated and when they are fully hydrated. Looking at the heavy metals, the sizes of the fully hydrated ions rank them from smallest to largest:  $\text{Pb}^{2+} < \text{Ni}^{2+} < \text{Cu}^{2+} < \text{Cd}^{2+} < \text{Zn}^{2+} < \text{Cr}^{3+}$ , with  $\text{Pb}^{2+}$  being the smallest with an assumed maximum diameter of 8.02 Å. This is larger than the largest size of the channels in the framework.

Table 6 also shows the free energy of hydration ( $\Delta\text{hydG}$ ), which quantifies the amount of energy that is released when an ion is hydrated. The ions with the highest  $\Delta\text{hydG}$  should prefer to remain in the solution phase [155]. To be able to pass through the pores/channels of the zeolite, the ions need to release some of the water molecules; hence, the ranking of the cations related to how easily they will do this is:  $\text{Pb}^{2+} < \text{Cd}^{2+} < \text{Zn}^{2+} < \text{Ni}^{2+} < \text{Cu}^{2+} < \text{Cr}^{3+}$ .

Table 7 summarizes the ranking results from several adsorption studies that have included multiple heavy metals in each test. As can be seen,  $\text{Pb}^{2+}$  ranks at the top in all studies. However,  $\text{Cr}^{3+}$ , which has the largest hydration radius and is the ion that is most

resistant to dehydration, ranked at the top or highest in several of the studies. Ref. [155] postulated that this was due to the precipitation of  $\text{Cr}^{3+}$  (and  $\text{Cu}^{2+}$ ) as metal hydroxides on the surface of the zeolite (4A) or inside the pore walls. A similar observation was reported by [156] on the adsorption of  $\text{Cu}^{2+}$  and  $\text{Cr}^{3+}$  ions on NaP1.

Synthetic zeolites are usually made to have larger cavities (i.e., a lower framework density) to facilitate transport into the zeolite [8]. Synthetic zeolites with larger pore openings, such as zeolites X and A, showed the highest removal capacity for  $\text{NH}_4^+$ .

**Table 6.** Unhydrated and hydrated radius and free energy of hydration ( $\Delta_{\text{hyd}}G$ ) of selected ions [157,158].

Ion	Unhydrated Radius	Hydrated Radius	$\Delta_{\text{hyd}}G$ kJ/mol	Ion	Unhydrated Radius	Hydrated Radius	$\Delta_{\text{hyd}}G$ kJ/mol
	Å	Å			Å	Å	
$\text{Li}^+$	0.60	3.82	−475	$\text{Cu}^{2+}$	0.72	4.19	−2010
$\text{Na}^+$	0.95	3.58	−365	$\text{Zn}^{2+}$	0.74	4.30	−1955
$\text{K}^+$	1.33	3.31	−295	$\text{Cd}^{2+}$	0.97	4.26	−1755
$\text{Ca}^{2+}$	0.99	4.12	−1505	$\text{Pb}^{2+}$	1.32	4.01	−1425
$\text{NH}_4^+$	1.48	3.31	−285	$\text{Cr}^{3+}$	0.64	4.61	−4010
$\text{NO}_3^-$	2.64	3.35	−300	$\text{Ni}^{2+}$	0.70	4.04	−1980
$\text{H}_2\text{PO}_4^-$	-	2.6	-				
$\text{PO}_4^{3-}$	-	7.9 <sup>1</sup>	−2765				

Note: <sup>1</sup> Stokes radius.

**Table 7.** Selectivity in competitive adsorption of heavy metals by different zeolites.

Zeolite	Origin	Si/Al	Selectivity	References
<i>Synthetic zeolites</i>				
FAU-type	Coal FA	2.5	$\text{Pb}^{2+} > \text{Cu}^{2+} > \text{Cd}^{2+} > \text{Zn}^{2+} > \text{Co}^{2+}$	[159]
NaP1	Coal FA	1.7	$\text{Cr}^{3+} > \text{Cu}^{2+} > \text{Zn}^{2+} > \text{Cd}^{2+} > \text{Ni}^{2+}$	[156]
4A	Coal FA	1.32	$\text{Cu}^{2+} > \text{Cr}^{3+} > \text{Zn}^{2+} > \text{Co}^{2+} > \text{Ni}^{2+}$	[155]
X	Egyptian kaolin and $\text{Na}_2\text{Si}_2\text{O}_5$	1.15	$\text{Pb}^{2+} > \text{Cd}^{2+} > \text{Cu}^{2+} > \text{Zn}^{2+} > \text{Ni}^{2+}$	[160]
A	Egyptian kaolin and $\text{Na}_2\text{Si}_2\text{O}_5$	1.04	$\text{Pb}^{2+} > \text{Cd}^{2+} > \text{Cu}^{2+} > \text{Zn}^{2+} > \text{Ni}^{2+}$	[160]
<i>Natural zeolites</i>				
Mordenite	Natural	4.4–5.5	$\text{Cu}^{2+} > \text{Co}^{2+} \approx \text{Zn}^{2+} > \text{Ni}^{2+}$	[161]
Clinoptilolite	Natural	4.9	$\text{Pb}^{2+} > \text{Zn}^{2+} > \text{Cu}^{2+} > \text{Ni}^{2+}$	[162]
Clinoptilolite	Natural	4.8	$\text{Cu}^{2+} > \text{Cr}^{3+} > \text{Zn}^{2+} > \text{Cd}^{2+} > \text{Ni}^{2+}$	[156]
Clinoptilolite	Natural	4.2	$\text{Pb}^{2+} > \text{Cd}^{2+} > \text{Zn}^{2+} \approx \text{Cu}^{2+}$	[163]
Clinoptilolite	Natural	2.7–5.3	$\text{Pb}^{2+} > \text{Ag}^+ > \text{Cd}^{2+} \approx \text{Zn}^{2+} > \text{Cu}^{2+}$	[161]
Phillipsite	Natural	2.4–2.7	$\text{Pb}^{2+} > \text{Cd}^{2+} > \text{Zn}^{2+} > \text{Co}^{2+}$	[163]
Chabazite	Natural	2.2–2.6	$\text{Pb}^{2+} > \text{Cd}^{2+} > \text{Cu}^{2+} > \text{Zn}^{2+} > \text{Co}^{2+}$	[163]
Scolecite	Natural	1.56	$\text{Cu}^{2+} > \text{Zn}^{2+} > \text{Pb}^{2+} > \text{Ni}^{2+} > \text{Co}^{2+} > \text{Co}^{2+}$	[164]

### 3.3.2. Cation Concentration and Competing Ions

As already mentioned, higher bulk concentrations cause faster diffusion as the gradient gets steeper. However, studies with natural zeolites from Australia and the USA have reported that the adsorption capacity of ammonium could be increased by 35–60% (up to 10–13 g  $\text{NH}_4^+$ /kg zeolite) by increasing the bulk concentration from 250 mg/L to 1000 mg/L [141] or by 230% (up to 13 g  $\text{NH}_4^+$ /kg zeolite) by increasing the concentration

from 50 mg/L to 800 mg/L [165], respectively. However, Lind et al. (2000) [166] reported equilibrium uptake of ammonium (ca. 40% adsorbed) by 20 g/L clinoptilolite (grain size of 71–125  $\mu\text{m}$ ) from a 1 M  $\text{NH}_4\text{Cl}$  solution (18 g  $\text{NH}_4^+$ /L) after just a few minutes of contact time, indicating an extreme adsorption capacity of 360 g N/kg zeolite (our calculations). Under normal conditions, there will often be several ions that compete for the adsorption sites on and in the zeolite. Besides the size of the ions compared to the cavities within the three-dimensional crystalline structure explained above, the concentrations of the competing ions impact the competition. These competing ions may, at least when considering the adsorption of  $\text{NH}_4^+$ , also be typical compensation ions such as  $\text{Na}^+$ ,  $\text{K}^+$ ,  $\text{Ca}^{2+}$ , and  $\text{Mg}^{2+}$ , as well as anions such as  $\text{NO}_3^-$ ,  $\text{SO}_4^{2-}$ , and  $\text{Cl}^-$  [97,167]. Furthermore, at low pH, the competition from  $\text{H}^+$  increases significantly [168].

### 3.3.3. Purity of the Zeolite

Natural zeolites will usually contain a variety of other minerals that may act as contaminants as they have no or low sorption capacity. Such minerals that are frequently found are quartz, albite, biotite, illite, montmorillonite, feldspar, calcite, halite, and heulandite [156,169,170]. Synthetic zeolites, however, usually contain a single framework type, giving them high uniformity.

### 3.3.4. Hydrophilicity/Hydrophobicity

Zeolites with low Si/Al ratios (e.g., zeolites A, X, and Y and natural zeolites in general) have a strong electrostatic field within their cavities, resulting in very strong interactions with polar molecules. By increasing the Si/Al ratio, the zeolite can be tuned to be more hydrophobic. This is beneficial when adsorbing non-polar compounds [132]. In other words, high silica zeolites tend to prefer cations with low charge density (large and monovalent), while low silica zeolites prefer cations with high charge density (small and multivalent) [171].

### 3.3.5. Compensation Cations

Natural zeolites will usually have more than one type of compensation cation in their crystalline structure. Modification of the zeolite with a solution of inorganic salts such as  $\text{NaCl}$ ,  $\text{CaCl}_2$ ,  $\text{NH}_4\text{Cl}$ , etc. will contribute to uniform compensation cations and thereby potentially optimize the cation exchange capacity [172]. For instance, Haji et al. (2016) [173] found that the removal of  $\text{NH}_4^+$  by zeolite Y was significantly better using  $\text{Na}^+$  as a compensation ion (92%) than with  $\text{Cs}^+$  (24.8%),  $\text{K}^+$  (24.3%),  $\text{Mg}^{2+}$  (18.5%), and  $\text{Ca}^{2+}$  (18.5%). Moreover, the effective dimensions of the pores of a given zeolite structure can be modulated by the appropriate choice of the extra-framework cations located within the pores to balance the negative framework charge (see also Figure 1) [174]. It has been shown that following dehydration and subsequent heat treatment of the zeolite, salt molecules with anions of up to two times the size of the  $\text{O}_6$ -ring's "free" opening of the sodalite-cage structural units are occluded in these cages [175].

### 3.3.6. Available Adsorption Surface and Size of the Zeolite Particles

The adsorption efficiency of an adsorbent is proportional to its specific surface area, defined as the total surface area available for adsorption. This area is dependent on the sizes of the zeolite particles, the pore size distribution, and surface roughness [176]. Smaller particles have larger specific surface areas per volume than larger particles. Due to their higher degree of crystalline ordering, compared to natural zeolites, synthesized zeolites have a greater specific surface area, which increases their efficiency as adsorbents [132].

Even if the availability of active sites is almost constant for both large and small particles, the accessibility of metal ions to adsorption sites is higher when the adsorbent consists of smaller particles because of the shorter diffusion paths for ions [177]. Hence, a smaller particle is expected to enhance the adsorption. The internal surface area is more

important than the external surface area in porous materials. Hence, changes on the external surface associated with grain size have very little effect on the adsorption efficiency [178].

By using more zeolite, the overall surface area will, of course, also increase.

### 3.3.7. pH

The pH affects both the surface charge (i.e., hydrophilicity) of the zeolite and the cationic character of the adsorbates; hence, it is important to control the pH both to optimize the adsorption rate of specific compounds and to maximize the adsorption capacity. In general, at higher pHs, the zeolite gets more negatively charged, but the adsorbates may lose their cationic character and be more neutrally charged or anionic. Apparently, most zeolites have points of zero charge (PZC) at a pH near neutral [132], though all PZCs of zeolites and other aluminosilicates reported by Kosmulski (2018,2020) [179,180] were typically <3. Kosmulski (2020) [180] argued also that often PZC was measured using methods that produced unreliable results (e.g., mass titration), but that this was less of a problem for metal oxides. Anyway, for zeolites to be negatively charged, the pH should be kept above their PZC. Hence, their PZC needs to be determined properly [180].

At increasing pH, heavy metals tend to precipitate as metal oxides and hydroxides, depending on their solubilities, thereby limiting their possibility of being adsorbed. This occurs at highly different pHs for the different metals, as indicated in Figure 4 by the theoretical hydroxide precipitation diagram based on the solubility constants ( $K_{S0}$ ) of the different metal hydroxides at 25 °C [181]:

$$\text{pH} = (\log K_{S0} - n \log K_w - \log [1])/n, \quad (5)$$

where  $M^{(n+)}$  is the molar activity (or equilibrium concentration) of the metal ion with valence  $n$ , while  $K_w$  is the dissociation constant of water. The diagram says that above a given metal concentration and pH, the metal hydroxide will precipitate out of solution. As this occurs at very different concentrations for different heavy metals, it has been used extensively in the separation of different metals in hydrometallurgical processes [181]. Note that at higher metal concentrations, the precipitation starts at a lower pH. However, the precipitation behavior is also very dependent on the presence of other anions such as carbonate, sulphate, and phosphate that can contribute to the precipitation of metal ions [181].

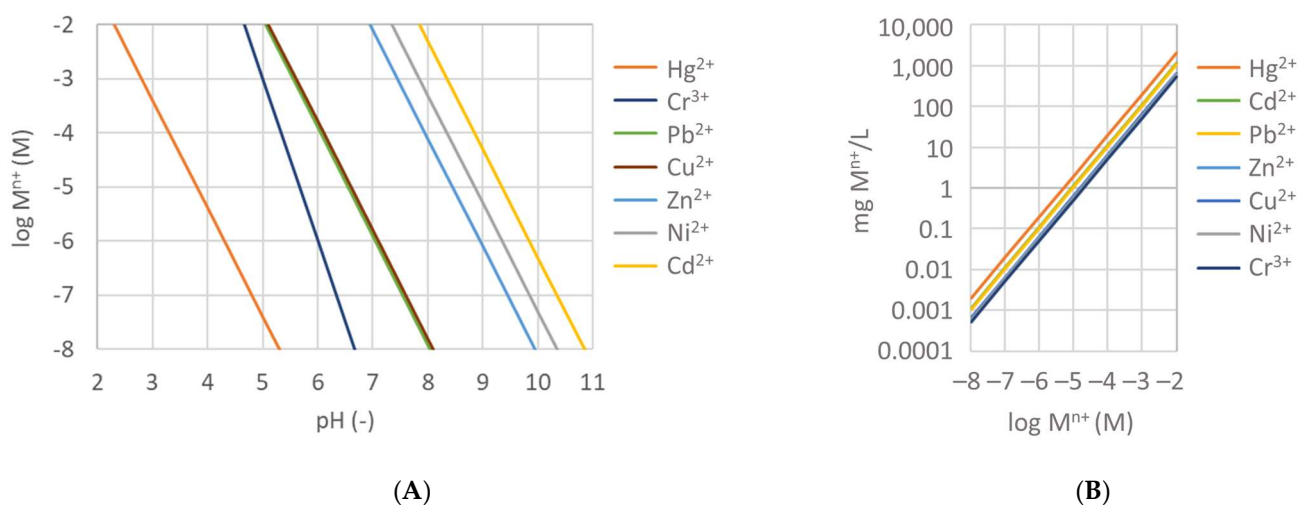


**Figure 4.** (A): Theoretical hydroxide precipitation diagram of selected heavy metals at pH 1–10 based on their respective metal hydroxide solubilities at 25 °C. To the left of each line, the hydroxide is still in solution, while to the right, it is expected to precipitate. Based on Monhemius (1977) [181]. (B): Calculated relationships between metal ion concentrations in molar (M) and mg/L within the concentration range used on the left side.

Also, the adsorption of ammonium ( $\text{NH}_4^+$ ) is strongly influenced by pH, as at high pH,  $\text{NH}_4^+$  is converted into ammonia ( $\text{NH}_3$ ) (pKa of 9.24), which will not have any affinity for hydrophilic zeolites due to the lack of any electrostatic attraction [132].

### 3.3.8. Temperature

An increase in temperature leads to changes in both process kinetics and equilibrium, including an increased diffusion rate, increased kinetic energy resulting in greater access of metal ions to adsorption sites, increased activity on the surface of the adsorbent resulting in greater affinity, and a decrease in mass transfer resistance [177]. The temperature may also expand the crystalline structure itself, thereby increasing the accessibility of the adsorbate to the interior of the zeolite. Furthermore, an increase in temperature is associated with a decrease in the thickness of the boundary layer surrounding the adsorbent (reduced hydration), such that the mass transfer resistance of the adsorbate decreases, which facilitates the diffusion of metals in the adsorbent. However, the electrostatic interactions are weaker at higher temperatures [177].

### 3.3.9. Contact Time

The adsorption process is quicker when the adsorbate concentration is high and/or when there is more space available for sorption on the zeolite. Hence, an increase in contact time allows reaching closer to equilibrium conditions and, hence, full utilization of the adsorption capacity. However, an increased contact time reduces the overall process efficiency as the adsorption rate is drastically reduced with time, requiring long retention/contact times. In a continuous filtration process, the contact time is given by the flow rate and liquid bed volume, and when the necessary exposure time to get additional adsorption is exceeded, there will be a breakthrough of the filter.

## 4. Sorption of Nitrate and Phosphate Using Zeolites

Anions such as nitrate ( $\text{NO}_3^-$ ) and phosphate ( $\text{H}_2\text{PO}_4^-$ ,  $\text{HPO}_4^{2-}$ , and  $\text{PO}_4^{3-}$ ) will not be efficiently captured by the hydrophilic zeolites described above as they will be repelled by the electrostatic forces otherwise attracting the cations, though zeolites derived from coal-FA have been shown to adsorb phosphate moderately well [182–184]. Moreover, increasing the Si/Al ratio to make the zeolite more hydrophobic is not very useful either since zeolites need to be modified to be able to adsorb these anions. Two different strategies can be used to modify zeolites:

1. Lowering the pH to make the zeolite cationic
2. Modifying the surface of the zeolite by cationic metal-doping or using surfactants.

### 4.1. pH-Derived Cationic Zeolites

The zeolite needs to be predominantly positively charged to be cationic. This may only occur at pHs below its PZC. As described above in Section 3.3.7, the actual PZC may, however, be challenging to measure correctly.

Phosphoric acid ( $\text{H}_3\text{PO}_4$ ) is a triprotic acid with three dissociation constants:  $\text{pKa},1 = 2.13$  (to  $\text{H}_2\text{PO}_4^-$ ),  $\text{pKa},2 = 7.20$  (to  $\text{HPO}_4^{2-}$ ), and  $\text{pKa},3 = 12.36$  (to  $\text{PO}_4^{3-}$ ) [185]. The ratio of the four different phosphate compounds is determined by the pH of the solution, as depicted in Figure 5. As shown in Table 6, the Stokes radius of  $\text{PO}_4^{3-}$  (7.9 Å) is very much larger than the hydrated radius of  $\text{H}_2\text{PO}_4^-$  (2.6 Å), hence  $\text{H}_2\text{PO}_4^-$  is more likely to penetrate the micropores of the zeolites.

Relatively few studies have apparently been conducted that have tried to adsorb phosphate to pH-derived cationic zeolites (see Table 8). However, Hamdi and Srasra (2012) [186] reported an adsorption capacity of 52.9 mg P/g for a synthetic zeolite A from purified clay T just by lowering the pH to 4–5. The zeolite had a measured PZC of 5.5. [184] reported efficient removal of phosphate at pHs between 3.5 and 9 when testing 15 different coal ash-derived zeolites. The zeolites were not metal-doped (see Section 4.2.1), but had variable levels of  $\text{Ca}^{2+}$ ,  $\text{Mg}^{2+}$ ,  $\text{Al}^{3+}$ , and  $\text{Fe}^{2+}$  in their framework due to their different

origins. The good removal at high pH (5.5–9) was attributed to the precipitation of calcium phosphate due to the  $\text{Ca}^{2+}$ -rich zeolite that was used. At acidic conditions (pH 3.5–5.5), the observed immobilization of phosphate was assumed to be due to the adsorption of  $\text{Fe}_2\text{O}_3$  through ligand exchange. Zhang et al. (2007) [104] treated a coal ash-derived zeolite with a low-concentrated (0.01 M)  $\text{H}_2\text{SO}_4$  solution that lowered the equilibrium pH of the zeolite to <10.5. This resulted in efficient removal of both  $\text{NH}_4^+$  and phosphate over the whole concentration range from 0.5 mg P/L to ca. 500 mg P/L with a S/L ratio of 10 g/L for 24 h. The formation of calcium phosphate precipitates was assumed to be the predominant mechanism for phosphate removal.

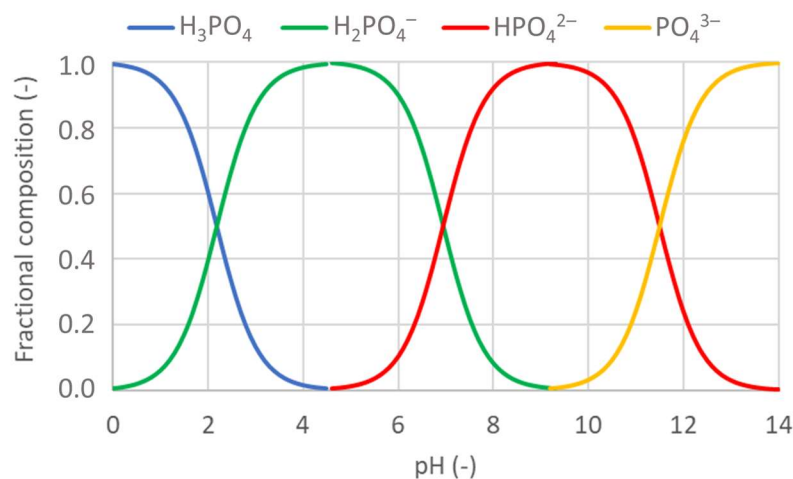


**Figure 5.** Fractional composition of different phosphate compounds depending on the pH. Based on the dissociation constants of phosphoric acid [185].

By decreasing the pH to <2, the dominant phosphate fraction will be  $\text{H}_3\text{PO}_4$ , which is uncharged (see Figure 5). At this low pH, zeolites are very likely to be neutral or positively charged [180]. Zhang et al. (2014) [187] demonstrated that it was possible to adsorb phosphate (as  $\text{H}_3\text{PO}_4$  and/or  $\text{H}_2\text{PO}_4^-$ ) at pH < 2. However, this requires considerable amounts of acid for pH adjustments and, subsequently, a potential equivalent amount of base to compensate for the low pH prior to release.

In theory, it should be possible to adsorb nitrate to positively charged zeolites, as has been documented for phosphorous (see above). Nitrate is 100% negatively charged at pH > 1.0 ( $\text{pK}_a = -1.37$ ), and its hydrated radius is close to that of  $\text{NH}_4^+$  and  $\text{K}^+$  (see Table 4). To the best of our knowledge, there have been no studies so far documenting the removal of nitrate by non-modified zeolites.

**Table 8.** Reported apparent sorption capacity of phosphate for non-modified and modified zeolites with test conditions (phosphate concentration range, S/L ratio, contact time, and temperature) and pH at optimum adsorption.

Zeolite	App. Sorption Capacity mg/g	Conc. Range mg P/L	S/L Ratio g/L	Contact Time h	Temp. °C	pH -	Ref.
<i>Non-modified zeolites</i>							
NaP1	11.4						
NaA	15.7	12.5–200	1	24	25	5.3	[182]
Clinoptilolite	20.2						
A	52.9	50–1000	6.6	4	70	5.5	[186]

Table 8. Cont.

Zeolite	App. Sorption Capacity	Conc. Range	S/L Ratio	Contact Time	Temp.	pH	Ref.
	mg/g	mg P/L	g/L	h	°C	-	
Clinoptilolite	1.3	10–100	48	2	25	2	[188]
Zeolite from coal-FA	11.7–42.4	1000	10	24	room	3.5–9	[184]
Clinoptilolite	0.77	0.03–3.1	8	24	room	3.0	[189]
NaP1-zeolite from coal-FA	34.7	0.5–1000	10	24	18–22	-	[183]
<i>Salt-modified zeolites</i>							
LaP1	58.2						
LaA	48.9	12.5–200	1	24	25	5.3	[182]
La-clinoptilolite	25.5						
TiO <sub>2</sub> -modified clinoptilolite	34.2	10–100	20	2	25	2	[188]
Ca-bearing K-zeolite	142–250	100–16,000	16.7	0.8–2.2	22	6–9	[190]
Zr oxide merlinoite	67.7	5–200	0.2–2	4	40	<5	[191]
CaP1-zeolite from coal-FA	49.5						
MgP1-zeolite from coal-FA	31.3						
AlP1-zeolite from coal-FA	29.9	0.5–1000	10	24	18–22	-	[183]
FeP1-zeolite from coal-FA	30.9						
Cu-zeolite X	87.7	10–200	1	24	25	5.0	[192]
<i>Surfactant-modified zeolites</i>							
HDTMA-Br clinoptilolite	20.9	0.03–3.1	8	24	room	12.0	[189]
HDP-Br clinoptilolite	11.6						

#### 4.2. Modification of Zeolites

The dominant method to increase the adsorption rate and capacity of anionic (and hydrophobic) compounds in zeolites has been to prepare modified zeolites. Two main methods have been used to modify the zeolites: metal doping and cationic surfactants, as discussed below.

##### 4.2.1. Metal-Doped Zeolites

Transition metal cations or oxides are doped into the zeolite framework, typically using oxides of lanthanides, aluminium, or zirconium to optimize the adsorption of anions [182,188,191]. The charge properties of the modified zeolites depend both on the kind of modifier and the conditions of preparation (temperature, amount of modifier) [191,193]. Calcination at rather high temperatures (200–800 °C) is frequently applied [194].

##### 4.2.2. Surfactant-Modified Zeolites (SMZs)

A cationic surfactant is used to create a hydrophobic monolayer (targeting hydrophobic compounds) or a cationic bilayer (targeting anions) on the external surface of the zeolite. Surfactants such as quaternary ammonium, sulphonium, arsonium, phosphonium, or idonium have typically been used [195–197].

Hexadecyltrimethylammonium (HDTMA) is a long-chain quaternary ammonium surfactant that has been widely used as a surfactant for generation SMZs. The large head group of the HDTMA molecule (three of the protons in NH<sub>4</sub><sup>+</sup> are replaced by three methyl groups, while the fourth is replaced by the long tail group) makes it too large to enter the zeolite channels for internal sorption sites, and the sorption of HDTMA is therefore limited to external cation-exchange sites on the zeolite surface [198]. The process of generating first

a monolayer and then a bilayer of the surfactant on the zeolite is illustrated in Figure 6, and a more detailed description is given in the figure text. It is important to note that a bilayer of the surfactant is needed for efficient adsorption of anions to the external surface of the SMZ by ion exchange, while hydrophobic compounds may still be adsorbed within the solvent-like hydrophobic bilayer [196,198,199]. According to Bowman (2003) [199], even cations still have access to the microporous structure of the zeolite despite the bilayer surrounding the zeolite. However, it has been challenging to find solid documentation that supports this statement or documentation of how much they are affected by this bilayer, first by the electrostatic repulsion exerted by the cationic heads of the surfactant and then by the hydrophobic region within the bilayer. A study by Baez-Alvarado and Olguín (2011) [200] indicates that some reduced adsorption capacity and rate can be expected. Though the adsorption of phosphate and nitrate to SMZs has been well documented, as summarized below:

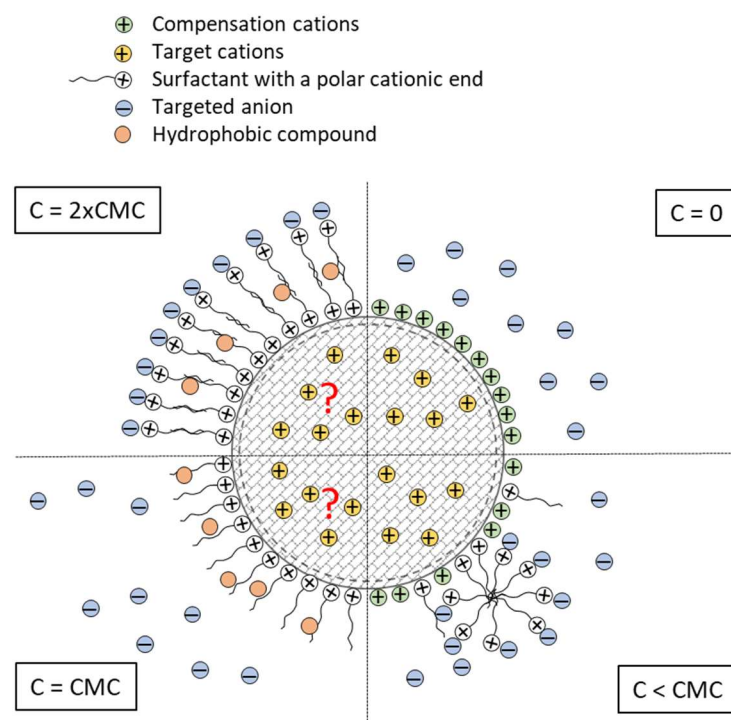


**Figure 6.** Illustration of the stepwise generation of a surface-modified zeolite using a surfactant:  $C = 0$ : the zeolite prior to any addition of surfactant attracting targeted cations that primarily adsorb to the micropore structure;  $C < CMC$ : the surfactant forms micelles that start adhering to the surface of the zeolite, replacing external compensation cations. When more surfactant molecules attach to the surface and the critical micelle concentration has been passed, breaking up the micelle, the surfactants spread out on the surface [198].  $C = CMC$ : Just enough surfactant has been added to create a monolayer of surfactants on the surface of the zeolite, held in place by electrostatic interaction between the negative surface charge of the zeolite and the positively charged end of the surfactant [196]. The hydrophobic tail of the surfactant attracts hydrophobic compounds in the water;  $C > CMC$ : a bilayer of the surfactant is evolving, driven by the hydrophobic affinity between surfactant tail groups, and eventually forms a fully saturated bilayer. The original net negative charge of the zeolite has been reversed to a net positive charge, attracting target anions in the water phase. Hydrophobic compounds are still attracted to the hydrophobic region within the bilayer [198,199], and according to Bowman (2003) [199], targeted cations still have access to the microporous structure, though a somewhat reduced adsorption capacity and adsorption rate can be expected (as indicated by red question marks) [200].

#### 4.2.3. Adsorption of Phosphate by Modified Zeolites

The majority of studies have been assessing the effect of metal-doped zeolites on the adsorption of phosphate, with very few using surfactant-modified zeolites. Some literature-reported studies are briefly summarized in Table 8 and briefly described below.

##### Results with Metal-Doped Zeolites

Wu et al. (2006) [183] tested the ability of salt-modified ( $\text{Ca}^{2+}$ ,  $\text{Mg}^{2+}$ ,  $\text{Al}^{3+}$ , and  $\text{Fe}^{3+}$ ) NaP1-zeolite derived from coal-FA to concomitantly adsorb ammonium and phosphate compared to non-modified NaP1. Only the Ca-modified zeolite improved the adsorption capacity for phosphate (from 34.7 mg/g to 49.5 mg/g), but Al- and Fe-modified zeolites improved the removal at relatively low phosphate concentrations (0.5–10 mg P/L), where the Ca-modified zeolite showed limited P removal. The mechanisms behind the phosphate removals were believed to be precipitation of calcium phosphate by the Ca-modified zeolite and ligand exchange for the Fe- and Al-zeolites. In addition, Xie et al. (2014) [154] observed efficient adsorption of phosphate using a coal FA-derived zeolite modified with lanthanum hydroxide ( $\text{La}(\text{OH})_3$ ) at  $\text{pH} > 2.5$  with an adsorption capacity of 71.9 mg P/g. The phosphate precipitated as  $\text{LaPO}_4$  on the zeolite. The sorption appeared to be insensitive to pH in the 3–10 range for low (5 mg P/L) and medium (100 mg P/L) concentrations but increased in the whole pH range 1–11 (highest at pH 1) at the highest tested concentration (500 mg P/L). At pH 3, La started to desorb from the zeolite, and at pH 2.3, 99.8% had desorbed. A similar study was conducted by [182] comparing the adsorption of phosphate by coal FA-derived zeolites (NaP1 and A) with that of a natural zeolite (clinoptilolite), all modified with lanthanum. The observed adsorption capacities were significantly higher with the coal FA-derived zeolites (44.0–58.2 mg P/g) than those with the natural zeolite (24.6 mg P/g), all with an apparent pH optimum at pH 5.3. The adsorption capacities appeared, however, to be only moderately affected by the pH in the range of 2–7. The experimental data fitted very well with the Langmuir isotherm model (much better than the Freundlich isotherm); hence, only a monolayer of phosphate was adsorbed to the surfactant-modified zeolite surface, and the thermodynamics showed that the phosphate adsorption was a spontaneous and endothermic process. In a recent study by Abdellaoui et al. (2021) [201], they used zirconium oxide-modified merlinoite obtained from coal fly to adsorb phosphate. The adsorption capacity was determined to be 67.7 mg P/g at  $\text{pH} < 5$  ( $\text{PZC} = 4.6$ ). Electrostatic interaction was found to be the predominant mechanism behind the observed adsorption. However, a part of the phosphate ions was adsorbed to the zeolite surface via strong bonding, presumably by coordination bonding, resulting in reduced desorption of the phosphate even if the pH was turned to strong alkaline conditions. The Freundlich isotherm gave an adequate fit to the data, indicating that the phosphate had adsorbed as a multilayer coverage over the heterogeneous distribution of active sites on the metal-doped zeolite.

##### Results with Surfactant-Modified Zeolites

Naghash and Nezamzadeh-Ejhieh (2015) [189] tested the adsorption capacity of phosphate by HDTMA bromide-modified clinoptilolite and hexadecylpyridinium (HDP) bromide clinoptilolite and found the optima at pH 12 at 675 mmol/kg (20.9 mg/g) and 376 mmol/kg (11.6 mg/g), respectively. Unmodified clinoptilolite had the optimum adsorption capacity at pH 3 at 25 mmol/kg (0.8 mg/kg). They explained the increased adsorption at high pH with a stronger attraction between the cationic head groups of the surfactants and the  $\text{PO}_4^{3-}$  form than any of the other phosphate forms. The Freundlich isotherm gave the best fit to the adsorption data, though the Langmuir isotherm also gave an acceptable correlation, suggesting that in addition to the monolayer of phosphate that was provided by the head ammonium group of the surfactant, some phosphate species may have been trapped between the organic chains within the bilayer [189].

#### 4.2.4. Adsorption of Nitrate by Surfactant-Modified Zeolites

As far as the authors have found, all available studies on the adsorption of nitrate on modified zeolites have been done on zeolites modified with different types of surfactants, primarily HDTMA. Table 9 summarizes the literature findings, which are also briefly presented below.

Li et al. (2017) [202] found that a clinoptilolite-rich turf modified with HDTMA-Br was able to sorb 5.0 mg NO<sub>3</sub>/g. In a later study with clinoptilolite from the same area, de Ganaro et al. (2014) [203] reported that HDTMA-Cl was better at exploiting its anion exchange capacity compared to the same zeolite modified with HDTMA-Br. Gouran-Orimi et al. (2018) [204] ran small-scale filtration tests on a polydopamine-coated clinoptilolite in fixed-bed columns for the removal of nitrate from deionized water with and without other competing anions. 2.47 mg NO<sub>3</sub>/g was adsorbed to the zeolite. Lower flow rate, pH (3–9), and temperature (10–35 °C), but higher influent concentration and bed height, increased the adsorption of nitrate. Lin et al. (2023) [205] used natural zeolite modified with HDTMA-Br in ballasted flocculation to improve the settling properties of activated sludge and, at the same time, remove nitrate and phosphate. When dosing 0.91 g modified zeolite per L sludge slurry with 4 g suspended solids/L and 5 mg NO<sub>3</sub>/L, the nitrate removal was ca. 44% (2.42 mg NO<sub>3</sub>/g) (our calculations). The adsorption of nitrate was only marginally impacted by competing anions when these were increased from 0 mg/L to 5 mg/L: 2.6% reduction by Cl<sup>−</sup> and 3.2% reduction by SO<sub>4</sub><sup>2−</sup>. When modifying natural zeolite with cetylpyridinium bromide (CPB), Zhan et al. (2011) [206] determined the maximum adsorption capacity to be 9.7 mg NO<sub>3</sub>/g from the Langmuir isotherm model, and the uptake of nitrate was only slightly impacted by competing anions (Cl<sup>−</sup>, HCO<sub>3</sub><sup>−</sup>, and SO<sub>4</sub><sup>2−</sup>) in the concentration range 0–200 mg/L. Interestingly, the adsorption was reported to be decreasing with temperature in the temperature range of 15–35 °C. They also found that the adsorption of nitrate onto the zeolite followed the pseudo-second-order kinetic model for the entire adsorption process and that both the Langmuir and the Freundlich isotherm models gave good fits with the adsorption data. In addition, Schick et al. (2010) [207] measured the adsorption of nitrate by a HDTMA-Br-modified clinoptilolite in batches and found that the maximum capacity was 6.1 mg NO<sub>3</sub>/g from the Langmuir isotherm model. The equilibrium time for uptake of nitrate was only 0.5–1 h, and the competition with other anions (Cl<sup>−</sup>, HCO<sub>3</sub><sup>−</sup>, and SO<sub>4</sub><sup>2−</sup>) only reduced the kinetics (uptake rate) and not the absolute removal capacity. However, in a later study with the same HDTMA-Br-modified clinoptilolite tested in a filter column, Schick et al. (2011) [208] reported that nitrate was significantly reduced in the presence of SO<sub>4</sub><sup>2−</sup>, with SO<sub>4</sub><sup>2−</sup> and NO<sub>3</sub><sup>−</sup> being similarly adsorbed to the zeolite. The same research group has also tested the adsorption of nitrate by differently nanostructured MFI-, ZSM-5-, and \*BEA-type zeolites modified with HDTMA-Br [39–41]. First, Schick et al. (2011) [40] obtained an adsorption of 37.2 mg NO<sub>3</sub>/g with HDTMA-Br-modified MFI-zeolite nanosheets. Then Hanache et al. (2019) [41], testing a HDTMA-Br-modified \*BEA-type zeolite nanosponge, reached a maximum adsorption capacity of 83 mg NO<sub>3</sub>/g. This was considerably better than the same HDTMA-Br-modified \*BEA-zeolite nanocrystals (19 mg NO<sub>3</sub>/g). Finally, Hanache et al. (2019) [39] tested different HDTMA-Br-modified nanostructured zeolites (nanosheets, nanocrystals, and nanosponges). Again, the nanosponge performed best with 132 mg NO<sub>3</sub>/g, compared to 120 mg NO<sub>3</sub>/g with nanosheets and 50 mg NO<sub>3</sub>/g with nanocrystals. The adsorption occurred very quickly; equilibrium occurred within about 2 min, fitting well with the pseudo-second-order model. A good fit with the Langmuir and the Dubinin-Radushkevich isotherm models confirmed that the adsorption mechanism was ion exchange and that the nitrate molecules formed a saturated monolayer on the surfactant at equilibrium [39,41].

**Table 9.** Reported apparent sorption capacity of nitrate for modified zeolites with test conditions (nitrate concentration range, S/L ratio, contact time, and temperature) and pH at optimum adsorption.

Zeolite	Surfactant	Amount Adsorbed	Conc. Range	S/L Ratio	Contact Time	Temp.	pH	Ref.
		mg NO <sub>3</sub> /g	mg NO <sub>3</sub> /L	g/L	h	°C	-	
Clinoptilolite	polydopamine	2.47	150	-	0.30	10	3	[204]
ZSM-5 nanocrystals	HDTMA-Br	50						
ZSM-5 nanosheets	HDTMA-Br	120	50–2500	0.5	24	room	6	[39]
ZSM-5 nanosponges	HDTMA-Br	132						
clinoptilolite-rich turf	HDTMA-Br	4.96	124–1240	100	24	room	-	[202]
Natural zeolite	HDTMA-Br	2.42	5	0.91	2	room	7	[205]
*BEA-type zeolite nanosponge	HDTMA-Br	83	50–1500	2	2 min	room	5.5	[41]
*BEA-type zeolite nanocrystals	HDTMA-Br	19		25	5 min			
Clinoptilolite-rich tuf	HDTMA-Br	6.07	1–113	20–200	24	room	5–6	[207]
Natural zeolite	CPB	9.68	89	2	0.5	15	6	[206]

#### 4.2.5. Leaching of Surfactants—A Potential Setback

An inherent challenge with using surfactants that are only adsorbed to the surface of the zeolites by ion exchange or electrostatic forces is that they may leach from the zeolites during actual use out in the field. Not surprisingly, the majority of available studies on surfactant-leaching from zeolites have been done on HDTMA [203,209–213].

A fully saturated bilayer of HDTMA on a clinoptilolite typically contains approximately 200 mmol HDTMA/kg (57 g/kg) [198]. Li et al. (2017) [202] studied the loss of HDTMA from clinoptilolite placed in a filter column continuously operated for 130–150 days. In one of the tests, only the medium-sized fraction (14–40-mesh) of the zeolite was used, resulting in a relatively high hydraulic conductivity of 0.01 cm/s, and the zeolite was only partially covered with a HDTMA-Br bilayer (150 mmol/kg). In this test, at the end of 150 days and 100 pore volumes (PV), 17% of the HDTMA had been lost. The loss followed a first-order model, but during the initial 70 PV, the loss was markedly faster ( $k = 0.003$ ) than the later 30 PV ( $k = 0.0003$ ), with a distinct transition between the two, corresponding to a quicker loss of the bilayer than the monolayer. In a second test, only the smallest size fraction (<40 mesh) of the zeolite was used (hydraulic conductivity of  $9 \cdot 10^{-6}$  cm/s), and this time it was fully covered with a HDTMA-Br bilayer (230 mmol/kg). Due to the smaller pore volume in the column, the linear velocity through the column was about 10 times faster, and at the end of the 130 days test period, 3000 PV had passed through, and 60% of the HDTMA was lost from the zeolite. In this case, there were two distinct transitions between an initial very rapid loss period (0–300 PV;  $k = 0.007$ ), a rapid loss period (300–1500 PV;  $k = 0.0003$ ), and a slow loss period (1500–3000 PV;  $k = 0.00008$ ), with the second transition corresponding to the external cation exchange capacity of the clinoptilolite. It was not suggested by Li et al. (2017) [202], but the first initial very rapid loss may potentially have been excess HDTMA not fully bound within the bilayer by hydrophobic forces. In summary, many factors may influence the loss of HDTMA from the modified zeolites, including the HDTMA coverage, flow rate, and conductivity (low conductivity increases the loss; [209]).

HDTMA has been shown to be toxic to soil bacteria in the dissolved state, but not when bound to the cation exchange sites present in soil [214]. It is also not biodegraded when bound to zeolites [209]. Hrenovic and Ivankovic (2007) [215] estimated the 50% growth inhibition concentration of HDTMA-Br (EC<sub>50</sub>) towards *Acinetobacter junii*, a phosphate-accumulating bacteria important for biological phosphorous removal in wastewater treatment plants, to be  $3.27 \pm 1.12 \cdot 10^{-7}$  mol/L (120 µg/L). Reeve and Fallowfield (2018) [196]

pointed to the lack of data connected to the toxicity of HDTMA-Br that is needed to determine the suitability of surfactant-modified zeolites in water remediation applications. Schick et al. (2011) [208] suggested that the residual amounts of surfactants leaching out could be lowered below the maximum residual concentration limit of ca.  $10^{-7}$  mol/L by filtration through a second column filled with activated carbon.

## 5. Practical Application of Zeolites as Adsorbent

When the zeolite is used as an adsorbent in practical applications, it is crucial to make sure that its adsorption characteristics (i.e., rate, kinetic, and capacity) are utilized to the fullest and that it will be a rather simple task to separate the zeolite from the water. Since synthesized zeolites are typically powders with particles in the nm-to- $\mu\text{m}$  size range, they will be very easily dispersed in water. Their small size is one of their main strengths as adsorbents, as their surface-to-volume ratio is very large. Hence, it will be beneficial if this can be retained in practical applications.

### 5.1. Production and Use of Shaped and Structured Zeolites

However, in practice, the zeolites are usually transformed into larger aggregates prior to industrial use, either by granulation into beads or pellets (i.e., structured zeolites) or by extrusion in the shapes of, e.g., cylinders (monoliths) (i.e., shaped zeolites) [171,216]. This is done to improve its mechanical and physical properties and to prevent or minimize pressure drop, material loss, and erosion of equipment when applied to, e.g., fixed-bed or expanded-bed filtration units [171]. In most cases, this includes the addition of water and other inorganic (e.g., clay, silica, or alumina) and/or organic binders that fill the gaps between the zeolite crystals and hold them together in the final material. Other additives may also be added to provide appropriate plasticity or porosity [216]. After shaping, the material is usually dried and calcined to remove water and labile components, and to achieve the final mechanical properties, residual binders typically constitute 5–30% of the final material [171,217]. However, this type of shaping or structuring can greatly affect the adsorption capacity and kinetics of the zeolite [216,218]. The introduction of different types of hierarchical aluminas (ordered and disordered mesoporous and macroporous structures) to improve the porosities in the binders has been suggested; see Bingre et al. (2018) [216] for a review.

### 5.2. Physical Separation of Powdered Zeolites—Magnetic Zeolites

Powdered zeolites may, as is frequently done with powdered activated carbon (PAC), be applied, e.g., directly to the aeration basin of an activated-sludge treatment process and to physical-chemical treatment processes in conjunction with chemicals used for the precipitation of specific constituents [219]. In both of these examples, the existing treatment train includes a unit (typically a sedimentation tank or rapid sand filter) to separate the sludge generated by the process, and the powdered zeolites (or PAC) will normally also be collected with the sludge. Otal et al. (2013) [152] added 1 g/L of a NaP1 zeolite synthesized from coal FA to a poorly settleable activated sludge, significantly improving the settling performance of the sludge and removing 30% of the nitrogen (13.7 mg  $\text{NH}_4/\text{g}$ ). It may also be applied to the effluent from a biological treatment process in a contacting basin. After a certain amount of time for contact, the zeolite particles (or PAC) are allowed to settle to the bottom of the tank, and the treated water is then removed from the tank [219]. In practice, to accelerate the settling rate of the powdered zeolites (or carbon), a flocculant (e.g., a polyelectrolyte) is added to aggregate the fine-grained particles. The flocculant must be removed (e.g., by calcination) if the powdered zeolites should be reused. To avoid using additional chemicals, filtration through a rapid sand filter may be used. However, the typical nm- $\mu\text{m}$  size range of powdered zeolites may imply that it will be challenging to get sufficient separation by traditional sand filtration without the aid of additional sludge or flocculant, as these typically have a cut-off range of 2–10  $\mu\text{m}$  [219].

The application of magnetic zeolites could, however, be a solution to this challenge [220]. By incorporating magnetic nanoparticles in the zeolite crystals, the composite will respond to an external magnetic field by forming aggregates (magnetic separation), which will settle much faster. When the magnetic field is removed, the aggregation will stop [220]. Hence, the magnetized zeolitic particle will replace the need for a flocculant and facilitate its reuse. Magnetic separation offers a significant improvement in operation efficiency and reduced costs [220].

It is important that the modification be strong enough to provide the zeolite particles with sufficient magnetic properties without altering the structure or adsorption properties of the zeolite [220]. Typical materials used to produce magnetic zeolites include metal nanoparticles (Fe, Co, Ni, etc.), ferrites ( $MFe_2O_4$ ;  $M = Mn^{2+}, Co^{2+}, Ni^{2+}$ , etc.), alloys ( $CoPt_5$ ,  $FePt$ , etc.), and iron oxides ( $Fe_3O_4$ ,  $\gamma-Fe_2O_3$ ) [221]. Magnetite ( $Fe_3O_4$ ) and maghemite ( $\gamma-Fe_2O_3$ ) are most commonly used as these are relatively cheap materials, biocompatible, and environmentally safe [220,222]. However, the clear drawbacks of using  $Fe_3O_4$  as a magnetic nanoparticle in the composite are that it tends to both agglomerate and react rapidly [223]. The often-preferred method to prepare iron oxide nanoparticles is by co-precipitation of  $Fe^{3+}$  and  $Fe^{2+}$  salts, as it is regarded as a facile and green synthesis method [220].

It is not the intention of this review to summarize all the different methods that have been used to prepare magnetic zeolites (see, e.g., Loiola et al. 2022 [220], Phouthavong et al. 2022) [224]); however, it should be noted that the embedding of magnetic nanoparticles in or on zeolites can be done both during and after the synthesis of zeolites, as described in Section 2.5.3.

Based on 25 years of published works, Loiola et al. (2022) [220] suggested that the numerous composite compounds that had been developed could be classified in five groups based on the position of the magnetic particles in the zeolite crystals: magnetic particles are encapsulated by the zeolitic structure (Type I), the zeolite surface is impregnated or decorated with magnetic nanoparticles (Type II), each magnetic particle is covered with zeolite layers (Type III), nanoagglomerates of small (<100 nm) particles of both zeolites and magnetic compounds (Type IV), and tri-modal composites in which the magnetic zeolite composite is dispersed in a polymer matrix. According to Loiola et al. (2022) [220], type II composites are currently the most relevant and common magnetic zeolites found in this literature, mainly for being easily obtained and usually for not having a negative impact when the nanoparticles are embedded. However, type V composites are the most promising ones in the long term since they solve problems related to agglomeration of constituents, oxidation, and leaching [220]. They are also more mechanically, chemically, and electrically stable [220].

However, improvements in magnetic adsorbent synthesis are still needed to make it more effective, give more uniform magnetic distribution, and break the barrier of the laboratory with scalable processes for their mass production [224].

## 6. Reuse of Adsorbed Compounds

There are two main strategies for reusing the adsorbed compounds:

1. Use them as they are, embedded in zeolite, typically as slow-release compounds, for instance, in fertilizers.
2. Recover them from the zeolite by controlled release.

There are at least two strengths of the first strategy: (1) There are no further treatments needed, implying limited added costs, and (2) depending on how it is applied, when the slow-released compounds in the zeolite are exhausted, potentially no residual waste zeolite needs to be managed.

The second strategy has several potential strengths: (1) the compounds can be recovered as a rich concentrate (2) that, depending on its purity and legal restrictions, can be utilized as a secondary raw material in commercial products (3), which could drastically broaden the range of reuse applications (4), hence also strengthening its potential role in the circular economy. (5) This also potentially enables multiple reuse cycles of the zeolite as an adsorbent, (6) thereby reducing the upstream costs per cycle, and (7) generates less residual zeolite waste that needs to be managed.

Both strategies require that it is possible to release the compounds of interest under conditions that can be controlled or naturally occur and that the release of unwanted compounds (e.g., toxic substances or compounds that limit further application) is within acceptable limits. These two topics are discussed in somewhat more detail in the following.

### 6.1. Slow Release of Compounds from the Zeolite during Application

Zeolites have been shown to be valuable in agriculture as soil conditioners due to their ability to improve soil chemical and physical properties such as the saturated hydraulic conductivity, the infiltration rate, their cation exchange capacity, and their great water-holding capacity [225]. They may also help the farmer with soil or water pollution, contamination by heavy metals, loss of nutrients, and loss of water-use efficiency in drylands [225]. Moreover, they have a large carrying capacity of slow-release macro- and micronutrients [20,225,226]. The slow release of ammonium from zeolites has been studied for decades [226]. Slow release from surfactant-modified zeolites loaded with nitrate has also been investigated [227]. In the case of phosphate, the ability to produce slow-dissolving calcium phosphate compounds such as brushite ( $\text{CaHPO}_4 \cdot 2\text{H}_2\text{O}$  (s)) during sorption in the pH range 6–9 is important, avoiding the formation of relatively insoluble Ca-phosphate minerals such as hydroxyapatite [200].

### 6.2. Controlled Release of Compounds of Interest

As discussed earlier, the main mechanism governing the adsorption of heavy metals and ammonium (Section 3.2) and phosphate and nitrate (Sections 4.1 and 4.2) to any zeolite, natural or synthetic, or modified by metal-doping or by surfactants appeared to be electrostatic interactions. Since electrostatic interactions by nature are reversible, it may be suggested that zeolites, under ideal conditions, could undergo a virtually unlimited number of adsorption–desorption cycles [8]. However, the real situation is never ideal, especially when the raw materials that the zeolites are synthesized from are far from homogeneous.

#### 6.2.1. Methods Used to Release the Compounds from Zeolites

Table 10 summarizes results from studies that have included the release of the compounds that have already been adsorbed to the zeolite, most often focusing on the possibility to regenerate the zeolite for additional sorption cycles to reduce the operational process costs. In general, to optimize the desorption of the compounds, the conditions that led to their optimum adsorption need to be reversed. There are typically two factors that are easy to manipulate that have been used extensively to desorb compounds from sorbents: the pH and the concentration of competing ions.

As mentioned in Section 3.3.7, at pHs below their PZC, zeolites become neutral or positively charged; hence, at these pHs, the electrostatic forces diminish or get reversed. Since heavy metals tend to precipitate as metal oxides and hydroxides at high pHs (see Figure 4), they are typically desorbed using strong acids (Table 10). Filatova and Pozhidaev (2020) [228] developed a scheme for a stepwise release of  $\text{Ni}^{2+}$ ,  $\text{Cu}^{2+}$ ,  $\text{Zn}^{2+}$ ,  $\text{Cr}^{3+}$ , and  $\text{Fe}^{3+}$  from a natural zeolite (70–75 wt% heulandite, 25–30 wt% potassium feldspar) using  $\text{H}_2\text{SO}_4$ . The zeolite had been used for adsorbing heavy metal-spiked wastewater from electroplating production. In four consecutive steps, 97% of  $\text{Ni}^{2+}$  was recovered as  $\text{NiSO}_4$  using 0.04 M  $\text{H}_2\text{SO}_4$  at 1.5 m/h (step 1), 95% of  $\text{Cu}^{2+}$  was recovered as  $\text{CuSO}_4$  with 0.15 M  $\text{H}_2\text{SO}_4$  at 1.2 m/h (step 2), 92% of  $\text{Zn}^{2+}$  was recovered as  $\text{ZnSO}_4$  with 0.30 M  $\text{H}_2\text{SO}_4$  at 1.0 m/h (step 3), and 90% of  $\text{Cr}^{3+}$  and 89% of  $\text{Fe}^{3+}$  were jointly recovered as  $\text{Cr}_2(\text{SO}_4)_3$  and  $\text{Fe}_2(\text{SO}_4)_3$ , respectively, with 1.0 M  $\text{H}_2\text{SO}_4$  at 0.5 m/h (step 4).

Ammonium can also be desorbed by pH adjustment, either by increasing the pH to drive the equilibrium between ammonium and ammonia towards ammonia and releasing the compound as partially dissolved and gaseous  $\text{NH}_3$  [229,230] or by decreasing the pH to reverse the electrostatic forces. However, the desorption process is typically further accelerated by adding competing ions (i.e., salts), as this will also contribute to the regeneration of the zeolite [150,160,231].

Adsorption of phosphate is usually done using metal-doped zeolites under slightly acidic conditions (Table 8). Xie et al. (2104) [154] recovered the phosphate by hydrothermal treatment at 250 °C in 3 M NaOH, as this also regenerated the La-doped zeolite.

Nitrate is typically captured using surfactant-modified zeolites (Table 9), and since the inner monolayer of surfactant is also kept in place by electrostatic forces [193], it is important to selectively target the nitrate during desorption. Gouran-Orimi et al. (2108) [204] did this by adding a weak basic solution (0.01–0.05 M NaOH), thereby reducing the positive charge of the polydopamine-coated clinoptilolite and increasing the concentration of OH<sup>−</sup> as a competing ion. However, the fraction of recovered nitrate was rather low (59–71%), and the loss of polydopamine during desorption was not reported, but 80–87% of the adsorption capacity of the polydopamine-coated clinoptilolite was recovered after three adsorption-desorption cycles. Schick et al. (2011) [208] recovered ca. 100% of nitrate from a HDTMA-modified clinoptilolite using 1 M NaBr. The loss of HDTMA from the surface of the clinoptilolite during desorption was apparently not substantial, but the slow leaching of HDTMA both during application (see Section 4.2.5) and desorption is a challenge both for repeated use of the adsorbent, for the environmental application, and potentially for the application of the recovered compounds.

In general, raising the temperature during desorption will most likely increase the rate and extent of desorption [232].

**Table 10.** Reported desorption of selected compounds from different types of zeolites under given conditions.

Compound	Zeolite	Release Conditions	Important Factors	Released Compound	Desorption Efficiency	Ref.
Cu <sup>2+</sup>	Synthetic from FA	0.1–0.8 M H <sub>2</sub> SO <sub>4</sub>	High conc. H <sub>2</sub> SO <sub>4</sub>	CuSO <sub>4</sub>	96–102% (four cycles)	[233]
Ni <sup>2+</sup>	Synthetic from FA	0.1–0.8 M H <sub>2</sub> SO <sub>4</sub>	High conc. H <sub>2</sub> SO <sub>4</sub>	NiSO <sub>4</sub>	84–98% (four cycles)	[233]
Cd <sup>2+</sup>	Natural zeolites	0.1 M HCl (54–80 bed volumes)	-	CdCl <sub>2</sub>	90% first cycle	[234]
Zn <sup>2+</sup>	Natural zeolites	0.1 M HCl (6–30 bed volumes)	-	ZnCl <sub>2</sub>	90% first cycle	[234]
Cr <sup>6+</sup>	HDTMA-modified clinoptilolite-rich tuff	0.28 M Na <sub>2</sub> CO <sub>3</sub> and 0.5 M NaOH (L/S: 3 mL/g); regeneration with 3 × 0.1 M HCl (L/S: 3 mL/g)	-	-	90% first cycle (100% regeneration)	[213]
NH <sub>4</sub> <sup>+</sup>	Alkali-treated clinoptilolite	0.5 M HCl	-	NH <sub>4</sub> Cl	Adsorption unaffected after 12 cycles	[235]
NH <sub>4</sub> <sup>+</sup>	Zeolite from FA	1 M NaCl (3 × 25 mL/2 g zeolite) at 25 °C for 1.25 h	-	NH <sub>4</sub> Cl	Ca. 10% loss in adsorbent capacity after one cycle	[236]
NH <sub>4</sub> <sup>+</sup>	Clinoptilolite	20 g NaCl/L for 15 h	High NaCl conc.	NH <sub>4</sub> Cl	100% (five cycles). Adsorption capacity increased from 9.2 mg/g to 10.9 mg/g (over first three cycles)	[237]
NH <sub>4</sub> <sup>+</sup>	Clinoptilolite	30 g NaCl/L (123–134 BV)	Low flow rate to get high conc.	NH <sub>4</sub> Cl	88–95%	[231]
NH <sub>4</sub> <sup>+</sup>	Synthetic NaA	30 g NaCl/L (43–46 BV)			92–95%	
NH <sub>4</sub> <sup>+</sup>	Clinoptilolite	10% NaCl and 0.6% NaOH	Increased desorption: 10–15% NaCl and 0–0.6% NaOH	NH <sub>3</sub>	100%	[229]
PO <sub>4</sub> <sup>3−</sup>	La-doped zeolite from FA	3 M NaOH (L/S ratio 80:1) at 250 °C for 5 h	High conc. NaOH (<4 M NaOH), high L/S ratio, high temp	Na <sub>3</sub> PO <sub>4</sub>	95% (five cycles)	[154]
NO <sub>3</sub> <sup>−</sup>	Polydopamin-coated clinoptilolite	0.01 M and 0.05 M NaOH	-	NaNO <sub>3</sub>	59–71% (three cycles)	[204]
NO <sub>3</sub> <sup>−</sup>	HDTMA-modified clinoptilolite	1 M NaBr (L/S: 5 mL/g) for 6 h	-	NaNO <sub>3</sub>	Ca. 100% first cycle	[208]

### 6.2.2. Downstream Concentration and Refinement

Ideally, the solution with the recovered compounds should be as concentrated and pure as possible, potentially just containing other compounds that would be beneficial for any downstream application. However, this is seldom the case. The concentrations are often low and variable, and the level of contaminants may be significantly higher than the concentrations of the compounds of interest. Hence, downstream processing to concentrate and refine the valuable compounds will normally be necessary. It is not within the scope of this review to summarize all these possibilities, but some general comments are discussed below.

#### Concentrating Ammonia by Stripping and Condensation

If ammonium is desorbed as ammonia by adding NaOH and NaCl, the partially dissolved and gaseous  $\text{NH}_3$  can be stripped off directly using air or hot steam in a stripping column and recovered as ammonium sulphate or ammonium nitrate by subsequent acid-washing with  $\text{H}_2\text{SO}_4$  or  $\text{HNO}_3$ , respectively, in a condenser column [19,238]. The stripping process is highly dependent on temperature and pH since both influence the equilibrium between ammonium and ammonia (both with positive correlations). Hence, the process is more efficient at elevated temperatures due to higher concentrations of ammonia and reduced solubility of gaseous ammonia at high temperatures, as well as reduced water viscosity at higher temperatures [239]. At ambient temperatures, the typical operating pH is  $>11$ , while it may be  $<10$  if the operating temperature is increased to  $60\text{ }^\circ\text{C}$  [240]. To avoid clogging due to scaling in the stripping column, it is advisable to avoid using calcium and magnesium salts for pH adjustments. However, problems with clogging due to scaling are avoided using jet loop reactors [241].

#### Concentrating by Precipitation

Precipitation as struvite (a slow-release fertilizer) is a common method to separate ammonium and phosphate from other dissolved compounds in a solution by adding a magnesium salt [166]. This may also be done to selectively separate different heavy metals in a stepwise precipitation process, taking into account their pH-dependent solubilities in the presence of anions such as carbonate, sulphate, and phosphate [181].

### 6.2.3. Regeneration of the Zeolite's Adsorption Capacity

To be able to reuse the zeolite as an adsorbent multiple times, it needs to be regenerated. The methods mentioned in Section 6.2.1 for the desorption of the compounds of interest may fully or partially regenerate the zeolite. Over time, after a few or several cycles of adsorption-desorption, the restorable adsorption capacity of the zeolite by simple desorption, as described in Section 6.2.1, will decline to a non-feasible/unacceptable level. This may be due to poisoning by strong chemisorption of (often polymerized) compounds on the active sites or pores of the zeolite, the formation of deposits on the zeolite by simple deposition and bacterial growth (fouling), chemical and structural alterations of the catalyst (e.g., noble metal sintering, dealumination, and collapse of the zeolite framework), and mechanical alterations due to mechanical stress (e.g., crushing, attrition, abrasion, or erosion) [242,243]. Chemisorption poisoning and fouling may be reversed, while chemical, structural, and mechanical alterations are irreversible, and, hence, in that case, recovery of the zeolite for resynthesis may be the best option.

There are available reviews focusing on the regeneration of catalytic zeolites (e.g., Daligaux et al. (2021) [244], but apparently none for zeolites used for adsorption). However, the focus is on the removal of coke, which is a heavy transformation product from the catalytic reactions facilitated by the zeolites [245]. Zeolites used for adsorption show less catalytic activity, and the expected formation of coke is therefore smaller, making these reviews less relevant.

Chemisorbed compounds will usually need to be decomposed to be efficiently removed; hence, thermal and chemical regeneration methods are most relevant [232,246],

e.g., high-temperature calcination, washing with a mixed solution of NaClO and NaCl, and Fenton oxidation [232,247,248]. In general, short contact times (<30 min) are needed to destroy organic contaminants [249], but thermal regeneration requires several hours of regeneration [247]. One of the advantages of zeolites is that they are stable in oxidative conditions, but when exposing them to high temperatures, it is important to take into account their temperature stability so as not to destroy their structure [250,251]. However, Wang et al. (2006) [247] found that calcination at 540 °C for 1 h of the synthetic zeolite MCM-22 saturated with the organic dye methylene blue was more efficient than using Fenton oxidation (0.01 M FeCl<sub>3</sub> and 3% H<sub>2</sub>O<sub>2</sub> for 48 h). The zeolite regenerated by calcination showed a higher adsorption capacity than the original zeolite, while the zeolite regenerated by Fenton oxidation only recovered 60% of the adsorption capacity. However, Chen et al. (2022) [3] found that the crystalline structure of the natural zeolite they tested (from Chifeng, Inner Mongolia) changed (due to dealumination) when the calcination temperature was raised to ≥450 °C.

Using microwave-assisted thermal generation may be an interesting option as it provides fast direct heating from the interior of the adsorbent instead of heating only from the outside, which occurs with traditional temperature swing adsorption or steaming [232]. The electromagnetic properties (e.g., dielectric constants) of the different components of the system (i.e., zeolite, water, and the chemisorbed compounds) determine where the energy is directed. Hence, the component with the highest dielectric constant gets heated first [252]. The typical wave frequency used on an industrial scale is 0.92 or 2.45 GHz [252]. While the penetration depth of water is around 1 cm, it is typically in the range of 10–100 cm in zeolites [252]. However, microwaves are mostly used for regenerating activated carbon [232], but also for zeolites used as catalysts [253]. We have found no studies documenting the effects of microwave-assisted thermal generation on zeolites used as adsorbents.

## 7. Discussion and Need for Further Studies

### 7.1. MSW-FA as a Source for Synthetic Zeolites

As outlined in Section 2.4, MSW-FA is far from being the best source for synthesizing zeolites meant for capturing cations. Its content of SiO<sub>2</sub> and Al<sub>2</sub>O<sub>3</sub>, the primary constituents in zeolites, is both relatively low, tending towards high Si/Al ratios (less useful for synthesizing low Si/Al zeolites with strong cation sorption) and variable (12–41 wt% and 5–24 wt%, respectively), and it usually has a relatively high level of contaminants that will hamper its appropriateness for any use. Hence, significant amendments are needed for it to be utilized as a source for zeolites, which may bring significant production costs.

On the other hand, the increasing awareness of the need to reduce waste, and particularly toxic waste, in combination with the large fractions of salts and certain heavy metals (e.g., zinc) in MSW-FA that could potentially have some commercial value, may provide additional options for utilizing these resources that are currently wasted. The processes needed to extract salts and heavy metals from MSW-FA are beneficial to the concomitant extraction and purification of zeolite precursor materials. A remaining important uncertainty is the level of impurities of residual heavy metals and organic micropollutants (e.g., dioxins and furans) in these precursor materials. The level of contamination will strongly restrict their range of applicability. However, it seems likely that it will be possible to solidify the heavy metals in the zeolitic structure, as well as to degrade dioxins and partially furans, during synthesis (see Sections 2.5.4 and 2.5.5), possibly without any substantial increase in the consumption of chemicals and energy. Though both the solidification of heavy metals and the degradation of dioxins may be improved by adding substantial amounts of phosphate or N<sub>2</sub>S (for heavy metals) during synthesis, if necessary, to control their release. However, as a result of the extractions of both salt, heavy metals, and zeolite precursors, the size of the hazardous waste fraction will be reduced, though the extraction process will generate a residual that may have higher specific toxicity, including the wastewater from the zeolite synthesis. Using, for instance, microwave-assisted hydrothermal treatment or other “green synthesis protocols” may reduce both energy consumption and waste volume.

An obvious drawback considering using MSW-FA as a source for Al- and Si-precursors for producing synthetic zeolites in the current situation is the almost complete lack of examples documenting that it will be possible, not the least, feasible. Hence, more studies focusing on optimizing the extraction and necessary purification steps to produce precursors with appropriate qualities, with and without supplements of Si and/or Al from other waste sources, are needed. Also, the impact of the variable composition of the initial MSW should be considered.

### 7.2. Capturing Efficiency

Since cation exchange will, in most cases, be the dominant mechanism for capturing the targeted compound (e.g., ammonium, nitrate, phosphate, or selected heavy metals), competition for available adsorption sites on the zeolite is crucial. Hence, tailoring the zeolite (i.e., framework type and necessary surface modifications) to the targeted compound will be important, as will optimizing the operating conditions (see Section 3.3). However, based on the rather large variability in the reported adsorption capacities and selectivity of the different types of zeolites, specific tailoring is challenging and may need to be adapted to the conditions in each case. Furthermore, this is made further difficult by the fact that most studies are done under relative ideal conditions and are not representative when applying zeolites as adsorbents in the “field”. From a recovery point of view, it is appropriate to harvest the targeted compounds from rich sources such as liquid manure fractions, rejection water after anaerobic digestion of food or sewage sludge, urine, concentrated black water after fermentation, industrial waste streams, or leachates from landfills or mines/mining areas. At high compound concentrations and low concentrations of competing ions, the need for tailored zeolites may be reduced [231]. In that regard, it is also interesting to note the reported increased adsorption capacity of zeolites at elevated bulk concentrations, particularly for ammonium (see Section 3.3.2), which would be beneficial when harvesting from high-strength sources.

There is also a balance between utilizing the whole adsorption capacity of the zeolite and the reduced adsorption kinetics when the capacity is close to being exhausted. This implies a need for increased exposure times or an increased risk of breakthrough (in flow-through applications if combined with treatment).

### 7.3. Acceptance and Need of Recovered End-Products

The above sections have described and discussed the feasibility of extracting Al- and Si-containing zeolite precursors from MSW-FA and using these precursors to synthesize tailored zeolites that could be used to harvest and recover nutrients and heavy metals as secondary raw materials. Hence, the intention is to turn hazardous waste (MSW-FA) into valuable products (zeolites) and secondary raw materials (zeolite precursors and recovered compounds) in a stepwise manner. However, within the European Union and the European Economic Area, waste management is strictly regulated through *The Waste Framework Directive 2000/98* (WFD). As a general measure to minimize waste generation, Article 6 (1) and (2) in the WFD have defined common end-of-waste criteria that specify when a certain waste ceases to be waste and becomes a product or a secondary raw material. End-of-waste may help to alleviate any user prejudice, increase the confidence of the users in quality standards, and encourage the use of secondary materials [254].

The two of the four criteria are that the substance (or object) is commonly used for specific purposes and that there is an existing market or demand for the substance (or object). Hence, end-of-waste criteria will not be defined for materials for which there is no demand or for which a market has not yet been developed. The global market for zeolites for all types of applications was ca. 6 million tons at a value of USD 13.2 billion in 2022 and is expected to increase by 4% annually to ca. 8.5 million tons at a value of USD 21.7 billion in 2030 [255]. The market for synthetic zeolites is still somewhat smaller than for natural zeolites, which are also expected to dominate due to a growing demand in various applications such as constructing and building materials, soil remediation,

and wastewater treatment. The largest bulk market for synthetic zeolites is as water softeners in detergents. However, the fastest-growing market is for synthetic zeolites as adsorbents/desiccants [256]. About 60 million tons of MSW-FA are generated globally each year. However, the typical contents of  $\text{SiO}_2$  and  $\text{Al}_2\text{O}_3$  are only in the range of 20% and 10%, respectively. This would anyway, more or less, cover the current global need for zeolite precursors. Nevertheless, the local availabilities of MSW-FA and demands for zeolite precursors are, of course, crucial to minimizing necessary transport from both cost and environmental perspectives. These need to be considered in each case.

The global market for recycled nutrients (i.e., N, P, and K) from waste streams such as wastewater, agricultural residues, and food waste is also relatively substantial at a value of USD 5.0 billion in 2023 and is expected to reach USD 7.4 billion in 2030 [257]. However, as for zeolite precursors, only the local or regional demands for recycled nutrients are relevant in this context, and these depend on local or regional traditional practices and are prone to seasonal changes. Moreover, this market is possibly more sensitive to transport costs due to smaller buyers. Hence, also here, the market potentials (as a part of a more thorough market analysis) need to be considered in each local case.

The third end-of-waste criteria is that the use is lawful, i.e., that the substance (or object) fulfils the technical requirements for the specific purposes and meets the existing legislation and standards applicable to products. In zeolite synthesis, both liquid and solid (crystalline or amorphous) Al- and Si precursors are utilized. The variation in precursors appears to be relatively broad and includes those precursors referred to in Section 2.5.2 [91]. The MSW-FA management plant(s) that will extract and purify the zeolite precursors will most probably receive MSW-FA from a large range of incineration facilities, implying a huge variation in FA composition within a waste fraction that is inherently heterogeneous. And importantly, the FA composition is also dependent on the type of incineration plant and how it is operated [3,7]. Hence, it may be challenging to determine optimum operational conditions for the extraction and purification processes, which may impact the composition and quality of the final precursors. It will be important to assess how easy it will be to control and predict the final product quality, identify any need for initial source separation or specific operational procedures carried out at the incineration plant to select or exclude particular MSW-FA fractions [254], and make sure that local legal requirements are fulfilled.

The fourth end-of-waste criteria is the most critical in this regard and states that the use should not lead to overall adverse environmental or human health impacts. As discussed in detail in Section 2.5.4, proper strategies that prevent the heavy metals and organic micropollutants embedded in the MSW-FA from being transferred to the zeolite precursors and to the recovered secondary raw materials need to be in place. Also in this regard, it must be determined if any hazard(s) associated with a particular MSW-FA source can be adequately controlled in some way during processing or whether they need to be excluded at the source to provide the requisite product quality [254]. The level of complexity needed in these assessments is difficult at the current state of development. The environmental risk assessment should include both chemical analyses, toxicity testing, and leaching rates of all relevant toxic compounds at different stages along the process train until the final products or secondary raw materials.

It should be noted that if a material does not meet the end-of-waste requirements, it does not imply that the material cannot be recycled and needs to be disposed of. Materials not fulfilling the end-of-waste requirements can be recycled and reused under the waste regime [254].

## 8. Concluding Remarks

MSW-FA is far from being the first option to use as a source for zeolite precursor, but if salts and heavy metals of potential commercial interest are extracted, then it should be more viable to also extract Al- and Si-containing precursor material from the residual matter and synthesize zeolites. Using “green synthesis protocols” such as microwave-assisted hydrothermal treatment for the synthesis process will reduce both the energy

consumption and the waste volume compared to traditional methods. There is also reason to believe that residual heavy metals will be solidified in the zeolitic structure and that dioxins, and partially furans, will be degraded during microwave-assisted hydrothermal synthesis. However, so far, very few attempts have been made to synthesize zeolites from MSW-FA without using any supplementary Si and/or Al sources. More studies are needed that include the upstream processes of extracting salts and heavy metals to improve the starting material for subsequent extraction of zeolite precursors (for tailored synthesis) or direct synthesis. It will also be important to understand how the expected variability in quality of the initial MSW-FA influences the final properties of the zeolites and how this variability can be controlled or counteracted. Moreover, the studies should look at how to minimize residual waste throughout the process, from MSW to zeolites, and consider the most appropriate and sustainable ways of minimizing the environmental and human risk of residual toxic compounds.

It is well established that zeolites may be used to adsorb compounds such as ammonium and heavy metals, and with necessary modifications of their surface, they may also be used to adsorb nutrients such as nitrate and phosphate. Zeolites with a low Si/Al ratio (negatively charged) have been found to be particularly good at adsorbing cations such as  $\text{NH}_4^+$ ,  $\text{Pb}^{2+}$ ,  $\text{Cd}^{2+}$ ,  $\text{Cr}^{3+}$ ,  $\text{Ni}^{2+}$ ,  $\text{Zn}^{2+}$ , and  $\text{Cu}^{2+}$ ; however, most MSW-FAs do typically have high Si/Al ratios, indicating that the precursor solution needs to be somewhat tailored. It is possible to both extract Al (by acid leaching) and Si (by alkali leaching), but these processes should be studied further on MSW-FA.

Adsorption and desorption for recovery are, in general terms, benefited by high concentrations of the target compounds and low concentrations of competing ions. In this review, we have not tried to collect and summarize all field trials that have been conducted, but our impression is that many more tests are needed, also with zeolites synthesized from MSW-FA, to document the best operating conditions for different adsorbates in different types of matrices, both for adsorption and desorption. An important aspect also here is the eventual leaching of toxic heavy metals and surfactant-modified zeolites (for the adsorption of nitrate and phosphate) from the zeolites to the environment and during desorption.

The main purpose here is to turn hazardous waste (MSW-FA) into valuable products (zeolites) and secondary raw materials (zeolite precursors and recovered compounds). The third and fourth end-of-waste criteria of the EU's WFD, relating to the lawful use of extracts from MSW-FA and potential environmental or human health impacts from their applications, respectively, are probably the most critical issues to consider in this process. Although fulfilling these criteria is currently far from being realized and is not absolutely required to recycle extracted fractions from MSW-FA, it is recommended to work towards such a goal since it would contribute to alleviating any user prejudice, increasing the confidence of the users in quality standards, encouraging the use of secondary materials, and supporting the EU common accepted end-of-waste strategy.

**Author Contributions:** Conceptualization, C.V.; investigation, C.V. and M.U.; writing—original draft preparation, C.V. and M.U.; writing—review and editing, C.V. and M.U.; visualization, C.V. All authors have read and agreed to the published version of the manuscript.

**Funding:** This research was funded by a grant from the internal Publication Fund at Norwegian Institute for Water Research.

**Data Availability Statement:** No new data were created or analysed in this study.

**Conflicts of Interest:** The authors declare no conflict of interest.

## References

1. Hoornweg, D.; Bhada-Tata, P. *What a Waste: A Global Review of Solid Waste Management*; The World Bank: Washington, DC, USA, 2012.
2. Kaza, S.; Yao, L.; Bhada-Tata, P.; Van Woerden, F. *What a Waste 2.0: A Global Snapshot of Solid Waste Management to 2050*; Urban Development: Washington, DC, USA, 2018.
3. Chen, D.; Zhang, Y.; Xu, Y.; Nie, Q.; Yang, Z.; Shenga, W.; Qian, G. Municipal solid waste incineration residues recycled for typical construction materials—A review. *RSC Adv.* **2022**, *12*, 6279. [[CrossRef](#)] [[PubMed](#)]

4. Lindberg, D.; Molin, C.; Hupa, M. Thermal treatment of solid residues from WtE units: A review. *Waste Manag.* **2015**, *37*, 82–94. [[CrossRef](#)] [[PubMed](#)]
5. Quina, M.J.; Bontempi, E.; Bogush, A.; Schlumberger, S.; Weibel, G.; Braga, R.; Funari, V.; Hyks, J.; Rasumssen, E.; Lederer, J. Technologies for the management of MSW incineration ashes from gas cleaning: New perspectives on recovery of secondary raw materials and circular economy. *Sci. Total Environ.* **2018**, *635*, 526–542. [[CrossRef](#)]
6. Weibel, G.; Zappatini, A.; Wolffers, M.; Ringmann, S. Optimization of metal recovery from MSWI fly ash by acid leaching: Findings from laboratory- and industrial-scale experiments. *Processes* **2021**, *9*, 352. [[CrossRef](#)]
7. Kanhar, A.H.; Chen, S.; Wang, F. Incineration fly ash and its treatment to possible utilization: A Review. *Energies* **2020**, *13*, 6681. [[CrossRef](#)]
8. Millini, R.; Bellussi, G. Zeolite science and perspectives. In *Zeolites in Catalysis: Properties and Applications*; Cejka, J., Morris, R.E., Nachtigall, P., Eds.; RSC Catalysis Series No. 28; The Royal Society of Chemistry: London, UK, 2017.
9. Ray, R.L.; Sheppard, R.A. Occurrence of zeolites in sedimentary rocks: An overview, in *Natural Zeolites: Occurrence, Properties, Applications*. *Rev. Miner. Geochem.* **2001**, *45*, 17–34.
10. MgBemere, H.E.; Ekpe, I.C.; Lawal, G.I. Zeolite synthesis, characterizations, and application areas—A review. *Int. Res. J. Environ. Sci.* **2017**, *6*, 45–59.
11. Khaleque, A.; Alam, M.M.; Hoque, M.; Mondal, S.; Haider, J.B.; Xuc, B.; Johir, M.A.H.; Karmakar, A.K.; Zhoud, J.L.; Ahmedb, M.B.; et al. Zeolite synthesis from low-cost materials and environmental applications: A review. *Environ. Adv.* **2020**, *2*, 100019. [[CrossRef](#)]
12. Cho, B.H.; Nam, B.H.; An, J.; Youn, H. Municipal Solid Waste Incineration (MSWI) Ashes as Construction Materials—A Review. *Materials* **2020**, *13*, 3143. [[CrossRef](#)]
13. Perego, C.; Bagatin, R.; Tagliabue, M.; Vignola, R. Zeolites and related mesoporous materials for multi-talented environmental solutions. *Microp. Mesop. Mater.* **2013**, *166*, 37–49. [[CrossRef](#)]
14. Karlfeldt Fedje, K.; Rauch, S.; Cho, P.; Steenari, B.M. Element associations in ash from waste combustion in fluidized bed. *Waste Manag.* **2010**, *30*, 1273–1279. [[CrossRef](#)] [[PubMed](#)]
15. Witek-Krowiak, A.; Gorazda, K.; Szopa, D.; Trzaska, K.; Moustakas, K.; Chojnacka, K. Phosphorus recovery from wastewater and bio-based waste: An overview. *Bioeng* **2022**, *13*, 13474–13506. [[CrossRef](#)]
16. Cordell, D. Peak phosphorous and the role of P recovery in achieving food security. In *Source Separation and Decentralization for Wastewater Management*; Larsen, T.A., Udert, K.M., Lienert, J., Eds.; IWA Publishing: London, UK, 2013; pp. 29–44.
17. Jenssen, T.K.; Kongshaug, G. *Energy Consumption and Greenhouse Gas Emissions in Fertiliser Production*; Proceeding, No. 509; The International Fertilizer Society: Paris, France, 2003.
18. European Commission Proposal for a Directive of the European Parliament and of the Council Concerning urban Wastewater Treatment (Recast) 541. 2022. Available online: [https://environment.ec.europa.eu/publications/proposal-revised-urban-wastewater-treatment-directive\\_en](https://environment.ec.europa.eu/publications/proposal-revised-urban-wastewater-treatment-directive_en) (accessed on 25 September 2023).
19. van Eekert, M.; Weijma, J.; Verdoes, N.; de Buissonjé, F.; Reitsma, B.; van den Bulk, J.; van Gastel, J. *Explorative Research on Innovative Nitrogen Recovery*; STOWA Report 51; Stichting Toegepast Onderzoek Waterbeheer: Amersfoort, The Netherlands, 2012.
20. Ganrot, Z. Use of zeolites for improved nutrient recovery from decentralized domestic wastewater. In *Handbook of Natural Zeolites*; Vassilis, J., Antonis, A.Z., Eds.; Bentham Science Publishers: Singapore, 2012; Chapter 17; pp. 410–435.
21. Bandala, E.R.; Liu, A.; Wijesiri, B.; Zeidman, A.B.; Goonetilleke, A. Emerging materials and technologies for landfill leachate treatment: A critical review. *Environ. Pollut.* **2021**, *291*, 118133. [[CrossRef](#)] [[PubMed](#)]
22. Ferrel-Luna, R.; García-Arreola, M.E.; González-Rodríguez, L.M.; Oredo-Cancino, M.; Escárcega-González, C.E.; de Haro-Del Río, D.A. Reducing toxic element leaching in mine tailings with natural zeolite clinoptilolite. *Environ. Sci. Pollut. Res.* **2023**. [[CrossRef](#)] [[PubMed](#)]
23. Helfferich, F. *Ion Exchange*; Dover Publishing: New York, NY, USA, 1995.
24. Inglezakis, V.J. The concept of “capacity” in zeolite ion-exchange systems. *J. Colloid. Inter. Sci.* **2005**, *281*, 68–79. [[CrossRef](#)]
25. Coombs, D.S.; Alberti, A.; Armbruster, T.; Artioli, G.; Colella, C.; Galli, E.; Grice, J.D.; Liebau, F.; Mandarino, J.A.; Minato, H.; et al. Recommended nomenclature for zeolite minerals: Report of the subcommittee on zeolites of the international mineralogical association, commission on new minerals and mineral names. *Can. Mineral.* **1997**, *35*, 1571–1606.
26. Derbe, T.; Temesgen, S.; Bitew, M. A Short Review on Synthesis, Characterization, and Applications of Zeolites. *Hindawi Adv. Mater. Sci. Eng.* **2021**, *2021*, 6637898. [[CrossRef](#)]
27. Wan, W.; Su, J.; Zou, X.D.; Wilhammar, T. Transmission electron microscopy as an important tool for characterization of zeolite structures. *Inorg. Chem. Front.* **2018**, *5*, 2836. [[CrossRef](#)]
28. Tsai, Y.T.; Huang, E.; Li, Y.; Hung, H.; Jiang, J.; Liu, T.; Fang, J.; Chen, H. Raman Spectroscopic Characteristics of Zeolite Group Minerals. *Minerals* **2021**, *11*, 167. [[CrossRef](#)]
29. Wang, T.; Luo, S.; Tompsett, G.A.; Timko, M.T.; Fan, W.; Auerbach, S.M. Critical Role of Tricyclic Bridges Including Neighboring Rings for Understanding Raman Spectra of Zeolites. *J. Am. Chem. Soc.* **2019**, *141*, 20318–20324. [[CrossRef](#)]
30. van Vreeswijk, S.H.; Weckhuysen, B.M. Emerging analytical methods to characterize zeolite-based materials. *Natl. Sci. Rev.* **2022**, *9*, nwac047. [[CrossRef](#)]
31. Barelocher, C.; McCuster, L.B.; Olson, H.D. *Atlas of Zeolite Framework Types*, 6th ed.; Elsevier: Amsterdam, The Netherlands, 2007.
32. Yu, J. Synthesis of zeolites. In *Introduction to Zeolite Science and Practice*, 3rd ed.; Čejka, J., Hv, B., Corma, A., Schüth, F., Eds.; Elsevier: Amsterdam, The Netherlands, 2007; Volume 168, Chapter 3.

33. Brännvall, E.; Kumpiene, J. Fly ash in landfill top covers—A review. *Environ. Sci. Proc. Impacts* **2016**, *18*, 11–21. [[CrossRef](#)]
34. Cundy, C.S.; Cox, P.A. The hydrothermal synthesis of zeolites: Precursors, intermediates and reaction mechanism. *Microp. Mesop. Mater.* **2005**, *82*, 1–78. [[CrossRef](#)]
35. Na, K.; Choi, M.; Ryoo, R. Recent advances in the synthesis of hierarchically nanoporous zeolites. *Microp. Mesop. Mater.* **2013**, *166*, 3–19. [[CrossRef](#)]
36. Gao, M.; Ma, Q.; Lin, Q.; Chang, J.; Bao, W.; Ma, M. Combined modification of fly ash with  $\text{Ca}(\text{OH})_2/\text{Na}_2\text{FeO}_4$  and its adsorption of Methyl orange. *App. Surf. Sci.* **2015**, *359*, 323–330. [[CrossRef](#)]
37. Perez-Ramirez, J.; Verboekend, D.; Bonilla, A.; Abello, S. Zeolite catalysts with tunable hierarchy factor by pore-growth moderators. *Adv. Funct. Mater.* **2009**, *19*, 3972. [[CrossRef](#)]
38. Ivanova, I.I.; Knyazeva, E.E. Micro-mesoporous materials obtained by zeolite recrystallization: Synthesis, characterization and catalytic applications. *Chem. Soc. Rev.* **2013**, *42*, 3671–3688. [[CrossRef](#)]
39. Hanache, L.E.; Sundermann, L.; Lebeau, B.; Toufaily, J.; Hamieh, T.; Daou, T.J. Surfactant-modified MFI-type nanozeolites: Super-adsorbents for nitrate removal from contaminated water. *Microp. Mesop. Mater.* **2019**, *283*, 1–13. [[CrossRef](#)]
40. Schick, J.; Daou, T.J.; Caulet, P.; Paillaud, J.L.; Patarin, J.; Mangold-Callarec, C. Surfactant-modified MFI nanosheets: A high capacity anion-exchanger. *Chem. Comm.* **2011**, *47*, 902–904. [[CrossRef](#)]
41. Hanache, L.E.; Lebeau, B.; Nouali, H.; Toufaily, J.; Hamieh, T.; Daou, T.J. Performance of surfactant-modified \*BEA-type zeolite nanosponges for the removal of nitrate in contaminated water: Effect of the external surface. *J. Hazard. Mater.* **2019**, *364*, 206–217. [[CrossRef](#)]
42. Mao, Y.; Wu, H.; Wang, W.; Jia, M.; Che, X. Pretreatment of municipal solid waste incineration fly ash and preparation of solid waste source sulphoaluminate cementitious material. *J. Hazard. Mater.* **2020**, *385*, 121580. [[CrossRef](#)] [[PubMed](#)]
43. Li, Y.; Cui, R.; Yang, T.; Zhai, Z.; Li, R. Distribution characteristics of heavy metals in different size fly ash from a sewage sludge circulating fluidized bed incinerator. *Energy Fuels* **2017**, *31*, 2044–2051. [[CrossRef](#)]
44. Fabricius, A.-L.; Renner, M.; Voss, M.; Funk, M.; Perfull, A.; Gehring, F.; Graf, R.; Fromm, S.; Duester, L. Municipal waste incineration fly ashes: From a multi-element approach to market potential evaluation. *Environ. Sci. Eur.* **2020**, *32*, 88. [[CrossRef](#)] [[PubMed](#)]
45. Bodéan, F.; Deniard, P. Characterization of flue gas cleaning residues from European solid waste incinerators: Assessment of various Ca-based sorbent processes. *Chemosphere* **2003**, *51*, 335–347. [[CrossRef](#)] [[PubMed](#)]
46. Chiang, K.-Y.; Jih, J.-C.; Chien, M.-D. The acid extraction of metals from municipal solid waste incinerator products. *Hydrometallurgy* **2008**, *93*, 16–22. [[CrossRef](#)]
47. Zhu, J.; Hao, Q.; Chen, J.; Hu, M.; Tu, T.; Jiang, C. Distribution characteristics and comparison of chemical stabilization ways of heavy metals from MSW incineration fly ashes. *Waste Manag.* **2020**, *113*, 488–496. [[CrossRef](#)]
48. Saakshy, K.; Singh, A.B.; Gupta Sharma, A.K. Fly ash as low cost adsorbent for treatment of effluent of handmade paper industry—Kinetic and modelling studies for direct black dye. *J. Clean. Prod.* **2016**, *112*, 1227–1240. [[CrossRef](#)]
49. Wesche, K. *Fly Ash in Concrete Properties and Performance*; RILEM Report 7; International Union of Testing and Research Laboratories: France; London, UK, 1991; p. 356.
50. Chen, Z.; Lu, S.; Tang, M.; Ding, J.; Buekens, A.; Yang, J.; Qiu, Q.; Yan, J. Mechanical activation of fly ash from MSWI for utilization in cementitious materials. *Waste Manag.* **2019**, *88*, 182–190. [[CrossRef](#)]
51. Fan, X.F.; Yuan, R.; Gan, M.; Ji, Z.; Sun, Z. Subcritical hydrothermal treatment of municipal solid waste incineration fly ash: A review. *Sci. Total Environ.* **2023**, *865*, 160745. [[CrossRef](#)]
52. Kim, S.Y.; Tanaka, N.; Matsuto, T.; Tojo, Y. Leaching behaviour of elements and evaluation of pre-treatment methods for municipal solid waste incinerator residues in column leaching tests. *Waste Manag. Res.* **2005**, *23*, 220–229. [[CrossRef](#)] [[PubMed](#)]
53. Kasina, M.; Kowalski, P.R.; Kajdas, B.; Michalik, M. Assessment of valuable and critical elements recovery potential in ashes from processes of solid municipal waste and sewage sludge thermal treatment. *Resources* **2020**, *9*, 131. [[CrossRef](#)]
54. Fan, Y.; Zhang, F.-S.; Zhu, J.; Liu, Z. Effective utilization of waste ash from MSW and coal co-combustion power plant—Zeolite synthesis. *J. Hazard. Mater.* **2008**, *153*, 382–388. [[CrossRef](#)] [[PubMed](#)]
55. Ohbuchi, A.; Koike, Y.; Nakamura, T. Crystal morphology analysis for heavy elements in municipal solid waste incineration fly ash and bottom ash by X-ray characterization techniques. *Anal. Sci.* **2020**, *6*, 471–477. [[CrossRef](#)] [[PubMed](#)]
56. Siddique, R. Utilization of municipal solid waste (MSW) ash in cement and mortar. *Resour. Conserv. Recycl.* **2010**, *54*, 1037–1047. [[CrossRef](#)]
57. Kowalski, P.R.; Kasina, M.; Michalik, M. Metallic elements fractionation in municipal solid waste incineration residues. *Energy Procedia* **2016**, *97*, 31–36. [[CrossRef](#)]
58. Weibel, G.; Eggenberger, U.; Schlumberger, S.; Mäder, U.K. Chemical associations and mobilization of heavy metals in fly ash from municipal solid waste incineration. *Waste Manag.* **2017**, *62*, 147–159. [[CrossRef](#)]
59. Rani, D.A.; Boccaccini, A.R.; Deegan, D.; Cheeseman, C.R. Air pollution control residues from waste incineration: Current UK situation and assessment of alternative technologies. *Waste Manag.* **2008**, *28*, 2279–2292. [[CrossRef](#)] [[PubMed](#)]
60. Saikia, N.; Kato, S.; Kojima, T. Production of cement clinkers from municipal solid waste incineration (MSWI) fly ash. *Waste Manag.* **2007**, *27*, 1178–1189. [[CrossRef](#)]
61. Wan, X.; Wang, W.; Ye, T.; Guo, Y.; Gao, X. A study on the chemical and mineralogical characterization of MSWI fly ash using a sequential extraction procedure. *J. Hazard. Mater.* **2006**, *134*, 197–201. [[CrossRef](#)]

62. IAWG (International Ash Working Group); Chandler, A.J.; Eighmy, T.T.; Hartlén, J.; Hjelmar, O.; Kosson, D.S.; Sawell, S.E.; van der Sloot, H.; Vehlow, J. *Municipal Solid Waste Incinerator Residues; Studies in Environmental Science*; Elsevier: Amsterdam, The Netherlands, 1997; Volume 67.
63. Zhao, Y.; Li, H. Understanding municipal solid waste production and diversion factors utilizing deep-learning methods. *Util. Policy* **2023**, *83*, 101612. [[CrossRef](#)]
64. Joseph, A.M.; Snellings, R.; van den Heede, P.; Matthys, S.; de Belie, N. The use of municipal solid waste incineration ash in various building materials: A Belgian Point of View. *Materials* **2018**, *11*, 141. [[CrossRef](#)]
65. Deng, L.; Xu, Q.; Wu, H. Synthesis of zeolite-like material by hydrothermal and fusion methods using municipal solid waste fly ash. *Proc. Environ. Sci.* **2016**, *31*, 662–667. [[CrossRef](#)]
66. Eighmy, T.T.; Eusden, J.D.; Krzanowski, J.E.; Domiango, D.S.; Stampfli, D.; Martin, P.M.; Erickson, P.M. Comprehensive approach toward understanding element speciation and leaching behavior in municipal solid waste incineration electrostatic precipitator ash. *Environ. Sci. Technol.* **1995**, *29*, 629–646. [[CrossRef](#)]
67. Hjelmar, O. Disposal strategies for municipal solid waste incineration residues. *J. Hazard. Mater.* **1996**, *47*, 345–368. [[CrossRef](#)]
68. Forestier, L.L.; Libourel, G. Characterization of flue gas residues from municipal solid waste combustors. *Environ. Sci. Technol.* **1998**, *32*, 2250–2256. [[CrossRef](#)]
69. Quina, M.J.; Bordado, J.C.; Quinta-Ferreira, R.M. Treatment and use of air pollution control residues from MSW incineration: An overview. *Waste Manag.* **2008**, *28*, 2097–2121. [[CrossRef](#)] [[PubMed](#)]
70. Song, G.J.; Kim, K.; Seo, Y.; Kim, S. Characteristics of ashes from different locations at the MSW incinerator equipped with various air pollution control devices. *Waste Manag.* **2004**, *24*, 99–106. [[CrossRef](#)]
71. Vavva, C.; Voutsas, E.; Magoulas, K. Process development for chemical stabilization of fly ash from municipal solid waste incineration. *Chem. Eng. Res. Des.* **2017**, *125*, 57–71. [[CrossRef](#)]
72. Li, X.; Chen, Q.; Zhou, Y.; Tyrer, M.; Yu, Y. Stabilization of heavy metals in MSWI fly ash using silica fume. *Waste Manag.* **2014**, *34*, 2494–2504. [[CrossRef](#)]
73. Karlfeldt, K.; Steenari, B.-M. Assessment of metal mobility in MSW incineration ashes using water as the reagent. *Fuel* **2007**, *86*, 1983–1993. [[CrossRef](#)]
74. Alba, N.; Gasso, S.; Lacorte, T.; Baldasano, J.M. Characterization of municipal solid waste incineration residues from facilities with different air pollution control systems. *J. Air Waste Manag. Assoc.* **1997**, *47*, 1170–1179. [[CrossRef](#)]
75. Romero, M.; Rincon, J.M.; Rawlings, R.D.; Boccaccini, A.R. Use of vitrified urban incinerator waste as raw material for production of sintered glass–ceramics. *Mat. Res. Bull.* **2001**, *36*, 383–395. [[CrossRef](#)]
76. Cheng, T.W.; Chen, Y.S. Characterisation of glass–ceramics made from incinerator fly ash. *Ceram. Intern.* **2004**, *30*, 343–349. [[CrossRef](#)]
77. Miyake, M.; Tamura, C.; Matsuda, M. Resource recovery of waste incineration fly ash: Synthesis of zeolites a and p. *J. Am. Ceram. Soc.* **2002**, *85*, 1873–1875. [[CrossRef](#)]
78. Yang, G.C.C.; Yang, T. Synthesis of zeolites from municipal incinerator fly ash. *J. Hazard. Mater.* **1998**, *62*, 75–89. [[CrossRef](#)]
79. Bac, B.H.; Song, Y.; Moon, Y.; Kim, M.H.; Kang, I.M. Effective utilization of incinerated municipal solid waste incineration ash: Zeolitic material synthesis and silica extraction. *Waste Manag. Res.* **2010**, *28*, 714–722. [[CrossRef](#)]
80. Lin, Y.-J.; Chen, J.-C. Resourcization and valorization of waste incineration fly ash for the synthesis of zeolite and applications. *J. Environ. Chem. Eng.* **2021**, *9*, 106549. [[CrossRef](#)]
81. Qiu, Q.; Jiang, X.; Lv, G.; Lu, S.; Ni, M. Stabilization of heavy metals in municipal solid waste incineration fly ash in circulating fluidized bed by microwave-assisted hydrothermal treatment with additives. *Energy Fuels* **2016**, *30*, 7588–7595. [[CrossRef](#)]
82. Qiu, Q.; Jiang, X.; Chen, Z.; Lu, S.; Ni, M. Microwave-assisted hydrothermal treatment with soluble phosphate added for heavy metals solidification in MSWI fly ash. *Energy Fuels* **2017**, *31*, 5222–5232. [[CrossRef](#)]
83. Chen, Q.; Long, L.; Liu, X.; Jiang, X.; Chi, Y.; Yan, J.; Zhao, X.; Kong, L. Low-toxic zeolite fabricated from municipal solid waste incineration fly ash via microwave-assisted hydrothermal process with fusion pretreatment. *J. Mater. Cycles Waste Manag.* **2020**, *22*, 1196–1207. [[CrossRef](#)]
84. Wang, K.-S.; Chiang, K.-Y.; Lin, K.-L.; Sun, C.-J. Effects of a water-extraction process on heavy metal behavior in municipal solid waste incinerator fly ash. *Hydrometallurgy* **2001**, *62*, 73–81. [[CrossRef](#)]
85. Chuai, X.; Yang, Q.; Zhang, T.; Zhao, Y.; Wang, J.; Zhao, G.; Cui, X.; Zhang, Y.; Zhang, T.; Xiong, Z.; et al. Speciation and leaching characteristics of heavy metals from municipal solid waste incineration fly ash. *Fuel* **2022**, *328*, 125338. [[CrossRef](#)]
86. Todorovic, J.; Ecke, H.; Lagerkvist, A. Solidification with water as a treatment method for air pollution control residues. *Waste Manag.* **2003**, *23*, 621–629. [[CrossRef](#)] [[PubMed](#)]
87. Glasser, F.P. Fundamental aspects of cement solidification and stabilisation. *J. Hazard. Mater.* **1997**, *52*, 151–170. [[CrossRef](#)]
88. Kiyaki, T.; Matsuda, M.; Wajima, T.; Matsui, T. Synthesis of zeolite from municipal solid waste incineration fly ash. *Waste Manag.* **2002**, *22*, 893–899. [[CrossRef](#)]
89. Shoppert, A.A.; Loginova, I.V.; Chaikin, L.I.; Rogozhnikov, D.A. Alkali fusion leaching method for comprehensive processing of fly ash. *KnE Mater. Sci.* **2017**, *2*, 89–96. [[CrossRef](#)]
90. Verboekend, D.; Pérez-Ramírez, J. Design of hierarchical zeolite catalysts by desilication. *Catal. Sci. Technol.* **2011**, *1*, 879–890. [[CrossRef](#)]

91. Sayehi, M.; Tounsi, H.; Garbarino, G.; Riani, P.; Busca, G. Reutilization of silicon- and aluminum- containing wastes in the perspective of the preparation of SiO<sub>2</sub>-Al<sub>2</sub>O<sub>3</sub> based porous materials for adsorbents and catalysts. *Waste Manag.* **2020**, *103*, 146–158. [CrossRef]
92. Boukerche, I.; Djerada, S.; Benmansoura, L.; Tifoutia, L.; Saleh, K. Degradability of aluminum in acidic and alkaline solutions. *Corros. Sci.* **2014**, *78*, 343–352. [CrossRef]
93. Lenntech. Iron Removal by Physical-Chemical Ways. Available online: <https://www.lenntech.com/processes/iron-manganese/iron/iron-removal-physicalchemical-way.htm> (accessed on 25 October 2023).
94. Faust, S.D.; Aly, O.M. *Chemistry of Water Treatment*; CRC Press: Boca Raton, FL, USA, 1988; p. 224.
95. Okada, K.; Arimitsu, N.; Kameshima, Y.; Nakajima, A.; MacKenzie, K.J.D. Preparation of porous silica from chlorite by selective acid leaching. *Appl. Clay Sci.* **2005**, *30*, 116–124. [CrossRef]
96. Temuujin, J.; Okada, K.; MacKenzie, K.J.D. Preparation of porous silica from vermiculite by selective leaching. *Appl. Clay Sci.* **2003**, *22*, 187–195. [CrossRef]
97. Adans, Y.F.; Martins, A.R.; Coelho, R.E.; das Virgens, C.F.; Ballarini, A.D.; Carvalho, L.S. A simple way to produce  $\alpha$ -alumina from aluminum cans by precipitation reactions. *Mat. Res.* **2016**, *19*, 977–982. [CrossRef]
98. Zong, Y.Z.; Chen, W.; Liu, Z. Extraction of alumina from high-alumina coal ash using an alkaline hydrothermal method. *SN Appl. Sci.* **2019**, *1*, 783. [CrossRef]
99. Zhao, X.; Zeng, L.; Guo, J.; Zhu, Q.; Huang, Z.; Lin, L.; Chen, X.; Cao, J.; Zhou, Z. Efficient separation and comprehensive extraction of aluminum, silicon, and iron from coal fly ash by a cascade extraction method. *J. Clean. Prod.* **2023**, *406*, 137090. [CrossRef]
100. Zhu, P.; Dai, H.; Han, L.; Xu, X.; Cheng, L.; Wang, Q.; Shi, Z. Aluminum extraction from coal ash by a two-step acid leaching method. *J. Zhejiang Univ.-Sci. A (Appl. Phys. Eng.)* **2015**, *16*, 161–169. [CrossRef]
101. Shoppert, A.; Veleev, D.; Loginova, I.; Chaikin, L. Complete extraction of amorphous aluminosilicate from coal fly ash by alkali leaching under atmospheric pressure. *Metals* **2020**, *10*, 1684. [CrossRef]
102. Kumar, A.; Agrawal, S.; Dhawan, N. Processing of coal fly ash for the extraction of alumina values. *J. Sustain. Metall.* **2020**, *6*, 294–306. [CrossRef]
103. Wu, C.; Yu, H.; Zhang, H. Extraction of aluminum by pressure acid-leaching method from coal fly ash. *Trans. Nonferrous Met. Soc. China* **2012**, *22*, 2282–2288. [CrossRef]
104. Zhang, B.H.; Wu, D.Y.; Wang, C.; He, S.B.; Zhang, Z.J.; Kong, H.N. Simultaneous removal of ammonium and phosphate by zeolite synthesized from coal fly ash as influenced by acid treatment. *J. Environ. Sci.* **2007**, *19*, 540–554. [CrossRef]
105. Wajima, T.; Ikegami, Y. Synthesis of zeolitic materials from waste porcelain at low temperature via a two-step alkali conversion. *Ceram. Int.* **2007**, *33*, 1269–1274. [CrossRef]
106. Lin, Y.-J.; Weng, C.-H.; Chen, C.-H. Synthesis of zeolite P from coal fly ash and its application in the removal of ammonium and phosphate ions. *Environ. Sci. Pollut. Res.* **2018**, *25*, 8339–8350.
107. Jin, Y.; Ma, X.; Jiang, X.; Liu, H.; Li, X.; Yan, J.; Cen, K. Effects of hydrothermal treatment on the major heavy metals in fly ash from municipal solid waste incineration. *Energy Fuels* **2013**, *27*, 394–400. [CrossRef]
108. Mossop, K.F.; Davidson, C.M. Comparison of original and modified BCR sequential extraction procedures for the fractionation of copper, iron, lead, manganese and zinc in soils and sediments. *Anal. Chim. Acta* **2003**, *478*, 111–118. [CrossRef]
109. Bayuseno, A.P.; Schmahl, W.W.; Muellejans, T. Hydrothermal processing of MSWI fly ash-towards new stable minerals and fixation of heavy metals. *J. Hazard. Mater.* **2009**, *167*, 250–259. [CrossRef]
110. Weibel, G.; Eggenberger, U.; Dmitrii, A.K.; Hummel, W.; Schlumberger, S.; Klink, W.; Fisch, M.; Mäder, U.K. Extraction of heavy metals from MSWI fly ash using hydrochloric acid and sodium chloride solution. *Waste Manag.* **2018**, *76*, 457–471. [CrossRef] [PubMed]
111. AWEL. *Stand der Technik für die Aufbereitung von Rauchgasreinigungsrückständen (RGRR) aus Kehrrechtverbrennungsanlagen*. Amt für Abfall, Wasser, Energie und Luft Abteilung Abfallwirtschaft und Betriebe Walchetur; Baudirektion Kanton Zürich: Zurich, Switzerland, 2013; p. 24.
112. Vassilev, S.V.; Vassileva, C.G. A new approach for the classification of coal fly ashes based on their origin, composition, properties, and behaviour. *Fuel* **2007**, *86*, 1490–1512. [CrossRef]
113. Lin, Y.-J.; Chen, J.-C. The optimum operating conditions for the synthesis of zeolite from waste incineration fly ash by alkali fusion and hydrothermal methods. *Int. Sch. Sci. Res. Innov.* **2018**, *12*, 669–675.
114. Xie, J.; Hu, Y.; Chen, D.; Zhou, B. Hydrothermal treatment of MSWI fly ash for simultaneous dioxins decomposition and heavy metal stabilization. *Front. Environ. Sci. Eng. China* **2010**, *4*, 108–115. [CrossRef]
115. Shi, D.; Hu, C.; Zhang, J.; Li, P.; Zhang, C.; Wang, X.; Ma, H. Silicon-aluminum additives assisted hydrothermal process for stabilization of heavy metals in fly ash from MSW incineration. *Fuel Process. Technol.* **2017**, *165*, 44–53. [CrossRef]
116. Qiu, Q.; Jiang, X.; Lv, G.; Lu, S.; Ni, M. Effects of microwave-assisted hydrothermal treatment on the major heavy metals of municipal solid waste incineration fly ash in a circulating fluidized bed. *Energy Fuels* **2016**, *30*, 5945–5952. [CrossRef]
117. Tong, H.; Shi, D.; Cai, H.; Liu, J.; Lv, M.; Gu, L.; Luo, L.; Wang, B. Novel hydroxyapatite (HAP)-assisted hydrothermal solidification of heavy metals in fly ash from MSW incineration: Effect of HAP liquid-precursor and HAP seed crystal derived from eggshell waste. *Fuel Process. Technol.* **2022**, *236*, 107400. [CrossRef]
118. Xu, Z.; Liang, Z.; Shao, H.; Zhao, Q. Heavy metal stabilization in MSWI fly ash using an additive-assisted microwave hydrothermal method. *J. Ind. Eng. Chem.* **2023**, *117*, 352–360. [CrossRef]

119. Kulkarni, P.S.; Crespo, J.G.; Afonso, C.A.M. Dioxins sources and current remediation technologies—A review. *Environ. Int.* **2008**, *34*, 139–153. [[CrossRef](#)]
120. Xue, Y.; Liu, X. Detoxification, solidification and recycling of municipal solid waste incineration fly ash: A review. *Chem. Eng. J.* **2021**, *420*, 130349. [[CrossRef](#)]
121. Hwang, I.-H.; Aoyama, H.; Matsuto, T.; Nakagishi, T.; Matsuo, T. Recovery of solid fuel from municipal solid waste by hydrothermal treatment using subcritical water. *Waste Manag.* **2012**, *32*, 410–416. [[CrossRef](#)]
122. Toor, S.S.; Rosendahl, L.; Rudolf, A. Hydrothermal liquefaction of biomass: A review of subcritical water technologies. *Energy* **2011**, *36*, 2328–2342. [[CrossRef](#)]
123. Jin, Y.-Q.; Ma, X.-J.; Jiang, X.-G.; Liu, H.-M.; Li, X.-D.; Yan, J.-H. Hydrothermal degradation of polychlorinated dibenzop-dioxins and polychlorinated dibenzofurans in fly ash from municipal solid waste incineration under non-oxidative and oxidative conditions. *Energy Fuel* **2013**, *27*, 414–420. [[CrossRef](#)]
124. Yamaguchi, H.; Shibuya, E.; Kanamaru, Y.; Uyama, K.; Nishioka, M.; Yamasaki, N. Hydrothermal decomposition of PCDDs/PCDFs in MSWI fly ash. *Chemosphere* **1996**, *32*, 203–208. [[CrossRef](#)]
125. Hu, Y.; Zhang, P.; Chen, D.; Zhou, B.; Li, J.; Li, X.-W. Hydrothermal treatment of municipal solid waste incineration fly ash for dioxin decomposition. *J. Hazard. Mater.* **2012**, *207*, 79–85. [[CrossRef](#)]
126. Chen, X.; Khunjar, W.; Jun, Z.; Li, J.; Yu, X.; Zhang, Z. Synthesis of nano-zeolite from coal fly ash and its potential for nutrient sequestration from anaerobically digested swine wastewater. *Bioresour. Technol.* **2012**, *110*, 79–85. [[CrossRef](#)]
127. Qiu, Q.; Chen, Q.; Jiang, X.; Lv, G.; Chen, Z.; Lu, S.; Ni, M.; Yan, J.; Lin, X.; Song, H.; et al. Improving microwave-assisted hydrothermal degradation of PCDD/Fs in fly ash with added Na<sub>2</sub>HPO<sub>4</sub> and water-washing pretreatment. *Chemosphere* **2019**, *220*, 1118–1125. [[CrossRef](#)] [[PubMed](#)]
128. Pan, T.; Wu, Z.; Yip, A.C.K. Advances in the Green Synthesis of Microporous and Hierarchical Zeolites: A Short Review. *Catalysts* **2019**, *9*, 274. [[CrossRef](#)]
129. Liu, Z.; Okabe, K.; Anand, C.; Yonezawa, Y.; Zhu, J.; Yamada, H.; Endo, A.; Yanaba, Y.; Yoshikawa, T.; Ohara, K.; et al. Continuous flow synthesis of ZSM-5 zeolite on the order of seconds. *Proc. Natl. Acad. Sci. USA* **2016**, *113*, 14091–14096. [[CrossRef](#)] [[PubMed](#)]
130. López-Delgado, A.; Robla, J.I.; Padilla, I.; López-Andrés, S. Zero-waste process for the transformation of a hazardous aluminum waste into a raw material to obtain zeolites. *J. Clean. Prod.* **2020**, *255*, 120178. [[CrossRef](#)]
131. Colella, C.; Wise, W.S. The IZA Handbook of Natural Zeolites: A tool of knowledge on the most important family of porous minerals. *Microp. Mesop. Mater.* **2014**, *189*, 4–10. [[CrossRef](#)]
132. de Magalhães, L.F.; da Silva, G.R.; Peres, A.C.E. Zeolite application in wastewater treatment. *Adsorp. Sci. Technol.* **2022**. [[CrossRef](#)]
133. Moshoeshe, M.; Nadiye-Tabbiruka, M.S.; Obuseng, V. A review of the chemistry, structure, properties and applications of zeolites. *Am. J. Mater. Sci.* **2017**, *7*, 196–221. [[CrossRef](#)]
134. Mumpton, F.A. La roca magica: Uses of natural zeolites in agriculture and industry. *Proc. Natl. Acad. Sci. USA* **1999**, *96*, 3463–3470. [[CrossRef](#)] [[PubMed](#)]
135. Yue, B.; Liu, S.; Chai, Y.; Wu, G.; Guan, N.; Li, L. Zeolites for separation: Fundamental and application. *J. Energy Chem.* **2022**, *71*, 288–303. [[CrossRef](#)]
136. Pérez-Botella, E.; Palomino, M.; Valencia, S.; Rey, F. *Nanoporous Materials for Gas Storage*; Springer: Singapore, 2019; pp. 173–208.
137. Lin, H.; Wu, X.; Zhu, J. Kinetics, equilibrium, and thermodynamics of ammonium sorption from swine manure by natural chabazite. *Sep. Sci. Technol.* **2015**, *51*, 202–213. [[CrossRef](#)]
138. Dong, L.D.; Zhu, Z.; Qiu, Y.; Zhao, J. Removal of lead from aqueous solution by hydroxyapatite/magnetite composite adsorbent. *Chem. Eng. J.* **2010**, *165*, 827–834. [[CrossRef](#)]
139. Langmuir, I. The constitution and fundamental properties of solid sand liquids. Part-I. Solids. *J. Am. Chem. Soc.* **1916**, *38*, 2221–2295. [[CrossRef](#)]
140. Freundlich, H. *Colloid and Capillary Chemistry*; Methuen: London, UK, 1926; p. 993.
141. Millar, G.J.; Winnett, A.; Thompson, T.; Couperthwaite, S.J. Equilibrium studies of ammonium exchange with Australian natural zeolites. *J. Water Process Eng.* **2016**, *9*, 47–57. [[CrossRef](#)]
142. Sprynskyy, M.; Buszewski, B.; Terzyk, A.P.; Namieśnik, J. Study of the selection mechanism of heavy metal (Pb<sup>2+</sup>, Cu<sup>2+</sup>, Ni<sup>2+</sup>, and Cd<sup>2+</sup>) adsorption on clinoptilolite. *J. Colloid Interface Sci.* **2006**, *304*, 21–28. [[CrossRef](#)] [[PubMed](#)]
143. Ugurlu, M.; Karaoglu, M.H. Adsorption of ammonium from an aqueous solution by fly ash and sepiolite: Isotherm, kinetic and thermodynamic analysis. *Microp. Mesop. Mater.* **2011**, *139*, 173–178. [[CrossRef](#)]
144. Ji, X.D.; Zhang, M.L.; Ke, Y.Y.; Song, Y.C. Simultaneous immobilization of ammonium and phosphate from aqueous solution using zeolites synthesized from fly ashes. *Water Sci. Technol.* **2013**, *67*, 6. [[CrossRef](#)] [[PubMed](#)]
145. Makgabutlane, B.; Nthunya, L.N.; Musyoka, N.; Dladla, B.S.; Nxumalo, E.N.; Mhlanga, S.D. Microwave assisted synthesis of coal fly ash-based zeolites for removal of ammonium from urine. *RSC Adv.* **2020**, *10*, 2416–2427. [[CrossRef](#)]
146. Zhang, M.; Zhang, H.; Xu, D.; Han, L.; Niu, D.; Zhang, L.; Wu, W.; Tianm, B. Ammonium removal from aqueous solution by zeolites synthesized from low-calcium and high-calcium fly ashes. *Desalination* **2011**, *277*, 46–53. [[CrossRef](#)]
147. Beler-Baykal, B.; Allar, A.D. Upgrading fertilizer production wastewater effluent quality for ammonium discharges through ion exchange with clinoptilolite. *Environ. Technol.* **2008**, *29*, 665–672. [[CrossRef](#)]
148. Liu, Y.; Yan, C.; Zhao, J.; Zhang, Z.; Wang, H.; Zhou, S. Synthesis of zeolite P1 from fly ash under solvent-free conditions for ammonium removal from water. *J. Clean. Prod.* **2018**, *202*, 11–22. [[CrossRef](#)]

149. Fu, H.; Li, Y.; Yu, Z.; Shen, J.; Li, J.; Zhang, M.; Ding, T.; Xu, L.; Lee, S.S. Ammonium removal using a calcined natural zeolite modified with sodium nitrate. *J. Hazard. Mater.* **2020**, *393*, 122481. [[CrossRef](#)] [[PubMed](#)]
150. Huang, X.; Wang, N.; Kang, Z.; Yang, X.; Pan, M. An Investigation into the Adsorption of Ammonium by Zeolite-Magnetite Composites. *Minerals* **2022**, *12*, 256. [[CrossRef](#)]
151. Shaban, M.; AbuKhadra, M.R.; Nasief, F.M.; El-Salam, H.M.A. Removal of Ammonia from Aqueous Solutions, Ground Water, and Wastewater Using Mechanically Activated Clinoptilolite and Synthetic Zeolite-A: Kinetic and Equilibrium Studies. *Water Air Soil Pollut.* **2017**, *228*, 450. [[CrossRef](#)]
152. Otal, E.; Vilches, L.F.; Luna, Y.; Poblete, R.; García-Maya, J.M.; Fernández-Pereira, C. Ammonium ion adsorption and settleability improvement achieved in a synthetic zeolite-amended activated sludge. *Chin. J. Chem. Eng.* **2013**, *21*, 1062–1068. [[CrossRef](#)]
153. Franus, M.; Wdowin, M.; Bandura, L.; Franus, W. Removal of environmental pollutions using zeolites from fly ash: A review. *Fresenius Environ. Bull.* **2015**, *24*, 854–866.
154. Xie, J.; Wang, Z.; Fang, D.; Li, C.; Wu, D. Green synthesis of a novel hybrid sorbent of zeolite/lanthanum hydroxide and its application in the removal and recovery of phosphate from water. *J. Colloid Inter. Sci.* **2014**, *423*, 13–19. [[CrossRef](#)]
155. Hui, K.S.; Chao, C.Y.; Kot, S. Removal of mixed heavy metal ions in wastewater by zeolite 4A and residual products from recycled coal fly ash. *J. Hazard. Mater.* **2005**, *127*, 89–101. [[CrossRef](#)]
156. Alvarez-Ayuso, E.; Garcia-Sanchez, A.; Querol, X. Purification of metal electroplating waste waters using zeolites. *Water Res.* **2003**, *37*, 4855–4862. [[CrossRef](#)]
157. Nightingale, E.R. Phenomenological theory of ion solvation. Effective radii of hydrated ions. *J. Phys. Chem.* **1959**, *63*, 1381–1387. [[CrossRef](#)]
158. Marcus, Y. Thermodynamics of solvation of ions. Part 5.—Gibbs free energy of hydration at 298.15 K. *J. Chem. Soc. Faraday Trans.* **1991**, *87*, 2995–2999. [[CrossRef](#)]
159. Joseph, I.V.; Tosheva, L.; Doyle, A.M. Simultaneous removal of Cd(II), Co(II), Cu(II), Pb(II), and Zn(II) ions from aqueous solutions via adsorption on FAU-type zeolites prepared from coal fly ash. *J. Environ. Chem. Eng.* **2020**, *8*, 103895. [[CrossRef](#)]
160. Ibrahim, H.S.; Jamil, T.S.; Hegazy, E.Z. Application of zeolite prepared from Egyptian kaolin for the removal of heavy metals: II. Isotherm models. *J. Hazard. Mater.* **2010**, *182*, 842–847. [[CrossRef](#)] [[PubMed](#)]
161. Kesraoui-Ouki, S.; Cheeseman, C.R.; Perry, R. Natural zeolite utilization in pollution-control—A review of applications to metals effluents. *J. Chem. Technol. Biotechnol.* **1994**, *59*, 121–126. [[CrossRef](#)]
162. Oter, O.; Akcay, H. Use of natural clinoptilolite to improve water quality: Sorption and selectivity studies of lead(II), copper(II), zinc(II), and nickel(II). *Water Environ. Res.* **2007**, *79*, 329–335. [[CrossRef](#)] [[PubMed](#)]
163. Caputo, D.; Pepe, F. Experiments and data processing of ion exchange equilibria involving Italian natural zeolites: A review. *Microp. Mesop. Mater.* **2007**, *105*, 222–231. [[CrossRef](#)]
164. Bosso, S.T.; Enzweiler, J. Evaluation of heavy metal removal from aqueous solution onto scolecite. *Water Res.* **2002**, *36*, 4795–4800. [[CrossRef](#)]
165. Deng, Q.; Dhar, B.R.; Elbeshbishy, E.; Lee, H.S. Ammonium nitrogen removal from the permeates of anaerobic membrane bioreactors: Economic regeneration of exhausted zeolite. *Environ. Technol.* **2014**, *35*, 2008–2017. [[CrossRef](#)]
166. Lind, B.-B.; Ban, Z.; Byden, S. Nutrient recovery from human urine by struvite crystallization with ammonia adsorption on zeolite and wollastonite. *Biores. Technol.* **2000**, *73*, 169–174. [[CrossRef](#)]
167. Zhao, Y.; Niu, Y.; Hu, X.; Xi, B.; Peng, X.; Liu, W.; Guan, W.; Wang, L. Removal of ammonium ions from aqueous solutions using zeolite synthesized from red mud. *Desalination Water Treat.* **2016**, *57*, 4720–4731. [[CrossRef](#)]
168. Zanin, E.; Scapinello, J.; de Oliveira, M.; Rambo, C.L.; Franscescon, F.; Freitas, L.; Maria, J.; de Mello, M.; Fiori, M.A.; Oliveira, J.V.; et al. Adsorption of heavy metals from wastewater graphic industry using clinoptilolite zeolite as adsorbent. *Process. Saf. Environ. Prot.* **2017**, *105*, 194–200. [[CrossRef](#)]
169. Dal Bosco, S.M.; Jimenez, R.S.; Carvalho, W. Removal of toxic metals from wastewater by Brazilian natural scolecite. *J. Colloid Interface. Sci.* **2005**, *281*, 424–431. [[CrossRef](#)] [[PubMed](#)]
170. Ćurković, L.; Cerjan-Stefanović, Š.; Filipan, T. Metal ion exchange by natural and modified zeolites. *Water Res.* **1997**, *31*, 1379–1382. [[CrossRef](#)]
171. Pérez-Botella, E.; Valncia, S.; Rey, F. Zeolites in Adsorption Processes: State of the Art and Future Prospects. *Chem. Rev.* **2022**, *122*, 17647–17695. [[CrossRef](#)] [[PubMed](#)]
172. Margeta, K.; Zabukovec, N.; Siljeg, M.; Farkas, A. Natural zeolites in water treatment—How effective is their use. In *Water Treatment*; IntechOpen: London, UK, 2013; Chapter 5.
173. Haji, S.; Al-Buqaishi, B.A.; Bucheeri, A.A.; Bu-Ali, Q.; Al-Aseeri, M.; Ahmed, S. The dynamics and equilibrium of ammonium removal from aqueous solution by Na-Y zeolite. *Desalination Water Treat.* **2016**, *57*, 18992–19001. [[CrossRef](#)]
174. Walton, K.S.; Abney, M.B.; LeVan, M.D. CO<sub>2</sub> adsorption in Y and X zeolites modified by alkali metal cation exchange. *Microporous Mesoporous Mater.* **2006**, *91*, 78. [[CrossRef](#)]
175. Rabo, J.A.; Schoonover, M.W. Early discoveries in zeolite chemistry and catalysis at Union Carbide, and follow-up in industrial catalysis. *Appl. Catal. A* **2001**, *222*, 261–275. [[CrossRef](#)]
176. Bujnova, A.; Lesny, J. Sorption characteristics of zinc and cadmium by some natural, modified, and synthetic zeolites. *Electron. J. Chem. Technol. Biotechnol.* **2004**, *59*, 121–126.

177. Inglezakis, V.J.; Loizidou, M.M.; Grigoropoulou, H.P. Ion exchange studies on natural and modified zeolites and the concept of exchange site accessibility. *J. Colloid Inter. Sci.* **2004**, *275*, 570–576. [[CrossRef](#)] [[PubMed](#)]
178. Oren, A.H.; Kaya, A. Factors affecting adsorption characteristics of  $Zn^{2+}$  on two natural zeolites. *J. Hazard. Mater.* **2006**, *131*, 59–65. [[CrossRef](#)]
179. Kosmulski, M. The pH dependent surface charging and points of zero charge. VII. Update. *Adv. Colloid Inter. Sci.* **2018**, *251*, 115–138. [[CrossRef](#)]
180. Kosmulski, M. The pH dependent surface charging and points of zero charge. VIII. Update. *Adv. Colloid Inter. Sci.* **2020**, *275*, 102064. [[CrossRef](#)] [[PubMed](#)]
181. Monhemius, A.J. Precipitation diagrams for metal hydroxides, sulphides, arsenates and phosphates. *Trans. Inst. Min. Metall.* **1977**, *6*, 203–206.
182. Goscianska, J.; Ptaszkowska-Koniarz, M.; Frankowski, M.; Franus, M.; Panek, R.; Franus, W. Removal of phosphate from water by lanthanum-modified zeolites obtained from fly ash. *J. Colloid Inter. Sci.* **2018**, *513*, 72–81. [[CrossRef](#)] [[PubMed](#)]
183. Wu, D.Y.; Zhang, B.H.; Li, C.J.; Zhang, Z.J.; Kong, H.N. Simultaneous removal of ammonium and phosphate by zeolite synthesized from fly ash as influenced by salt treatment. *J. Colloid Inter. Sci.* **2006**, *304*, 300–306. [[CrossRef](#)] [[PubMed](#)]
184. Chen, J.G.; Kong, H.N.; Wu, D.Y.; Hu, Z.B.; Wang, Z.S.; Wang, Y.H. Removal of phosphate from aqueous solution by zeolite synthesized from fly ash. *J. Colloid Interface Sci.* **2006**, *300*, 491–497. [[CrossRef](#)]
185. Aylward, G.H.; Findlay, T.J.V. *SI Chemical Data*, 2nd ed.; John Wiley & Sons: Hoboken, NJ, USA, 1974.
186. Hamdi, N.; Srasra, E. Removal of phosphate ions from aqueous solution using Tunisian clays minerals and synthetic zeolite. *J. Environ. Sci.* **2012**, *24*, 617–623. [[CrossRef](#)]
187. Zhang, Y.; Kou, X.; Lu, H.; Lv, X. The feasibility of adopting zeolite in phosphorus removal from aqueous solutions. *Desalination Water Treat.* **2014**, *52*, 4298–4304. [[CrossRef](#)]
188. Alshameri, A.; Yan, C.; Lei, X. Enhancement of phosphate removal from water by  $TiO_2$ /Yemeni natural zeolite: Preparation, characterization and thermodynamic. *Microporous Mesoporous Mater.* **2014**, *196*, 145–157. [[CrossRef](#)]
189. Naghash, A.; Nezamzadeh-Ejehieh, A. Comparison of the efficiency of modified clinoptilolite with HDTMA and HDP surfactants for the removal of phosphate in aqueous solutions. *J. Ind. Eng. Chem.* **2015**, *31*, 185–191. [[CrossRef](#)]
190. Hermassi, M.; Valderrama, C.; Font, O.; Moreno, N.; Querol, X.; Batis, N.; Cortina, J. Phosphate recovery from aqueous solution by K-zeolite synthesized from fly ash for subsequent valorisation as slow release fertilizer. *Sci. Total Environ.* **2020**, *731*, 139002. [[CrossRef](#)]
191. Ciesla, J.; Franus, W.; Franus, M.; Kedziora, K.; Gluszczyk, J.; Szerement, J.; Jozefaciuk, G. Environmental-friendly modifications of zeolite to increase its sorption and anion exchange Properties, Physicochemical Studies of the Modified Materials. *Material* **2019**, *12*, 3213. [[CrossRef](#)] [[PubMed](#)]
192. Mokrzycki, J.; Fedyna, M.; Marzec, M.; Szerement, J.; Panek, R.; Klimek, A.; Bajda, T.; Mierzwa-Hersztek, M. Copper ion-exchanged zeolite X from fly ash as an efficient adsorbent of phosphate ions from aqueous solutions. *J. Environ. Chem. Eng.* **2022**, *10*, 108567. [[CrossRef](#)]
193. Mahmoodi, N.; Saffar-Dastgerdi, M.H. Zeolite nanoparticle as a superior adsorbent with high capacity: Synthesis, surface modification and pollutant adsorption ability from wastewater. *Microchem. J.* **2019**, *145*, 74–83. [[CrossRef](#)]
194. Swiderska-Dabrowska, R.; Schmidt, R.; Sikora, A. Effect of calcination temperature on chemical stability of zeolite modified by iron ions. In *Polish Environmental Engineering 2012*; Environmental Engineering Committee PAS, Ed.; Environmental Engineering Committee PAS: Lublin, Poland, 2012; pp. 307–317.
195. Glassman, H.N. Surface active agents and their application in bacteriology. *Bacteriol. Rev.* **1948**, *12*, 105. [[CrossRef](#)]
196. Reeve, P.J.; Fallowfield, H.J. Natural and surfactant modified zeolites: A review of their applications for water remediation with a focus on surfactant desorption and toxicity towards microorganisms. *J. Environ. Manag.* **2018**, *205*, 253–261. [[CrossRef](#)]
197. Ivankovic, T.; Hrenovic, J. Surfactants in the environment. *Arch. Ind. Hyg. Toxicol.* **2010**, *61*, 95–110. [[CrossRef](#)]
198. Li, Z. Sorption kinetics of hexadecyltrimethylammonium on natural clinoptilolite. *Langmuir* **1999**, *15*, 6438–6445. [[CrossRef](#)]
199. Bowman, R.S. Applications of surfactant-modified zeolites to environmental remediation. *Microporous Mesoporous Mater.* **2003**, *61*, 43–56. [[CrossRef](#)]
200. Baez-Alvarado, M.D.; Olguín, M.T. Surfactant-modified clinoptilolite-rich tuff to remove barium ( $Ba^{2+}$ ) and fulvic acid from mono- and bi-component aqueous media. *Microporous Mesoporous Mater.* **2011**, *139*, 81–86. [[CrossRef](#)]
201. Abdellaoui, Y.; Oualid, H.A.; Hsini, A.; Ibrahim, B.E.; Laabd, M.; Ouardi, M.E.; Giacomani-Vallejos, G.; Gamero-Melo, P. Synthesis of zirconium-modified Merlinoite from fly ash for enhanced removal of phosphate in aqueous medium: Experimental studies supported by Monte Carlo/SA simulations. *Chem. Eng. J.* **2021**, *404*, 126600. [[CrossRef](#)]
202. Li, Z.; Willims, C.; Roy, S.; Bowman, R.S. Desorption of hexadecyltrimethylammonium from charged mineral surfaces. *Environ. Geosci.* **2017**, *10*, 37–45. [[CrossRef](#)]
203. de Gennaro, B.; Catalanotti, L.; Bowman, R.S.; Mercurio, M. Anion exchange selectivity of surfactant modified clinoptilolite-rich tuff for environmental remediation. *J. Colloid Inter. Sci.* **2014**, *430*, 178–183. [[CrossRef](#)]
204. Gouran-Orimi, R.; Mirzayi, B.; Nematollahzadeh, A.; Tardast, A. Competitive adsorption of nitrate in fixed-bed column packed with bio-inspired polydopamine coated zeolite. *J. Environ. Chem. Eng.* **2018**, *6*, 2232–2240. [[CrossRef](#)]

205. Lin, H.; Huang, X.; Chang, J.; Li, B.; Bai, Y.; Su, B.; Shi, L.; Dong, Y. Improving sludge settling performance of secondary settling tank and simultaneously adsorbing nitrate and phosphate with surfactant modified zeolite (SMZ) ballasted flocculation. *J. Environ. Chem. Eng.* **2023**, *11*, 109650. [[CrossRef](#)]
206. Zhan, Y.; Lin, J.; Zhu, Z. Removal of nitrate from aqueous solution using cetylpyridinium bromide (CPB) modified zeolite as adsorbent. *J. Hazard. Mater.* **2011**, *186*, 1972–1978. [[CrossRef](#)]
207. Schick, J.; Caullet, P.; Paillaud, J.-L.; Patarin, J.; Mangold-Callarec, C. Batch-wise nitrate removal from water on a surfactant-modified zeolite. *Microporous Mesoporous Mater.* **2010**, *132*, 395–400. [[CrossRef](#)]
208. Schick, J.; Caullet, P.; Paillaud, J.-L.; Patarin, J.; Mangold-Callarec, C. Nitrate sorption from water on a Surfactant-Modified Zeolite. Fixed-bed column experiments. *Microporous Mesoporous Mater.* **2011**, *142*, 549–556. [[CrossRef](#)]
209. Li, Z.; Roy, S.J.; Zou, Y.; Bowman, R.S. Long-Term chemical and biological stability of surfactant-modified zeolite. *Environ. Sci. Technol.* **1998**, *32*, 2628–2632. [[CrossRef](#)]
210. Hrenovic, J.; Rozic, M.; Sekovanic, L.; Anic-Vucinic, A. Interaction of surfactant-modified zeolites and phosphate accumulating bacteria. *J. Hazard. Mater.* **2008**, *156*, 576–582. [[CrossRef](#)]
211. Li, Z. Chromate transport through surfactant-modified zeolite columns. *Groundw. Monit. Remediat.* **2006**, *26*, 117–124. [[CrossRef](#)]
212. Li, Z.; Hong, H. Retardation of chromate through packed columns of surfactant-modified zeolite. *J. Hazard. Mater.* **2009**, *162*, 1487–1493. [[CrossRef](#)] [[PubMed](#)]
213. Li, Z.; Bowman, R.S. Retention of inorganic oxyanions by organo-kaolinite. *Water Res.* **2001**, *35*, 3771–3776. [[CrossRef](#)]
214. Nye, J.V.; Guerin, W.F.; Boyd, S.A. Heterotrophic activity of microorganisms in soils treated with quaternary ammonium compounds. *Environ. Sci. Technol.* **1994**, *28*, 944–951. [[CrossRef](#)] [[PubMed](#)]
215. Hrenovic, J.; Ivankovic, T. Toxicity of anionic and cationic surfactant to *Acinetobacter junii* in pure culture. *Cent. Eur. J. Biol.* **2007**, *2*, 405–414.
216. Bingre, R.; Louis, B.; Nguyen, P. An overview on zeolite shaping technology and solutions to overcome diffusion limitations. *Catalysts* **2018**, *8*, 163. [[CrossRef](#)]
217. Gleichmann, K.; Unger, B.; Brandt, A. Manufacturing of industrial zeolite molecular sieves. *Chem. Ing. Technol.* **2017**, *89*, 851–862. [[CrossRef](#)]
218. Amir, C.; Mohammad, K.; Javad, A.S.; Sareh, A.A. Effect of bentonite binder on adsorption and cation exchange properties of granulated nano zeolite. *Adv. Mater. Res.* **2011**, *335–336*, 423–428. [[CrossRef](#)]
219. Tchobanoglous, G.; Burton, F.L.; Stensel, H.D. *Wastewater Engineering: Treatment and Reuse*, 4th ed.; Metcalf & Eddy, Inc.; McGraw-Hill: New York, NY, USA, 2003; pp. 1138–1162.
220. Loiola, A.R.; Bessa, R.A.; Oliveira, C.P.; Freitas, A.D.L.; Soares, S.A.; Bohn, F.; Pergher, S.B.C. Magnetic zeolite composites: Classification, synthesis routes, and technological applications. *J. Magn. Magn. Mater.* **2022**, *560*, 169651. [[CrossRef](#)]
221. Lu, A.-H.; Salabas, E.L.; Schüth, F. Magnetic nanoparticles: Synthesis, protection, functionalization, and application. *Angew. Chem. Int. Ed.* **2007**, *46*, 1222–1244. [[CrossRef](#)]
222. Kharisov, B.I.; Dias, H.V.R.; Kharissova, O.V.; Jiménez-Pérez, V.M.; Pérez, B.O.; Flores, B.M. Iron-containing nanomaterials: Synthesis, properties, and environmental applications. *RSC Adv.* **2012**, *2*, 9325–9358. [[CrossRef](#)]
223. Popescu, R.C.; Andronescu, E.; Vasile, B.S. Recent advances in magnetite nanoparticle functionalization for nanomedicine. *Nanomaterials* **2019**, *9*, 1791. [[CrossRef](#)] [[PubMed](#)]
224. Phouthavong, V.; Yan, R.; Nijpanich, S.; Hagio, T.; Ichino, R.; Kong, L.; Li, L. Magnetic adsorbents for wastewater treatment: Advancements in their synthesis methods. *Materials* **2022**, *15*, 1053. [[CrossRef](#)]
225. Cataldo, E.; Salvi, L.; Paoli, F.; Fucile, M.; Masciandaro, G.; Manzi, D.; Masini, C.M.; Mattii, G.B. Application of zeolites in agriculture and other potential uses: A review. *Agronomy* **2021**, *11*, 1547. [[CrossRef](#)]
226. Pond, W.G.; Mumpton, F.A. *Zeo-Agriculture—Use of Natural Zeolites in Agriculture and Aquaculture*; Westview Press: Brockport, NY, USA, 1984.
227. Li, Z. Use of surfactant-modified zeolite as fertilizer carriers to control nitrate release. *Microporous Mesoporous Mater.* **2003**, *61*, 181–188. [[CrossRef](#)]
228. Filatova, E.G.; Pozhidaev, Y.N. Development of natural zeolites regeneration scheme. *IOP Conf. Ser. Earth Environ. Sci.* **2020**, *459*, 032035. [[CrossRef](#)]
229. Zhang, Y.; Prigent, B.; Geißen, S.-U. Adsorption and regenerative oxidation of trichlorophenol with synthetic zeolite: Ozone dosage and its influence on adsorption performance. *Chemosphere* **2016**, *154*, 132–137. [[CrossRef](#)]
230. Lubensky, J.; Ellersdorfer, M.; Stocker, K. Ammonium recovery from model solutions and sludge liquor with a combined ion exchange and air stripping process. *J. Water Process Eng.* **2019**, *32*, 100909. [[CrossRef](#)]
231. Malovanyy, A.; Sakalova, H.; Yatchyshyn, Y.; Plaza, E.; Malovanyy, M. Concentration of ammonium from municipal wastewater using ion exchange process. *Desalination* **2013**, *329*, 93–102. [[CrossRef](#)]
232. Salvador, F.; Martin-Sanchez, N.; Sanchez-Hernandez, R.; Sanchez-Montero, M.J.; Izquierdo, C. Regeneration of carbonaceous adsorbents. Part I: Thermal Regeneration. *Microporous Mesoporous Mater.* **2015**, *202*, 259–276. [[CrossRef](#)]
233. Sireesha, S.; Agarwal, A.; Sopanrao, K.S.; Sreedhar, L.; Anitha, K.L. Modified coal fly ash as a low-cost, efficient, green, and stable adsorbent for heavy metal removal from aqueous solution. *Biomass Convers. Biorefinery* **2022**. [[CrossRef](#)]
234. Batjargal, T.; Yang, J.-S.; Kim, D.-H.; Baek, K. Removal characteristics of Cd(II), Cu(II), Pb(II), and Zn(II) by natural Mongolian zeolite through batch and column experiments. *Sep. Sci. Technol.* **2011**, *46*, 1313–1320. [[CrossRef](#)]

235. Bolan, N.S.; Mowatt, C.; Adriano, D.C.; Blennerhassett, J.D. Removal of ammonium ions from fellmongery effluent by zeolite. *Commun. Soil Sci. Plant Anal.* **2003**, *34*, 1861–1872. [CrossRef]
236. Zhang, M.; Zhang, H.; Xu, D.; Han, L.; Niu, D.; Tian, B.; Zhang, J.; Zhang, L.; Wu, W. Removal of ammonium from aqueous solutions using zeolite synthesized from fly ash by a fusion method. *Desalination* **2011**, *271*, 111–121. [CrossRef]
237. Karadag, D.; Tok, S.; Akgul, E.; Turan, M.; Ozturk, M.; Demir, A. Ammonium removal from sanitary landfill leachate using natural G<sup>o</sup>ordes clinoptilolite. *J. Hazard. Mater.* **2008**, *153*, 60–66. [CrossRef]
238. Lorick, D.; Ahlström, M.; Grimvall, A.; Harder, R. Effectiveness of struvite precipitation and ammonia stripping for recovery of phosphorus and nitrogen from anaerobic digestate: A systematic review. *Environ. Evid.* **2020**, *9*, 27. [CrossRef]
239. Huang, J.-C.; Shang, C. Air stripping. In *Handbook of Environmental Engineering. Vol. 4: Advanced Physicochemical Treatment Processes*; Wang, L.L., Hung, Y.-T., Shammass, N.K., Eds.; The Humana Press Inc.: Totowa, NJ, USA, 2006.
240. Katehis, D.; Diyamandoglu, V.; Fillos, J. Stripping and recovery of ammonia from centrate of anaerobically digested biosolids at elevated temperatures. *Water Environ. Res.* **1998**, *70*, 231–240. [CrossRef]
241. Değermenci, N.; Yildiz, E. Ammonia stripping using a continuous flow jet loop reactor: Mass transfer of ammonia and effect on stripping performance of influent ammonia concentration, hydraulic retention time, temperature, and air flow rate. *Environ. Sci. Pollut. Res.* **2021**, *28*, 31462–31469. [CrossRef]
242. Guisnet, M.; Ribeiro, F.R. Chapter 1 Deactivation and regeneration of solid catalysts. In *Deactivation and Regeneration of Zeolite Catalysts*; Catalytic Science Series; Guisnet, M., Robeiro, F.R., Eds.; Imperial College Press: London, UK, 2011; Volume 9, p. 360. [CrossRef]
243. Chen, S.; Popovich, J.; Zhang, W.; Ganser, C.; Hadel, S.E.; Seo, D.-K. Superior ion release properties and antibacterial efficacy of nanostructured zeolites ion-exchanged with zinc, copper, and iron. *RSC Adv.* **2018**, *8*, 37949–37957. [CrossRef]
244. Daligaux, V.; Richard, R.; Manero, M.-H. Deactivation and Regeneration of Zeolite Catalysts Used in Pyrolysis of PlasticWastes—A Process and Analytical Review. *Catalysts* **2021**, *11*, 770. [CrossRef]
245. Guisnet, M.; Ribeiro, F.R. Fundamental description of deactivation and regeneration of acid zeolites. *Stud. Surf. Sci. Catal.* **1994**, *88*, 53–68.
246. Salvador, F.; Martin-Sanchez, N.; Sanchez-Hernandez, R.; Sanchez-Montero, M.J.; Izquierdo, C. Regeneration of carbonaceous adsorbents. Part II: Chemical, Microbiological and Vacuum Regeneration. *Microporous Mesoporous Mater.* **2015**, *202*, 277–296. [CrossRef]
247. Wang, S.; Li, H.; Xie, S.; Liu, S.; Xu, L. Physical and chemical regeneration of zeolitic adsorbents for dye removal in wastewater treatment. *Chemosphere* **2006**, *65*, 82–87. [CrossRef]
248. Zhang, Z.Y.; Shi, T.B.; Jia, C.Z.; Ji, W.J.; Chen, Y.; He, M.Y. Adsorptive removal of aromatic organosulfur compounds over the modified Na-Y zeolites. *Appl. Catal. B Environ.* **2008**, *82*, 1–10. [CrossRef]
249. Fujita, H.; Izumi, J.; Sagehashi, M.; Fujii, T.; Sakoda, A. Decomposition of trichloroethene on ozone-adsorbed high silica zeolites. *Water Res.* **2004**, *38*, 166–172. [CrossRef]
250. Lee, D.-G.; Kim, J.-H.; Lee, C.-H. Adsorption and thermal regeneration of acetone and toluene vapors in dealuminated Y-zeolite bed. *Sep. Purif. Technol.* **2011**, *77*, 312–324. [CrossRef]
251. Simancas, R.; Chokkalingam, A.; Elangovan, S.P.; Liu, Z.; Sano, T.; Iyoki, K.; Wakihara, T.; Okubo, T. Recent progress in the improvement of hydrothermal stability of zeolites. *Chem. Sci.* **2021**, *12*, 7677. [CrossRef]
252. Bathen, D. Physical waves in adsorption technology—An overview. *Sep. Purif. Technol.* **2003**, *33*, 163–177. [CrossRef]
253. Abdelsayed, V.; Shekhawat, D.; Tempke, R.S. Zeolites interactions with microwaves during methane non-oxidative coupling. *Catal. Today* **2021**, *365*, 88–102. [CrossRef]
254. Delgado, L.; Catarino, A.S.; Eder, P.; Litten, D.; Luo, Z.; Villanueva, A. *End-of-Waste Criteria*; EUR—Scientific and Technical Research series; European Commission Joint Research Centre: Seville, Spain, 2009. [CrossRef]
255. Grand View Research, Market Analysis Report: Zeolite Market Size, Share & Trends Analysis Report By Application (Catalyst, Adsorbent, Detergent Builder), By Product (Natural, Synthetic), By Region (North America, Europe, APAC, CSA, MEA), And Segment Forecasts, 2022–2030. Grand View Research, India & US, Report 978-1-68038-601-1, p. 114. Available online: <https://www.grandviewresearch.com/industry-analysis/zeolites-market> (accessed on 25 October 2023).
256. Markets and Markets, Market Research Report: Zeolites Market by Type (Natural, Synthetic), Function (Ion-Exchange, Catalyst, Molecular Sieve), Synthetic Zeolites Application (Detergent, Catalyst), Natural Zeolites Application, and Regional-Global Forecast to 2026. Markets and Markets, India, Report CH 8006. 2021. Available online: <https://www.marketsandmarkets.com/Market-Reports/zeolites-market-76442083.html> (accessed on 25 October 2023).
257. Coherent Market Insights (2023) Nutrient Recycling Market. Coherent Market Insights, India, Report CM15972, p. 154. Available online: <https://www.coherentmarketinsights.com/market-insight/nutrient-recycling-market-5972> (accessed on 25 October 2023).

**Disclaimer/Publisher’s Note:** The statements, opinions and data contained in all publications are solely those of the individual author(s) and contributor(s) and not of MDPI and/or the editor(s). MDPI and/or the editor(s) disclaim responsibility for any injury to people or property resulting from any ideas, methods, instructions or products referred to in the content.